

**CHARACTERIZATION OF THE C-TERMINAL DOMAIN OF
THE P53 TUMOR SUPPRESSOR**

by

BAHAR SHAMLOO

Submitted to the

Graduate School of Engineering and Natural Sciences

in partial fulfillment of

the requirements for the degree of

Doctor of Philosophy

Sabanci University

July 2016

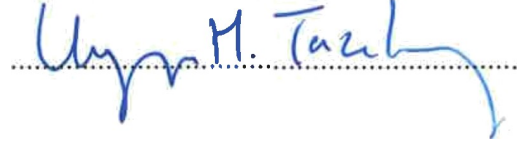
**CHARACTERIZATION OF THE C-TERMINAL DOMAIN OF
THE P53 TUMOR SUPPRESSOR**

APPROVED BY:

Prof. Dr. Batu Erman
(Thesis Supervisor)



Prof. Dr. Uygur Halis Tazebay



Prof. Dr. Canan Atılğan



Prof. Dr. Uğur Sezerman



Prof. Dr. Selim Çetiner



DATE OF APPROVAL: 25.07.2016

© Bahar Shamloo 2016

All Rights Reserved

ABSTRACT

CHARACTERIZATION OF THE C-TERMINAL DOMAIN OF THE P53 TUMOR SUPPRESSOR

Bahar Shamloo

Molecular Biology, Genetics, and Bioengineering, PhD Thesis, 2016

Thesis supervisor: Batu Erman

Keywords: p53, p53 CTM, CRISPR/Cas9 system, Human Colon Cancer

Half of all cancer cases have a mutated p53 gene. The p53 protein's C-terminal domain plays an important role in its post-translational modification. We studied the function of this domain in endogenous p53 in HCT116 human colon cancer cell lines. We generated several C-terminal mutant (CTM) cell lines through CRISPR-Cas9 mediated genome editing. The focus of this study is three of these p53 CTM cell lines that encode 1) a truncated p53 protein (p53 $\Delta 21$ / $\Delta 21$); 2) a single amino acid deleted p53 protein (p53 $\Delta R379$ / $\Delta R379$); and 3) a p53 protein missing the C-terminus encoded by the last p53 exon (p53 $\Delta 26$ / $\Delta 26$). We show that cells which express the p53 $\Delta R379$ protein (with deleted Arg379), grow slower than their wild type counterparts and cannot bind to DNA targets as efficiently as WT p53. The p53 $\Delta 21$ mutant lacks 21 amino acids at the C-terminus. This mutant p53 can accumulate after DNA damage and can bind to DNA targets efficiently; nevertheless, it shows a different transcription pattern for some genes that play important roles in ribosome biogenesis stress. The p53 $\Delta 26$ expressing mutant cell line lacks the last exon of p53 on both alleles, behaves in a very different way. The phenotype of this mutant is similar to HCT116KO cells that do not express p53. These mutant cells express truncated p53 and they grow much slower and go to senescence twice as fast as HCT116KO counterparts. This p53 mutant cannot translocate into the nucleus after DNA damage induced by Doxorubicin treatment. We assessed the expression of p53 target genes by quantitative RT PCR and found defects in the expression of these genes for all our CTM cell lines. These results indicate that the p53 C-terminal domain is very critical for the protein's function.

Özet

P53 TÜMÖR BASKILAYICI PROTEİNİNİN C-TERMINAL DOMAIN KARAKTERİZASYONU

Bahar Shamloo

Moleküler Biyoloji, Genetik ve Biyomühendislik, PhD Tezi, 2016

Tez danışmanı: Batu Erman

Anahtar kelimeler: p53, p53 CTM, CRISPR/Cas9 sistemi, İnsan Kolon Kanseri

Tüm kanser vakalarının yarısında mutasyona uğramış p53 geni görülmektedir. P53 proteininin c-terminal domaini post-translasyon modifikasyonlarında önemli bir rol sahibi. Bu çalışmada, HCT116 insan kolon kanser hücre hatlarında bulunan endojen p53'te bu domainin fonksiyonu çalışılmıştır. CRISPR-Cas9 aracılı genom düzenleme tekniği ile C-terminal mutant (CTM) hücre hatları oluşturulmuştur. Bu çalışmada oluşturulan p53 CTM hücre hatlarından; 1) kesilmiş p53 proteini (p53 $\Delta 21$ / $\Delta 21$), 2) tek amino asidi silinmiş p53 proteini (p53 $\Delta R379$ / $\Delta R379$), 3) son p53 eksonu tarafından kodlanan C-terminali içermeyen p53 proteini; içerenler üzerinde durulmuştur. Elde edilen veriler ışığında, p53 $\Delta R379$ proteinini (silinmiş Arg379 ile) ifade eden hücrelerin doğal fenotipe (WT p53) göre daha yavaş büyüdükleri ve DNA hedeflerine WT p53 kadar verimli bağlanmadıkları belirlenmiştir. The p53 $\Delta 21$ mutantının C-terminalinde 21 amino asidi bulunmamaktadır. Bu mutant p53 DNA hasarı sonrası birikebilmekte ve DNA hedeflerine verimli bir şekilde bağlanabilmektedir, buna rağmen bu hücreler ribozom biyogenez stresinde önemli rol oynayan genler özelinde daha farklı bir transkripsiyon şablonuna sahiptir. p53 $\Delta 26$ biyosentezleyen mutant hücre hattı ise her iki alelde p53'ün son eksonunu içermemektedir ve çok farklı bir davranış sergilemektedir. Bu mutantın fenotipi p53'ü ifade etmeyen HCT116KO hücreleri ile benzerdir. Bu mutant hücreler kesik p53 proteini ifade ederler ve çok daha yavaş büyümektedirler ve HCT116KO mukabillerine göre iki kat hızlı hücre yaşlanmasına (senesans) girerler. Bu p53 mutantı Doxorubicin tedavisi ile indüklenen DNA hasarı sonrasında hücre çekirdeğine doğru yer değiştirememektedir. Bütün CTM hücre hatlarında, p53 hedef genlerinin ifade seviyeleri kantitatif RT PCR ile incelenmiş ve bu genlerde kusurlar tespit edilmiştir. Bu sonuçlar, p53 C-terminal domaininin proteinin fonksiyonu için çok hassas olduğunu göstermektedir.

To My Beloved Ana...

ACKNOWLEDGEMENTS

I am so happy that I am given a chance to express my gratitude to the one who helped me in every way through the difficulties of these five years, Prof. Dr. Batu Erman. I believe that being a teacher is the most crucial responsibility in the world. Teachers are leaders, are those who shape the culture of the society. Prof. Dr. Batu Erman is a great teacher, a sincere friend, a caring father, and a wise leader. The most important thing he taught me was to always wonder, to be curious, and to yearn for the answers. I am grateful to him for the rest of my life.

I am very thankful to all my teachers, Prof. Dr. Uygur Tazebay for his support and his faith in me, Prof. Dr. Canan Atılgan for her precious scientific comments during these years, Prof. Dr. Uğur Sezerman for introducing bioinformatics to me in the best possible way and his support, Prof. Dr. Selim Çetiner for his support whenever I needed help and making me smile all the time. I also want to express my gratitude to Prof. Dr. Hikmet Budak who never withheld his assistance from me during these years. I am grateful to my M.Sc. advisor, Prof. Dr. Eda Tahir Turanlı, who never gave up on me and stood by me even after so many years. I also want to thank Prof. Dr. Nader Pourmand for opening new horizons for me and for helping me to look in a different way. I am

grateful to Dr. Tolga Stl and Dr. Adil Doęanay Duru for their scientific comments and support.

I am eternally grateful to my friends and colleagues who made this period extremely joyful and full of memories. I thank our post-doctoral research fellows, Dr. Emre Tařkin and Dr. Belkıs Atasever Arslan for their help and support during the first year of my Ph.D. Nearly all the molecular biology and cell culture methods I learnt was because of endless help and support of Dr. Nazlı Keskin and Dr. Emre Deniz. I also want to thank my undergraduate colleagues, Liana Behmoiras and Sinem Usluer who bestowed their friendship on me. I feel incredibly lucky to spend the last year of my Ph.D. studies in the most friendly and helpful laboratory that could ever exist. I am obliged to Canan Seyitoęlu, Ronay etin, Melike Gezen, Hlya Yılmaz, Nazife Tolay, and most importantly, Asma Al-Murtadha, who gave their pure friendship and support to me. They made me enjoy every hour I spent in the laboratory with them.

I am much obliged to TBİTAK-BİDEB 2215 program that supported me financially for the first four years of my PhD, and also Sabanci University Dean office full-scholarship that supported me during my fifth year.

It wouldn't be possible to fulfill my studies if it wasn't for all the love and friendship I received from my friends, Forough Hafezi, Leila Haghighi, Sina Kia, Kaveh Rahimzadeh, Pozhhan Mokhtari, Dr. Raghu Mokkaapati, and Glperi Yalın.

The last but not the least gratitude goes to my family. My beloved mother who means the world to me, my dear father who always believed in me, my brother who supported me in every way, and my dear Mert, who stood by me through these years with his endless faith in me. At the end, I want to send my love to the memory of my grandfather, Hamid Shamloo, whose love and support is always felt deeply in my heart.

TABLE OF CONTENTS

1. INTRODUCTION	1
1.1. The p53 Protein	1
1.1.1. p53; Guardian of the Genome	1
1.1.2. p53 Structure	4
1.1.3. p53 Evolution	8
1.1.4. p53 Mutations and Cancer and Therapeutic Approaches.....	9
1.2. Genome Editing Tools	14
1.2.1. A Brief History of Genome Engineering.....	14
1.2.2. TALEN Proteins.....	15
1.2.3. CRISPR Technology	16
2. AIM OF THE STUDY	18
3. MATERIALS AND METHODS	20
3.1. Materials.....	20
3.1.1. Chemicals	20
3.1.2. Equipment	20
3.1.3. Buffers and Solutions	20
3.1.4. Growth Media.....	22
3.1.5. Commercial Molecular Biology Kits	23
3.1.6. Enzymes	23
3.1.7. Bacterial Strains	23
3.1.8. Mammalian Cell Lines	24
3.1.9. Plasmids and Primers	24
3.1.10. DNA and Protein Molecular Weight Markers.....	29
3.1.11. DNA Sequencing.....	29
3.1.12. Software, Computer-Based Programs, and Websites.....	30
3.2. Methods.....	31
3.2.1. Bacterial Cell Culture	31
3.2.2. Plasmid Construction	32
3.2.3. Mammalian Cell Culture	34
3.2.4. TALEN Protein Assembly	35
3.2.5. CRISPR/Cas9 and CRISPR/Cas9n Gene Editing	36

3.2.6. RNA-Sequencing.....	37
4. RESULTS	38
4.1. Screening Homozygous CTM Cell Lines Created by Genome Editing Tools ...	38
4.1.1. TALEN-Mediated CTM Cell Lines	39
4.1.2. CRISPR-Mediated CTM Cell Lines.....	42
4.2. Homology Directed CTMs.....	47
4.3. NHEJ Mediated CTM: mut#4, mut#5, and mut#9.....	49
4.3.1. Phenotypic Specificities of the CTM Cell Lines.....	55
4.3.2. The p53 Protein Expression in CTM Cell Lines	56
4.3.3. DNA-Binding Activity of p53 in CTM Cell Lines	60
4.3.4. p53 Translocation into the Nucleus in CTM Cell Lines.....	61
4.3.5. mRNA Amount for p53 and p53 Target Genes in CTM Cell Lines	63
4.3.6. Cell Doubling Time Increase in CTM Cell Lines	68
5. DISCUSSION.....	71
REFERENCES	75

LIST OF FIGURES

Figure 1.1: p53/MDM2/MDMX regulation loop	2
Figure 1.2: Post-translational modification of the p53 protein.....	7
Figure.4.1: TALEN proteins designed to create P53 CTD mutant cells	40
Figure 4.2: Transfection control using GFP expressing plasmids and RFLP analysis of TALEN transfected cell pools	41
Figure 4.3: TALEN transfected single cell clone RFLP and heterozygous mutant	42
Figure 4.4: Annotation of Primers used for RFLP and CRISPR target sites.....	44
Figure 4.5: Annealing of DNA oligonucleotides for cloning into Guide RNA expression plasmids	44
Figure 4.6: Experimental design of genome editing using the CRISPR/Cas9 system ...	45
Figure 4.7: The mechanism of CRISPR/Cas9 interaction with DNA	46
Figure 4.8: Design of the donor DNA for homology directed mutation of HEK293 cells	47
Figure 4.9: Homology directed mutagenesis using the CRISPR/Cas9 system with ss- oligonucleotides	48
Figure 4.10: Non-Homologous End Joining mediated random mutations using the CRISPR/Cas9 system	50
Figure 4.11: Single cell clone screening of CTM cell lines.....	51
Figure 4.12: Sequencing analysis of mut#4, mut#5, and mut#9	53
Figure 4.13: Predicted p53 gene DNA, RNA and protein structure of mut#4, mut#5, and mut#9	54
Figure 4.14: Analysis of p53 protein expression in HCT116WT and CTM cells by western blotting	56
Figure 4.15: Analysis of p53, p21, PUMA protein expression in mut#4 and mut#9	57
Figure 4.16: Analysis of p53 protein expression in WT, mut#9, and mut#5 under different types of genotoxic stress	58
Figure 4.17: Analysis of p53 expression in WT, KO, and mut#5	59
Figure 4.18: p53 protein expressed by mut#9 cells binds less efficiently to target DNA	60
Figure 4.19: p53 nuclear translocation is inhibited in mut#5 cells under stress.....	61
Figure 4.20: Confocal microscopic analysis of WT and mut#5 cells with and without stress	62

Figure 4.21: Quantitative realtime PCR analysis of p53, p21, MDM2, PUMA mRNA expression from WT, mut#4, mut#5, mut#9 cells, normalized to WT un-treated.....	64
Figure 4.22: Quantitative realtime PCR analysis of p53, p21, MDM2, PUMA mRNA expression from WT, mut#4, mut#5, mut#9 cells, normalized to the each cell's own untreated	65
Figure 4.23: Quantitative realtime PCR analysis of p53, p21, MDM2, PUMA mRNA expression from HCT116WT, HCT116KO, and mut#5.....	66
Figure 4.24: CTM cell lines have differentially expressed telomere genes.....	66
Figure 4.25: Doubling time analysis of HCT116WT cells in comparison with mut#4 and mut#9	68
Figure 4.26: Growth rate comparison of HCT116WT and HCT116KO and mut#5 cells	69
Figure 4.27: Analysis of doubling time in WT, mut#5, and mut#9 cells with or without stress	69
Figure 4.28: mut#5 and mut#9 cells grow slower than HCT116WT cells.....	70

LIST OF TABLES

Table 3.1: The list of the plasmids used in this thesis.....	24
Table 3.2: The list of the primers used in this thesis	27
Table 3.3: The list of the software, programs and websites used in this thesis.....	30
Table 3.4: Optimized PCR conditions	33

LIST OF SYMBOLS AND ABBREVIATIONS

α	Alpha
β	Beta
μ	Micro
A	Ampere
Amp	Ampicillin
AP	Alkaline Phosphatase
ATM	Ataxia Telangiectasia Mutated
bGH PA	Bovine Growth Hormone Polyadenylation
Cas	CRISPR associated
CIAP	Calf Intestine Alkaline Phosphatase
CMV	Cytomegalovirus
CRISPR	Clustered Regularly Interspaced Short Palindromic Repeat
crRNA	CRISPR RNA
CTD	C-Terminal Domain
CTM	C-Terminal Mutant
DBD	DNA-Binding Domain
DMEM	Dulbecco's Modified Eagle Medium
DMSO	Dimethylsulfoxide
DNA	Deoxyribonucleic Acid
DSB	Double Strand Break

E.coli	Escherichia coli
FACS	Fluorescence Activated Cell Sorting
FBS	Fetal Bovine Serum
GFP	Green Fluorescent Protein
gRNA	Guide RNA
h	Hour
HBS	HEPES-Buffered Saline
HCC	Hepatocyte Carcinoma
HDR	Homology-Directed Repair
INDEL	Insertion Deletion
JNK	c-Jun activator kinase
KO	Knock-out
LB	Luria Broth
MDM2	Mouse Double Minute 2
MDMX/MDM4	Mouse Double Minute 4
mRNA	Messenger RNA
mtDNA	Mitochondrial DNA
NCBI	National Center for Biotechnology
NHEJ	Non-Homologous End Joining
NLS	Nuclear Localization Signal
NMD	Nonsense-Mediated mRNA Decay
nt	Nucleotide
PAM	Protospacer-adjacent motif
PBST	PBS-Tween20
PEI	Polyethylenimine
PI	Propidium Iodide
Pol	Polymerase
PRR	Proline Riche Region
PSA	Prostate-Specific Antigen
PTM	Post-Translational Modification
PUMA	p53 Up-regulated Modulator of Apoptosis
QRT PCR	Quantitative Real Time PCR
REG	C-terminal Regulatory Domain
RFLP	Restriction Fragment Length Polymorphism
RNA	Ribonucleic Acid

RNA-Seq	RNA Sequencing
ROS	Reactive Oxygen Species
RP	Ribosomal Protein
rpm	Rotation per minute
rRNA	ribosomal RNA
RT-PCR	Real Time Polymerase Chain Reaction
RVD	Repeat-Variable Di-residue
SDM	Site-Directed Mutagenesis
SDS PAGE	Sodium Dodecyl Sulfate Polyacrylamide Gel Electrophoresis
sgRNA	Single-Guide RNA
sIL-1Ra	Secretory Interleukin-1 Receptor Antagonist
SIRT1	Sirtulin (silent mating type information regulation homolog) 1
ss-oligo	single-stranded oligodeoxynucleotide
TAL	Transcription Activator-Like
TALEN	Transcription Activator-Like Effector Nuclease
TBE	Tris Borate EDTA
TET	Tetramerization Domain
TIGAR	Tp53-induced glycolysis and apoptosis regulator
tracrRNA	Trans-Activating CRISPR RNA
UTR	Un-Translated Region
V	Volt
Wip1	wild-type p53-induced phosphatase-1
WT	Wild Type
ZFN	Zinc Finger Nuclease

1. INTRODUCTION

1.1. The p53 Protein

1.1.1. p53; Guardian of the Genome

The p53 protein is mutated in more than 50% of human cancer cases. The prevalence of the p53 mutation depends on the cancer type, ranging from 80-90% in ovarian or lung cancer to as low as 5% in cervical cancer¹. Whether by mutation in the *TP53* gene or by the perturbation of p53 associated pathways, p53 is inactivated in almost every tumor². Li and Fraumeni first discovered germline mutations in the *Tp53* gene in 1969 and defined these mutations as familial cancer syndrome^{3,4}. Although p53 is the most studied protein during the last 40 years in over 80,000 articles, there is still much to discover about the complexities of this protein.

p53-mediated cellular responses: p53 is involved in many cellular responses such as cell cycle arrest, induction of senescence, DNA repair, and apoptosis by controlling transcription of its target genes⁵. Upon cellular stress signals such as hypoxia, oncogenic stress, oncogene activation, DNA damage, telomere erosion, or ribosomal stress, p53 protein becomes stabilized. This stabilization is mediated by multiple post-translational modifications such as methylation, phosphorylation and acetylation. p53 stabilization results in its translocation into the nucleus and the induction of transcription of p53 target genes. Transcriptional regulation of p53 target genes leads to cellular responses such as cell cycle arrest or apoptosis, depending on the severity and irreparability of the damage⁶. One of the p53 protein's transcriptional

targets is the *mdm2* gene that encodes the MDM2 protein. MDM2 keeps cellular p53 protein levels under strict control along with its homolog, MDMX, by forming a heterodimer and acting as an E3 ubiquitin ligase⁷. MDMX acts as a p53 negative regulator in two ways; first by preventing MDM2 from auto-ubiquitination, and second by binding to the transactivation domain of p53 and inhibiting its activation^{8,9} (Figure 1.1).

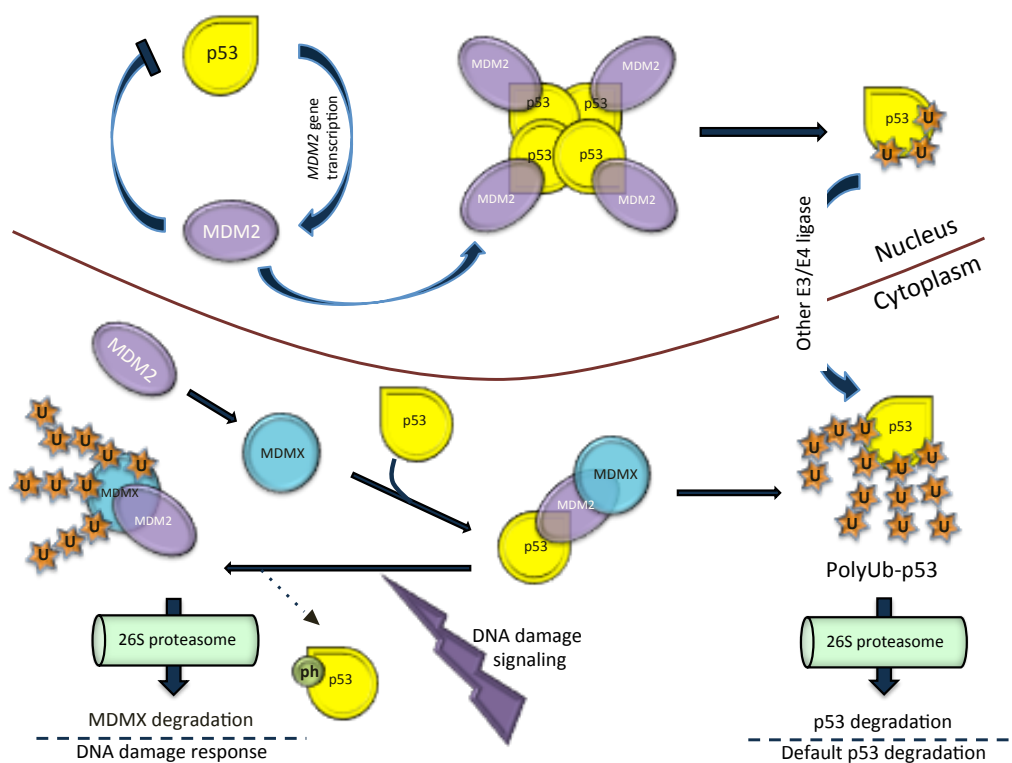


Figure 1.1: p53/MDM2/MDMX regulatory loop. The MDM2/p53 autoregulatory feedback loop is shown at the top left. Mono-ubiquitination of p53 by MDM2 binding to its N-terminal leads to p53 nuclear export (top right). The activation of MDM2/MDMX and other E3 ligases or E4 factors in the cytoplasm leads to the poly-ubiquitination and 26S proteasomal degradation of p53 (bottom right). Following DNA damage stress, p53 N-terminal gets phosphorylated and MDMX is poly-ubiquitinated in the MDM2/MDMX complex (bottom left). This results in MDMX degradation, loss of the activator component of MDM2/MDMX E3 complex, p53 stabilization and accumulation¹⁰.

p53 and ribosome biogenesis stress: Ribosomal stress affects the p53/MDM2 interaction¹¹. The nucleolus is a sub-nuclear compartment in which ribosome biogenesis occurs. rRNA genes in tandem repeats are translocated to the nucleolus and are transcribed by RNA polymerase I (Pol I) in a strictly regulated manner. Because ribosome biogenesis is an extremely energy-consuming process for cells that requires high fidelity, it is suppressed under cellular stress¹¹. The misregulation of ribosome biogenesis is detected in various human cancer cases¹². The rRNA together with ribosomal proteins (RPs) are assembled in the nucleolus hub to construct the 40S and 60S ribosomal subunits¹³. 40S subunit has 18S RNA and 33 proteins; 60S subunit has 5S, 28S, and 5.8S RNA subunits and 46 proteins¹⁴. The nucleolus and the ribosome biogenesis apparatus play an important role in sensing cellular stress. Upon severe cellular stress, such as Doxorubicin treatment, the nucleolus is condensed and nucleolar proteins and RNAs are packed in structures called nucleolar caps¹⁵. This alteration in nucleolar morphology is an important factor in p53 activation upon stress¹⁶. Inhibition of rRNA processing and transient knock down of the activator subunit of PolI is followed by p53-dependent cell cycle arrest^{17,18}. Ribosomal proteins, such as RPL11, similar to the ARF tumor suppressor, bind to MDM2 and inhibit its interaction with p53 by generating a stable complex with MDM2¹⁹. Two main models are suggested for the RP/MDM2/p53 interaction: a) upon ribosomal stress, RPs are diffused into the nucleus and bind to MDM2, inhibiting its nuclear export into the cytoplasm, b) following the 40s depletion, translation of RPL11 is enhanced from its mRNA, it accumulates and induces p53 activity; the RPL11-MDM2 complex binds to the RPL11 promoter and induces its transcription as well²⁰. RPL11 and RPL5 are transferred from nucleolus into the nucleus, bind to MDM2 and activate p53²¹. Other RPs cannot enter the nucleus and are quickly degraded^{12,21}. It should be noted that PRs, not only increase p53 activity in an MDM2-dependent manner, but they could also bind to the promoter of a number of the p53 regulatory genes. As an example, RPL11 is important in the recruitment of p300/CBP (a p53 transcriptional co-activator), which leads to p53 K382 acetylation and p53 activation²⁰.

1.1.2. p53 Structure

The human p53 protein consists of 393 amino acids and forms a homo-tetramer when active. p53 protein is composed of 5 domains: the transactivation domain (TAD; divided into TAD1 and TAD2), the proline rich region (PRR), the DNA binding domain (DBD), the tetramerization domain, and the C-terminal regulatory domain²². In addition to these structurally well defined domains, the p53 protein has intrinsic disordered regions to provide its conformational adaptability²³. Post-translational modification (PTM) occurs under various conditions to regulate p53 stability, activity, and protein-protein interactions (Figure. 2)²⁴.

Transactivation Domain: The N-terminal transactivation domain of p53 is divided into two sub-domains: TAD1 (amino acid 1-40) and TAD2 (amino acid 41-61). TAD is important in activation of the p53 protein by interacting with the p300, CREB binding proteins (CBP), and MDM2/MDMX proteins²⁵. Phosphorylation of this domain is important because it specifies the group of proteins that can interact with the p53 protein and turn its function on and off²⁶. p300/CBP and MDM2 compete over their binding site on the p53 N-terminal domain and depending on the post-translational modification of this domain, the affinity of MDM2 or p300/CBP changes^{27,28}. Hydrophobic amino acids in TAD1 (such as L22 and W23) are important in MDM2 binding²⁹. MDM2 binding to the TAD results in the ubiquitination of the CTD of p53. The interaction of MDM2 with the TAD must required the CTD as CTD mutant p53 proteins cannot interact with MDM2³⁰. Under DNA damage stress, post-translational modification of TAD1 (e.g. T18 phosphorylation) and CTD (e.g. K382 acetylation) results in the decrease of the affinity of MDM2 to its N-terminal p53 binding site decreases and the affinity of p300-CBP for p53 increases. These modifications transcriptionally activate the p53 protein^{31,32}. Some modifications (such as S15 phosphorylation) can directly increase p53 affinity for p300/CBP as well³³.

DNA binding Domain: The p53 protein binds to DNA response elements with two half-site motifs with variable spacer lengths (0-13 base pair). Each of these motifs has a general sequence of RRRCWWGYYY (R = A or G; W= A or T; Y = C or T)^{34,35}.

In a tetramerized p53, all four DBD bind to these binding sites cooperatively³⁶. Thus the p53 tetramer binds to the sequence RRRCWWGYYYN₍₀₋₁₃₎RRRCWWGYYY, where each half site is bound by a dimer. The DBD consists of two anti-parallel β sheets that make a β -sandwich. These two sheets join using several elements such as β hairpins, α -helix “H1”, and α -helix “H2”. The latter interacts with C-terminal end of the DBD. α -helix “H1” and loop L3 have Zn-chelating residues that coordinate a zinc atom (zinc finger motif)^{37,38}. L120 (in contact with second R of the p53 response element) and R273 that contacts with DNA phosphate backbone are examples of amino acids that are important in DNA binding. Mutations in these amino acids are frequently reported in tumor genomes as carcinogenic mutations. Mostly, mutations in cancer cases reside in the DBD and these mutations either disturb p53 DNA binding (class I mutations) or change the p53 conformation (class II mutations)³⁹. Class I mutations refer to surface residues and do not change p53 conformation as much as class II. DBD mutations are generally associated with cancer onset due to three reasons: a) they affect transcription activation by p53, because DNA binding efficiency changes⁴⁰, b) mutations affect the folding of p53 protein at body temperature⁴¹, and c) Arginine residues are abundant in the DBD and these amino acids are susceptible to mutation because their codons are affected by CG dinucleotide error-prone repair⁴². In addition to DNA, the DBD also interacts with p53-binding proteins, which change the protein's conformation. For example, 53BP1 and 53BP2 (ASPP2) proteins bind to the DBD. These interactions are important for the function of p53 as 53BP1 activates ataxia-telangiectasia mutated (ATM) in response to DNA damage^{43,44}. ATM and ATR are two proteins that are important for the pathway that results in the phosphorylation of the N-terminal TAD of p53 that results in its dissociation from MDM2.

Tetramerization Domain: The tetramerization domain of p53 starts from amino acid 324 to 355; β -strand (326-333) and α -helix (335-354) in each of four monomers form a V-like shape. G334 is very important in the secondary structure and its mutation leads to cancer⁴⁵. M330 and L344 reside in the center of the tetramer are responsible for the stoichiometry of the structure⁴⁶. In cancer studies, mutation rate in the tetramerization domain is many folds (~100 folds) less than the mutation rate in DBD⁴⁷; one reason is the high melting temperature (70°C) of the oligomerization domain that inhibits unfolding of the domain in body temperature following mutations⁴⁸, and the second reason is that generally dominant negative activity of the

mutant protein does not happen for this domain⁴⁹. The side chain size of the hydrophobic residues is extremely critical for the folding of this domain and oligomerization stoichiometry as the V-shape folding changes to L-shape following specific mutations (such as for F341 and L344)^{50,51}. Tetramerization of p53 leads to masking of the Leucine rich nuclear export signal that resides in the tetramerization domain and determines cellular p53 localization. This structural change is also a hallmark for stressed cells since in normal cells, all monomer, dimer, and tetramer states of p53 are present in different ratios; on the other hand, cells under stress stabilize amount of tetramer p53 even before p53 level increase⁵². Generally various modifications on p53 can favor a protein-protein interaction, or vice versa.

Proline-Rich Region: Proline-rich regions reside in the N-terminus (amino acid 71-93; ten Proline residues) and C-terminus (294-323; seven Proline residues). Proline amino acids are important for an efficient folding of the p53 protein⁵³ and its interaction with SH3 domain containing proteins (such as 53BP2)⁵⁴. Poly-proline regions have been shown to be critical for the activity of p53, specially its role in inducing apoptosis⁵⁵.

C-Terminal Domain: C-terminal basic domain starts from amino acid 356 until the last amino acid of the p53 protein (393). This domain is flexible and is exposed to many post-translational modification^{56,57,58}. p53 CTD post-translational modification plays an important role in p53 conformational change, DNA-binding specificity, oligomerization state, and nuclear import/export⁵⁹. p53 CTD has been solved in complex with Sir2 (a protein deacetylase) and S100B (Calcium binding p53 inhibitor); both change p53 conformation completely differently^{60,61}. Sir2 family has roles in DNA repair, genome stability and transcriptional silencing⁶². For example, miR-34a/sirtuin 1(SIRT1)/p53 is a p53 regulatory pathway in which p53 is suppressed by SIRT1 deacetylase activity under normal unstressed conditions. miR-34a modulates expression of numerous genes, including SIRT1. p53 increases transcription of this microRNA; this up-regulation in turn leads to suppression of SIRT1 and increasing p53-dependent apoptosis⁶³. Another member of this complicated circuit is the c-Jun protein and its activator, JNK (c-Jun activator kinase), which are responsible for re-directing p53 cell cycle arrest activity to robust apoptosis. JNK also plays a role in cell proliferation and cell cycle progression⁶⁴. The positive feedback loop between p53 and

JNK is not completely known, but the p53 protein induces pro-oxidant genes, which increase reactive oxygen species (ROS), promoting JNK activation⁶⁵.

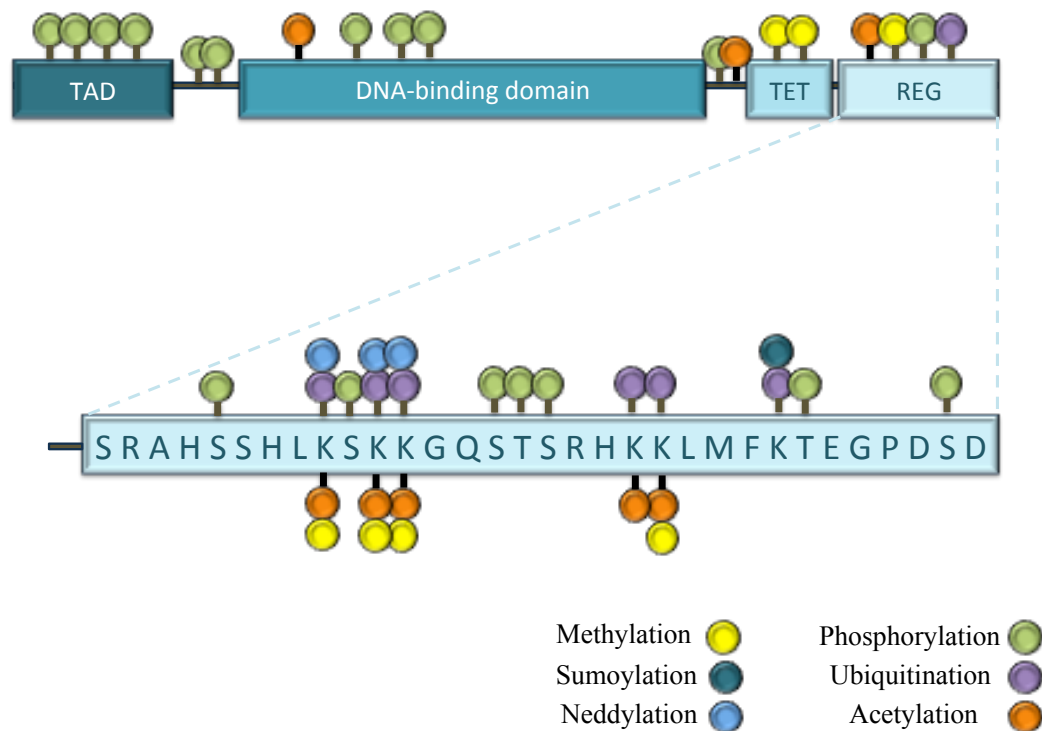


Figure 1.2: Post-translational modification (PTM) of the p53 protein. At the top, p53 domains are shown as: TAD (Transactivation domain), TET (Tetramerization domain), REG (C-terminal regulatory domain). Upon stress, several PTMs accumulate and activate p53. Different PTM patterns regulate p53 protein-protein interactions, transactivation activity and stability.

1.1.3. p53 Evolution

The history of the p53 protein goes back to the appearance of early metazoan sponges, cnidarians, placozoan and even protists, about 1-2 billion years ago. This history shows the importance of p53 in cancer development ever since^{66,67}. Even in unicellular close relatives of metazoans (*M. brevicollis*) some metazoan-specific p53 transcription factor family member proteins are detected. This finding shows the role of p53 family proteins in the evolution of multicellular organisms by playing a role in the maintenance of genome integrity under stress conditions^{68,69}. p53, p63, and p73 are three family members found in vertebrates that evolved from a primordial common ancestor gene. The proteins encoded by these three genes have distinct responsibilities; p63 and p73 participate in developmental and differentiation, while p53 functions as a tumor suppressive protein⁷⁰. These three paralogs are present in the cartilaginous fishes and the jawless lamprey, showing the evolutionary path of the p53 family⁷¹. p63 and p73 have evolved slower compared to p53 in vertebrates⁷². Structurally, the DNA binding domain in p53 is more stable compared to those of p63 and p73; p53 has evolved slightly according to the organismal temperature and thermodynamics of the protein^{71,73}. p63 and p73 need their second helix in their tetramerization domain which is lost during the evolution of the p53 protein; this region can be traced in many fish p53 sequences such as in zebrafish. In human, p53 C-terminal indiscriminating binding site and also the flexible linker in between tetramerization and C-terminal regulatory domains compensate lack of this second helix^{74,75}. Shortening of tetramerization domain is most probably directly related to the p53 protein's novel functions in genome stability, while C-terminal domain maintains its length and features during vertebrate evolution of the protein to a great extent⁷⁵. As a consequence, tetramerization and DNA binding domain have changed in p53 to obtain additional adaptive functions, while keeping their key role in cell integrity maintenance. MDM2 family protein is highly conserved in primitive metazoans, but MDM2 gene is lost in some organism, for example in *C. elegans* and *Drosophila*, which are rapidly evolving organisms^{75,76}. Homologs of p53- and MDM2-family in primitive protozoans (*T. adhaerens*) interact through the N-terminal domain of MDM2-like protein and TAD of putative p53 family

protein^{77,78}. p53-MDM2 regulation has grown more complicated during divergence of MDM2 and MDMX from an ancestral MDM2-like gene⁷⁹.

MDM2 consists of four evolutionary conserved regions: N-terminal domain, acidic region, zinc-finger, and RING domain, among which RING domain is the most conserved. This domain is responsible for homo- and hetero-dimerization of MDM2 family members and also mediates E3 ubiquitin ligase activity of MDM2, established nearly 500 million years ago in vertebrates⁸⁰. As mentioned before, MDMX doesn't have intrinsic E3 ubiquitin ligase activity⁸. Other than MDM2 family as the master regulator of p53, there are other E3 ubiquitin ligase proteins, such as TRIM24, TOPORS, and CARPs that evolved independently and are probably more important in N-terminally truncated p53 isomers^{81,82}. There still remains much to be discovered about these non-MDM2, E3 ubiquitin ligases; if they are expressed in a tissue specific manner in an indicated developmental stage or if signal transduction pathways control them. Answering these questions could lead to new therapeutic strategies for cancer treatment in the future.

1.1.4. p53 Mutations and Cancer and Therapeutic Approaches

Mutations that affect transcriptional activity of the p53 protein: Up to now, many mutations in different domains of the *Tp53* gene have been reported. Tp53 is polymorphic in coding and non-coding regions. Mutant p53 protein are able to change the microenvironment of the solid tumor in several ways such as modulation of extracellular matrix components, changing the secretion pattern of interleukins, cytokines, enzymes, and generally the secretome of the tumor cells, and last but not least, affecting the crosstalk between stromal and tumor cells⁸³. For instance, mutant p53 binds to the promoter of the secretory interleukin-1 receptor antagonist (sIL-1Ra) gene, suppressing its production and generating a chronic pro-inflammatory microenvironment, whereas wild type p53 is unable to interact with this interleukin gene under normal conditions⁸⁴. Also, prostate-specific antigen (PSA) mRNA levels is directly correlated with mutant p53 mRNA, associated with more aggressive cancer

while wild type p53 strongly suppresses PSA gene transcription⁸⁵. Mutant p53 can also trigger neo-vascularization by increasing the activity of transcription factors (e.g. E2F1) of pro-angiogenic cytokine stabilizers (IL8 and GRO- α)⁸⁶. Importantly, the Warburg effect is stimulated by mutant p53⁸⁷; cancer cells with mutant p53 induce glycolysis by targeting genes that are responsible for energy metabolism (such as *Parkin*) and promote glucose transporter 1 (GLUT1) translocation to the plasma membrane, increased glucose uptake and lactate production^{88,89}. Most of these pro-cancer mutations reside in the DNA binding domain of the p53 protein, inhibiting its binding to target gene control elements upon stress. Some of these somatic mutations are R175H, Y220C, G245S, R248Q/W, R249S, R273C/H, and R282W. The most frequent germ-line mutation in tetramerization domain is R337H^{1,90}. Yet another class of pro-cancer p53 mutations do not alter the transcription activity of the p53 protein, but lead to defects in mRNA stabilization and control by micro RNAs^{91,92}. Surprisingly, very few p63 or p73 mutations are reported in relation with cancer cases.

Even a single amino acid change in the *Tp53* gene can cause developmental or metabolic changes. As an example, the P72R mutation causes metabolism defects. R allele variants are found mostly in cold climates and are related to obesity and metabolic dysfunction⁹³. High cancer prevalence in African and African-American individuals with the P47S polymorphism was recently identified. This study identified that even heterozygote carriers of the S47 mutation develop carcinoma (HCC). A possible explanation for this phenotype is that HCC patients might have lost their wild type p53 allele at some point during disease development⁹⁴. The interesting fact about *Tp53* gene mutations is that the effect of the mutation on the p53 protein function is allele dependent, meaning that depending on which allele is mutant, a dominant-negative phenotype or a gain of function is possible; invasion or metastasis phenotypes in the tumors are an example of this phenomenon⁹⁵.

Mutations that affect the stability of the p53 protein: Some p53 mutations affect the structural stability of the protein by disturbing its kinetics, while other mutations inhibit DNA-p53 interactions^{96,97}. Mutation in any one of R248, R273, or R280 perturbs transcription activity of p53⁹⁸. The DNA binding domain of the p53 protein has a rather low melting point at 44-45°C (temperature-sensitivity phenotype). This intrinsic property results in the destabilization and unfolding of mutant p53 proteins (e.g. V143A, Y220C, and F270L) at body temperature^{98,99,100}. Small-molecule

stabilizers could be introduced to regain the functionality of these mutant proteins. There are other structural mutations that change wild type folding of the p53 protein, regardless of the melting point such as R249S that effect p53 hairpin conformation, caused by aflatoxin B1¹⁰¹. Zinc binding is extremely important for p53- DNA minor groove interactions, therefore if any mutation occurs in this region of DBD (C176F, H179R, C238Y, and C242S) it would be deleterious to DNA binding⁹⁷. R175 is also a hotspot for DBD mutations; it resides close to Zinc binding region; if a histidine substitutes for arginine, not only is the melting point of the mutant p53 drastically decreased, but also its affinity for zinc-binding is reduced⁹⁸. Nevertheless, if an amino acid with a smaller side chain (e.g. alanine) replaces arginine, the mutation would be less damaging⁹⁷. Aside from the changes mentioned above, some mutations in DBD lead to aggregation of p53 as an amorphous and fibrillar nucleation due to unfolding and again irreversible aggregation of DBD in dominant negative unstable mutants^{97,102}. For instance, unfolding of the p53 protein leads to Ile254 exposure that causes aggregation of p63 and p73 and formation of co-aggregates in mutant cells¹⁰³. Tetramerization domain mutations are not as frequent as DBD mutations. R337H is the most common mutation in this domain that disturbs the salt bridge between R337 and Asp352 leading to the destabilization of p53 tetramers in a pH dependent manner¹⁰⁴. R175H and R273H *Tp53* missense mutations are also responsible for aggressive and metastatic cancer in which mutant p53 accumulates in cancer cells^{105,106}.

Mutations that affect the stability of the p53 mRNA and protein: Eight percent of somatic p53 mutations lead to premature stop codons that result in the rapid degradation of the mRNA encoded by the *TP53* gene in a process called nonsense mediated mRNA decay (NMD)¹⁰⁷. Nonsense mutations, such as R196X or R213X cause more than 500,000 new cancer cases every year^{1,90}. Aminoglycins and antibiotics (e.g. gentamicin), despite their toxicity, are used as therapeutic strategies to suppress NMD by binding to the ribosomal decoding center^{107,108}.

Mutations in p53 protein regulators: In many cancer cases the p53 protein is wild type but MDM2 and MDMX are over-expressed which leads to excess p53 degradation⁷. Small molecules such as RITA that binds to the N-terminal domain of p53, or Nutlin that binds to the N-terminal domain of MDM2 abolish the p53-MDM2

interaction, are used as cancer drugs for such cases^{109,110}. The p53 binding pocket of MDM2 and MDMX are structurally different. Activating p53 at its utmost level in therapeutic approaches requires dissociation from both MDM2 and MDMX⁷. MDMX has an auto-inhibitory motif in which the amino acids W200 and W201 fold back and mimic the MDMX-p53 TAD. This motif reduces the inhibitory effect of MDMX up to 100 fold compared to MDM2. Under normal conditions, casein kinase I α binds to these amino acids to prevent auto-inhibition^{111,112}; blocking this interaction triggers auto-inhibition of MDMX and therefore could be an effective application in therapy. Stabilization of MDM2 also causes p53 degradation. Some MDM2 stabilizers such as wild-type p53-induced phosphatase-1 (Wip1) are over-expressed in tumor cells. This molecule is also a target for small-molecule inhibitors for cancer therapy^{113,114}.

Mutation in the p53 protein that affects metabolism: Glycolysis is an important pathway that plays a role in carcinogenesis. p53 is an inhibitor of the gene encoding *Tp53*-induced glycolysis and apoptosis regulator (TIGAR)⁸⁸. Colon cancer cells with mutant p53 were shown to benefit from the over expression of TIGAR which increased the antioxidant response, supporting cancer progression¹¹⁵. In the absence of wild type p53, the insulin-receptor gene is also overexpressed. Increased insulin signaling interferes with the glycolysis pathway and promotes tumor growth¹¹⁶. The role of p53 in metabolism is very important but this connection has been underestimated in many cancer studies¹¹⁷. Mostly, cell cycle arrest and apoptosis has been the main focus for cancer cells with mutant p53. A recent study with a with p53^{3KR/3KR}, a mouse model where three Lysine residues in the p53 C-terminal were mutated, showed that senescence, apoptosis, and cell cycle arrest were defective as expected. Unexpectedly the same study found that glycolysis was inhibited while the generation of reactive oxygen species (ROS) was maintained. This mutant p53 was responsible for sending cells to ferroptotic cell death in response to stress¹¹⁸. Although mutant p53 can have a dominant negative effect on wild type p53 in p53 heterozygous mutants, at some point mutant p53 can retain their metabolic activities due to the dissociation between metabolic and cell cycle arrest activities of the p53 protein, such as what happens in Li-Fraumeni syndrome^{119,120}.

The p53 protein's metabolic responsibilities are partly mitochondria related. p53 is known to translocate to the mitochondria and regulate the expression of mitochondrial genes. p53 is also important for mitochondrial genome (mtDNA)

homeostasis^{121,122}. The metastatic potential of cancer cells with mutated *TP53* was recently found to be correlated with to their increased mitochondrial respiration and antioxidant capacity¹²³.

Mutations in the C-terminal domain of the p53 protein: The C-terminal domain (CTD) of p53 where many post-translational modifications occur, is also target of many cancerous mutations. For example, K382 deacetylation is induced by NAD⁺-dependent sirtuin deacetylases (SIRT1) and SIRT2; this deacetylation has an inhibitory effect on p53. SIRT1/SIRT2 overexpression is the main reason for chronic myelogenous leukemia and inhibition of these proteins is an effective anticancer therapy¹²⁴. Lysine residues in the CTD take part in DNA binding and transcriptional activation by p53. These residues act as an anchor for the DNA phosphate backbone while p53 binds to its target genes^{125,126}. Another study found that the CTD was necessary for tetramer formation using an induced-fit mechanism¹²⁷. The CTD results in the stabilization of the DNA-p53 complex by changing the conformation of the DBD. Laptchenko *et al.* compared the DNA binding capability of three CTD mutants by ChIP-Seq¹²⁸. While p53 with wild type CTD binds to 335 target genes, the p53^{6KR} mutant binds to 278 targets; even less binding is reported for the mutant p53^{6KQ} and the $\Delta 30$ mutant (175 sites)¹²⁸. Therefore, the CTD is a positive regulator of DNA binding by the p53 protein¹²⁹. These recent findings contradict earlier experiments that identified the p53 CTD as an inhibitor of DNA binding¹³⁰. CTD mutations may change the stability of p53-DNA complex in a target dependent manner. If we divide p53-binding sites into three subgroups, they could be: a) high affinity distal binding sites (such as the site in the p21 gene), b) medium affinity distal binding sites (such as the site in the PUMA gene), and c) closely-spaced low affinity binding sites (such as those in the MDM2 gene). Truncated p53 CTD mutation (p53 ^{$\Delta 30$}) and p53^{6KQ} completely lose their affinity to the third group, unlike wild type p53 and p53^{6KR}^{128,131}. It is known that the DBD of p53 changes the conformation of its loop L1 from inward to outward to sit in the major groove of its DNA target. When a p53 tetramer interacts with a target sequence, three parts of the p53 protein is involved in the binding; Zn-coordinated H1 helix with its H178 interact with the N-terminus; H179 in the helix communicate with p53 regulatory CTD (last 30 amino acids); β -sandwich and the DBD cooperation¹³². These three mentioned interactions are all crucial for transcriptional activity of the p53 protein. The

link between the CTD and the DBD could potentially result in the functional regulation of p53 DNA binding by the CTD¹³³.

The p53 C-terminal domain also has an important effect on its nuclear translocation¹²⁸. A nuclear localization signal was found both in the N-terminal and C-terminal regions of the p53 protein^{134,135}. As mentioned before, MDM2 ubiquitination leads to the destabilization of p53 protein, but this post-translational modification by MDM2 is also important for the nuclear localization of the p53 protein to the extent that in the absence of the six lysine residues in CTD, nuclear export of p53 is perturbed^{136,137}. Our study, which created new mutant cell lines that express various CTD mutants of p53 addresses the importance of this domain in p53 functions outlined here.

1.2. Genome Editing Tools

1.2.1. A Brief History of Genome Engineering

“Genome engineering can be defined as directed modification of the gene complement of a living organism”, as John F. Morrow described in his article in 1976. Treatment of inherited diseases and genetic transformation of plants are the most crucial beneficial uses of genetic engineering¹³⁸. The aim of genome engineering is to target a specific region to introduce a desired mutation without off-targeting any other sequence in the genome. After years of unsuccessful attempts at genome engineering, recently genome editing proteins such as Zinc Finger Nuclease (ZFN), Transcription Activator-Like Effector Nuclease (TALEN), and Clustered Regularly Interspaced Short Palindromic Repeats (CRISPR) were discovered.

Introducing viral DNA in mammalian cells (infection) in 1968 by J. Sambrook et al., was the preliminary efforts in gene delivery¹³⁹. However, infection was efficient but not site-specific. Genetic manipulation of genomes with rare-cutting homing endonucleases, with recognition sites much longer than bacterial restriction enzymes, were used to introduce a limited number of double strand breaks (DSB) in the genome¹⁴⁰. However, this method was not applicable for many regions on the genome. An ideal genome engineering system needs to target a specific genomic region. In 2004 Akiko Nomura and Yukio Sugiura succeeded in creating mutant Zinc finger proteins, which could function as a novel artificial nuclease that targeted desired genomic sequences. They showed selective hydrolysis of DNA duplexes by three tandem zinc finger mutants¹⁴¹. ZFN was a great step forward in site-specific genome engineering, but target selectivity was limiting and their construction was expensive and technically challenging¹⁴².

1.2.2. TALEN Proteins

In 2011, transcription activator-like (TAL) effectors, started a new trend in user-friendly genome engineering tools. TAL effectors were discovered in the genus *Xanthomonas*, a plant pathogenic bacteria that uses these proteins to regulate DNA expression in host plant cells by binding the promoters of target genes. TALE proteins were found to have 12-27 tandem repeats of 33-35 amino acids, each repeat specifically binding one base of the targeted DNA sequence¹⁴³. The base preference of the repeats is specified by the 12th and 13th adjacent amino acid residues in each repeat, which are called 'repeat-variable di-residue' (RVD). A code specifies the target specificity of these RVDs whereby a repeat containing NI at the RVD position binds Adenine, NG binds Thymine, HD binds Cytosine, and NN/NK binds Guanine¹⁴⁴. The simplicity of this system enabled molecular biologists to manipulate the repeats to recognize any desired sequence in the genome.

DNA editing at the genomic scale is possible with TALE nuclease (TALEN) proteins, which are designed to have a FokI restriction enzyme domain fused to the TALE DNA binding domain. TALEN proteins are designed as heterodimers that bind to DNA and

generate double-strand breaks (DSBs) in the spacer region between the two recognition sequences¹⁴³.

1.2.3. CRISPR Technology

Clustered regularly interspaced short palindromic repeats (CRISPR)/CRISPR-associated (Cas) systems are the adaptive immune defenses that are found in bacteria and archaea. In this system, short RNA is used to direct degradation of foreign nucleic acids (DNA/RNA). There are three types of CRISPR systems. Single effector enzyme (i.e. cas9) is used to cleave double-strand (ds) DNA in the Type II CRISPR systems. In contrast, multiple effectors are used in the type I and type III¹⁴⁵. A The CRISPR system consists of a cluster of CRISPR-associated genes, noncoding RNAs, and a distinctive array of repetitive elements (direct repeats). There are short variable sequences that are derived from exogenous DNA targets, known as protospacers, between these repeats. A protospacer is always associated with a protospacer adjacent motif (PAM: 5'-NGG) within the DNA target. DSBs are created by the Cas9 nuclease 3 bp upstream of the PAM (Figure. 4.5). Type II CRISPR systems consist of: 1) the Cas9 nuclease; 2) the CRISPR RNA (crRNA) array, which encodes guide RNAs (gRNA); and 3) the auxiliary trans-activating crRNA (tracrRNA) that assists the processing of the crRNA array into discrete units. Artificially fusing crRNA and tracrRNA together creates chimeric, single-guide RNA (sgRNA) (which we use in this thesis). The RNA-guided Cas9 nuclease increases the efficiency of genome engineering in eukaryotic cells by specifying a 20-nt targeting sequence within its guide RNA¹⁴⁶. Assembly of CRISPR/Cas9 enzymes is straightforward. Annealed single stranded oligonucleotides encoding the target gRNA with BbsI recognition sequences are cloned into the pSpCas9(BB) plasmid. The pSpCas9(BB) plasmid includes selection markers such as a puromycin resistance gene or a GFP gene to select transfected cells. The CRISPR-Cas9/Cas9n system creates double strand breaks (DSBs) that are repaired by eukaryotic cells, either by non-homologous end joining (NHEJ) or by homology directed repair (HDR) in the presence of a homologous DNA sequences. NHEJ causes small insertions, deletions, or base substitutions (INDEL)¹⁴⁶ (Figure. 4.6). The NHEJ pathway is error-prone. The endogenous DNA repair machinery processes the ends of DSBs. During this

process, random INDEL mutations can occur at the site of junction so frame-shifts and premature stop codons arise if the target sequence is in a coding region of the genome. The HDR pathway requires a repair template in the form of either a plasmid with a sequence homologous to the target site or single-stranded DNA oligonucleotides (ss-oligo)^{146,147}.

2. AIM OF THE STUDY

p53 protein levels are tightly regulated in normal cells. Cellular stresses, such as DNA double-strand breaks results in the stabilization and accumulation of p53 protein in the nucleus. The p53 protein is a transcription factor that directly controls numerous genes that are related to cellular functions such as cell cycle arrest and apoptosis. The p53 C-terminal regulatory domain is the target of several post-translational modifications (PTM); this helps cells to strictly regulate the p53 protein activity in basal conditions or under stress.

The last exon of the C-terminus, which is investigated in detail in this study, is a subject of many PTMs. We studied how endogenous p53 behaves when it lacks several amino acids in its C-terminus. The C-terminal mutant (CTM) cells were obtained using genome engineering tools (TALEN proteins and the CRISPR/Cas9 system). We found out that even a single amino acid deletion, which is R379 in this study, could cause a major difference in the transcription of many genes, and even in the doubling time of the CTM cell lines. There are nuclear import/export sites on the p53 protein, but none has been reported in the C-terminus encoded by the last exon. Unexpectedly, we found that a truncated p53 protein ($\Delta 26/ \Delta 26$) that lacks the last exon of the *Tp53* gene, cannot translocate into the nucleus after genotoxic stress. We assessed p53 protein expression (by western blot) in CTM cell lines. We also examined the subcellular localization of mutant p53 proteins using confocal microscopy. Both types of experiments indicated that the CTM cell line ($\Delta 26/ \Delta 26$) had a p53 nuclear accumulation defect under stress. We checked if the p53 protein could bind to its target DNA efficiently, using pull-down

experiments. We identified differentially transcribed genes in p53 CTM cell lines by Quantitative RT PCR. We also analyzed changes in cell growth rate by xCELLigence real time cellular analysis equipment. To have a broader view of what happens in cells with mutated p53, we also conducted RNA sequencing (RNASeq) to compare the transcriptome of our CTM cell lines with wild type cells. We demonstrated that p53 C-terminus is crucial for the accumulation of p53 and some of its target proteins under stress conditions; we confirmed that p53 CTM cell doubling time increases in some of the mutants, perhaps pointing to the relationship between CTD and telomere length¹⁴⁸. The p53 C-terminus controls DNA binding activity of the p53 protein, which we confirmed here. Our RNASeq experiments indicate that p53 may be playing a role in ribosomal biogenesis by coordinately controlling ribosomal protein gene expression.

3. MATERIALS AND METHODS

3.1. Materials

3.1.1. Chemicals

All the chemicals used in this thesis are listed in Appendix A.

3.1.2. Equipment

All the equipment used in this thesis is listed in Appendix B.

3.1.3. Buffers and Solutions

Standard buffers and solutions used in the project were prepared according to the protocols in Sambrook et al., 2001.

Agarose Gel: For 100 ml 1% w/v gel, 1 g of agarose powder was dissolved in 100 ml 0.5X TBE buffer by heating. 0.01% (v/v) ethidium bromide was added to the solution.

Calcium Chloride (CaCl₂) Solution: 60mM CaCl₂ (diluted from 1M stock), 15% Glycerol, and 10mM PIPES (pH 7.00) were mixed and the solution was filter-sterilized and stored at +4°C.

Blocking Buffer: For 10ml, 0.5 g skim milk powder was dissolved in 10 ml PBS.

FACS Buffer: For 500ml 1X solution, 2.5 g bovine serum albumin (BSA) and 0.5 g sodium azide were mixed in 500 ml 1X PBS and the solution was kept at +4°C.

HEPES-buffered saline (HBS): For 100 ml 2X solution 0.8 g NaCl, 0.027 g Na₂HPO₄·2H₂O and 1.2 g HEPES were dissolved in 90 ml of ddH₂O. pH was adjusted to 7.05 with 0.5 M NaOH and the solution was completed to 100 ml with distilled water. The buffer was filter-sterilized and stored at -20°C.

PBS-Tween20 (PBST) Solution: For 1 L 1X solution, 0.5 mL Tween20 was added in 1 L 1X PBS.

Phosphate-buffered saline (PBS): For 200 ml 1X solution, 1 tablet of PBS (Sigma P4417) was dissolved in 200 ml ddH₂O and the solution was filter-sterilized.

Polyethylenimine (PEI) Solution: For 1 mg/ml solution, 100 mg polyethylenimine powder was dissolved in 100 ml ddH₂O and the pH was adjusted to 7.0 with HCl. The solution was filter sterilized and kept at -20°C.

Protein Loading Buffer: Commercial buffer (Fermentas #R0891) that includes 5X loading dye (0.313 M Tris HCl (pH 6.8 at 25°C), 10% SDS, 0.05% bromophenol blue, 50% glycerol) and 20X reducing agent (2 M DTT) were mixed.

SDS Separation Gel: For 10ml 13% gel, 2.5 ml Tris (1.5M pH 8.8), 3 ml H₂O, 4.34 ml Acryl: Bisacryl (30%), 100 µl 10% SDS, 100 µl 10% APS, and 10 µl TEMED were mixed.

SDS Running Buffer: For 1 L 10X stock solution, 30.3 g Tris base, 144 g Glycine, and 10 g SDS were dissolved in 1L ddH₂O.

SDS Stacking Gel: For 5 ml 4% gel, 1.25 ml Tris (0.5 M pH 6.8), 2.70 ml H₂O, 1 ml Acryl-Bisacryl (30%), 50 µl 10% SDS, 15 µl 10% APS, and 7.5 µl TEMED were mixed.

Transfer Buffer: For 1 L 10X stock solution, 14.5 g Tris and 72 g Glycine was dissolved in 1 L ddH₂O. Final pH was adjusted to 8.3.

Transfer Buffer: For 800 ml 1X, 80 ml 10X Transfer Buffer, 160 ml methanol, and 560 ml ddH₂O were mixed.

Tris-Borate-EDTA (TBE) Buffer: For 1 L 10X stock solution, 104 g Tris-base, 55 g boric acid, and 40 ml 0.5M EDTA (pH 8.0) were dissolved in 1 L of ddH₂O. The solution is kept at room temperature.

Blocking solution: 5% skimmed milk in 1X PBS

Antibody dilution solution: 0.5% 100 Triton X – 100 with 1% BSA in 1X PBS

Propidium Iodide (PI) staining solutions: Propidium iodide (1mg/ml), 60µl

Triton X-100 and 100µl RNase (stock: 10mg/ml) and the volume were adjusted to 10 ml with cold FACS incubation buffer.

3.1.4. Growth Media

Luria Broth (LB): For 1 L 1X LB media, 20 g LB powder was dissolved in 1 L ddH₂O and then autoclaved at 121°C for 15 minutes. For selection, kanamycin at a final concentration of 50 µg/ml or ampicillin at a final concentration of 100 µg/ml was added to liquid medium just before use.

LB-Agar: For 1 L 1X agar medium, 20 g LB powder and 15 g bacterial agar powder were dissolved in 1 L ddH₂O and then autoclaved at 121°C for 15 minutes. Autoclaved medium was poured onto sterile Petri dishes after cooling down to 50°C. For selection, kanamycin at a final concentration of 50 µg/ml or ampicillin at a final concentration of 100 µg/ml was added to the medium before pouring onto petri dishes. Sterile solid agar plates were kept at 4°C for maximum 3 month.

DMEM: HEK293T, HCT116 (HCT116WT), and HCT116p53^{-/-} (HCT116KO) cell lines were maintained in filter-sterilized DMEM that is supplemented with 10% heat-inactivated fetal bovine serum, 2mM L-Glutamine, 100 U/ml penicillin and 100 U/ml streptomycin.

Freezing medium: All the cell lines were frozen in heat-inactivated fetal bovine serum containing 10% DMSO (v/v).

3.1.5. Commercial Molecular Biology Kits

- QIAGEN Plasmid Midi Kit, 12145, QIAGEN
- QIAGEN Plasmid Maxi Kit, 12163, QIAGEN
- Qiaprep Spin Miniprep Kit, QIAGEN
- Qiaquick Gel Extraction Kit, 28706, QIAGEN
- Qiaquick PCR Purification Kit, 28106, QIAGEN
- RevertAid First Strand cDNA Synthesis Kit, K1622, FERMENTAS
- SuperScript Double-Stranded cDNA Synthesis Kit, 11917-020, INVITROGEN
- Golden Gate TALEN and TALE Effector kit 2.0, Addgene #1000000024
- TOPO® TA Cloning Kits, Thermo Fisher Scientific
- LightCycler® 480 SYBR Green I Master, Roche

3.1.6. Enzymes

All the restriction enzymes, DNA modifying enzymes and polymerases and their corresponding buffers used in this study were from either Fermentas or NEB.

3.1.7. Bacterial Strains

Escherichia coli DH-5α (F- endA1 glnV44 thi-1 relA1 gyrA96 deoR nupG lacZdeltaM15 hsdR17) competent cells were used for bacterial transformation of general plasmid DNAs.

3.1.8. Mammalian Cell Lines

HEK293T: Derivative of human embryonic kidney 293 (HEK293) cell line that stably express the large T antigen of SV40 virus (ATCC: CRL-1573™).

HCT116 and HCT116p53-/-: Human colorectal carcinoma cell line and its p53-null derivative (ATCC CCL-247™)

3.1.9. Plasmids and Primers

The plasmids and the primers used in this thesis are listed in Table 3.1 and Table 3.2, respectively.

PLASMID NAME	PURPOSE OF USE	SOURCE
PCDNA	Transfection efficiency Control	Lab Construct
pHD1	TALEN Cloning	Golden Gate TALEN Kit #1000000024
pHD2	TALEN Cloning	Golden Gate TALEN Kit #1000000024
pNI3	TALEN Cloning	Golden Gate TALEN Kit #1000000024
pNI4	TALEN Cloning	Golden Gate TALEN Kit #1000000024
pNI5	TALEN Cloning	Golden Gate TALEN Kit #1000000024
pNI6	TALEN Cloning	Golden Gate TALEN Kit #1000000024
pNI7	TALEN Cloning	Golden Gate TALEN Kit #1000000024

pNN8	TALEN Cloning	Golden Gate TALEN Kit #1000000024
pNN9	TALEN Cloning	Golden Gate TALEN Kit #1000000024
pNN10	TALEN Cloning	Golden Gate TALEN Kit #1000000024
pNG1	TALEN Cloning	Golden Gate TALEN Kit #1000000024
pNN4	TALEN Cloning	Golden Gate TALEN Kit #1000000024
pHD5	TALEN Cloning	Golden Gate TALEN Kit #1000000024
pHD6	TALEN Cloning	Golden Gate TALEN Kit #1000000024
pLR-NG	TALEN Cloning	Golden Gate TALEN Kit #1000000024
pNN1	TALEN Cloning	Golden Gate TALEN Kit #1000000024
pNG2	TALEN Cloning	Golden Gate TALEN Kit #1000000024
pHD3	TALEN Cloning	Golden Gate TALEN Kit #1000000024
pNG4	TALEN Cloning	Golden Gate TALEN Kit #1000000024
pNG5	TALEN Cloning	Golden Gate TALEN Kit #1000000024
pNN6	TALEN Cloning	Golden Gate TALEN Kit #1000000024

pNI7	TALEN Cloning	Golden Gate TALEN Kit #1000000024
pNI8	TALEN Cloning	Golden Gate TALEN Kit #1000000024
pHD9	TALEN Cloning	Golden Gate TALEN Kit #1000000024
pNI10	TALEN Cloning	Golden Gate TALEN Kit #1000000024
pNG1	TALEN Cloning	Golden Gate TALEN Kit #1000000024
pNN2	TALEN Cloning	Golden Gate TALEN Kit #1000000024
pNN4	TALEN Cloning	Golden Gate TALEN Kit #1000000024
pNG5	TALEN Cloning	Golden Gate TALEN Kit #1000000024
pLR-NN	TALEN Cloning	Golden Gate TALEN Kit #1000000024
pFUS_A	TALEN Cloning	Golden Gate TALEN Kit #1000000024
pFUS_B6	TALEN Cloning	Golden Gate TALEN Kit #1000000024
pFUS_B7	TALEN Cloning	Golden Gate TALEN Kit #1000000024
pC-GoldyTALEN	TALEN Cloning	Golden Gate TALEN Kit #1000000024
pSpCas9(BB)-Puro	CRISPR Cloning	Zhang Lab
pSpCas9n(BB)-Puro	CRISPR Cloning	Zhang Lab

PTZ57 R/T	Sequencing	InsTAclone PCR cloning kit
-----------	------------	----------------------------

Table 3.1: The list of the plasmids used in this thesis. Plasmid names, their purpose of uses and sources are given.

PRIMER NAME	SEQUENCE	PURPOSE OF USE
h_p21rt_FW D	GCAGACCAGCATGACAGATTT	p21 qPCR
h_p21rt_rev	GGATTAGGGCTTCCTCTTGGA	p21 qPCR
puma fwd	ACCAGCCCAGCAGCACTTAG	PUMA qPCR
puma rev	TCTTCTTGTCTCCGCCGCTC	PUMA qPCR
gapdh fwd	TCCTGCACCACCAACTG	GAPDH qPCR
gapdh rev	TCTGGGTGGCAGTGATG	GAPDH qPCR
p53_GADD 45_fwd	(Biotin)GAACATGTCTAAGCATGCTG	Pull down
p53_GADD 45_rev	(Biotin)CAGCATTCTTAGACATGTTC	Pull down
GAPDH-FWD-long	GTCAAGGCTGAGAACGGGAAG	RNA-sequencing quality control
GAPDH-REV-long	GTCAAAGGTGGAGGAGTGGGT	RNA-sequencing quality control
beta_actin-FWD-long	GTTGGGGGACAAAAAAGGGGGA	RNA-sequencing quality control
beta_actin-REV-long	TCTTCATTGTGCTGGGTGCC	RNA-sequencing quality control

p53K381A_ Fwd primer	ACCTCCCGCCATAAAGCACTCATGTTCAAGAC	PCR
p53K381A_ Rev primer	AGACTGACCCTTTTGGACTTCAGGTGG	PCR
TP53-for	CCCCAGCCCCCTAGCAGAGA	PCR
TP53-rev	CAGGAAGCCAAAGGGTGAAGAGG	PCR
TP53- long primer-fwd	ATCCTCCTCCCCACAACAAAACACC	PCR
TP53- long primer-rev	TCTCTCCTCCCTGCTTCTGTCTCCT	PCR
ss oligo-HR TP53	AAAGGGTCAGTCTACCTCCCGCCATAAAAAG CTTATGTTCAAGACAGAAGGGCCTGACT	HDR
hp53 fwd	CCCAAGCAATGGATGATTGA	qPCR
hp53 rev	GGCATTCTGGGAGCTTCATCT	qPCR
Cas9 p53- fwd	CACCGCATGAGTTTTTTATGGCGGG	CRISPR/Cas9 design
Cas9 p53K382rev	AAACCCCGCCATAAAAACTCATGC	CRISPR/Cas9 design
Left Cas9n p53-fwd	CACCGGGAGGTAGACTGACCCTTTT	CRISPR/Cas9 n design
Left Cas9n p53- rev	AAACAAAAGGGTCAGTCTACCTCCC	CRISPR/Cas9 n design
Right Cas9n- fwd	CACCGAACTCATGTTCAAGACAGA	CRISPR/Cas9 n design
Right Cas9n p53K382rev	AAACTCTGTCTTGAACATGAGTTTC	CRISPR/Cas9 n design
pJET1.2 Forward	CGACTCACTATAGGGAGAGCGGC	Pre- Sequencing control
pJET1.2 Reverse	AAGAACATCGATTTTCCATGGCAG	Pre- Sequencing

		control
Dkc1-FWD	CTCGGAAGTGGGGTTTAGGT	qPCR
Dkc1 REV	ACCACTTCAGCAACCACCTC	qPCR
hTERT FWD	TGTACTTTGTCAAGGTGGATGTGA	qPCR
hTERT REV	TTGATGATGCTGGCGATGA	qPCR
Rtel1 FWD	GCCAGGGAGCTACATCTTTG	qPCR
Rtel1 REV	CCCTTGGTCTGAAACGTGAT	qPCR
Terf1 FWD	GCAACAGCGCAGAGGCTATTATT	qPCR
Terf1 REV	AGGGCTGATTCCAAGGGTGTA	qPCR

Table 3.2: The list of the primers used in this thesis. Primer names, their sequences, and their purpose of uses are given.

3.1.10. DNA and Protein Molecular Weight Markers

DNA ladders and protein molecular weight markers used in this thesis are listed in Appendix C.

3.1.11. DNA Sequencing

McLab (CA-USA) commercially provided sequencing service.
(<http://www.mclab.com/>)

3.1.12. Software, Computer-Based Programs, and Websites

The software and computer based programs used in this project are listed in Table 3.3

SOFTWARE, PROGRAM, WEBSITE NAME	COMPANY/WEBSITE ADDRESS	PURPOSE OF USE
NCBI BLAST	Http://blast.ncbi.nlm.nih.gov/Blast.cgi	Basic local alignment search tool
FlowJo V10	Tree Star Inc.	Viewing and analyzing flow cytometry data
ImageJ	http://imagej.nih.gov/ij/	Visualizing and calculating p53 amount in WT cells versus CTM cell lines/ Comparing western blot band intensities
CLC Main Workbench	CLC bio	Genomics and Transcriptome analysis
Ensembl Genome Browser	http://www.ensembl.org/index.html	Human and mouse genome
LightCycler 480 SW 1.5	ROCHE	Analyzing qPCR results
RTCA Software 2.0	ACEA Biosciences	Real-time cell growth analysis
CRISPR design	http://crispr.mit.edu/	CRISPR designer
Visual Molecular Dynamics	http://www.ks.uiuc.edu/Research/vmd/	Display and analyzing TALEN proteins

NAMD-Scalable Molecular Dynamics	http://www.ks.uiuc.edu/Research/namd/	Stimulation of TALEN proteins
--	---	----------------------------------

Table 3.3: The list of the software, programs and websites used in this thesis. Name of the software, programs, and websites, their producers/websites and purpose of uses are given.

3.2. Methods

3.2.1. Bacterial Cell Culture

Bacterial Culture Growth: *Escherichia coli* (*E. coli*) DH5 α strain was grown in Luria Broth (LB) or 2XLB (low salt), overnight at 37°C, shaking at 250 rpm. For long-term storage of bacterial cells, glycerol was added to the overnight grown culture to a final concentration of 10% in 1 mL in a cryo-vial. Bacterial glycerol stocks were stored at -80°C. In order to obtain single colonies, bacteria were spread on LB/agar containing petri dishes using glass beads and incubated overnight at 37°C without any shaking. All growth media were supplemented with or without selective antibiotic prior to any application.

Preparation and Transformation of Competent Bacteria: A single colony of *E.coli* DH5 α was picked from an LB/agar petri dish (incubated overnight without any antibiotic selection). The colony was inoculated in 50 mL LB without any selective antibiotics in a 200 mL flask and incubated at 37°C overnight, shaking at 250 rpm. The next day, 4 mL from this overnight culture was diluted in 400 mL LB medium in a 2 L flask and incubated at 37°C overnight, shaking at 250 rpm until the optical density (at 590 nm) reached 0.375. The culture was then transferred into 50 ml polypropylene tubes (8 tubes in total) and incubated on ice for 10 min, followed by a centrifugation at 1600 g for 10 min at 4°C. After centrifugation, each pellet was resuspended in 10 mL ice-cold CaCl₂ solution and centrifuged at 1100 g for 5 min at 4°C. The pellets were again resuspended in 10mL ice-cold CaCl₂ solution and incubated on ice for 30 min.

Following the final centrifugation at 1100 g for 10 min at 4°C, this time the pellets were resuspended in 2mL ice-cold CaCl₂ solution and pooled in a single polypropylene tube (16 ml bacterial solution in total). This solution was dispensed into 200µL aliquots into pre-chilled 1.5ml centrifuge tubes. Competent cells were frozen immediately in liquid nitrogen and then stored at -80°C for later use. Transformation efficiency of the competent cells (typically 10⁷-10⁸ cfu/µg) was tested by pUC19 plasmid transformation, using different concentrations of the plasmid DNA.

Chemically competent cell was taken out from -80°C and mixed with 100 pg of plasmid DNA. The cells were then incubated on ice for 30 min. After the incubation period, the cells were heat shocked for 90 s at 42°C and transferred back on ice for 60 s. 800 µL of LB (without any antibiotics) was added on the cells and this culture was incubated for 45 min at 37°C. After 45 min, the cells were spread with glass beads on LB/agar petri dishes containing appropriate antibiotic for selection. The plate was incubated overnight at 37°C without any shaking.

Plasmid DNA Isolation: Plasmid DNA isolation was performed using either the alkaline lysis protocol from Molecular Cloning: A Laboratory Manual (Sambrook *et al*) or Qiagen Mini-Midiprep Kits according to the manufacturer protocols. The concentration and purity of the DNA isolated were determined by using a UV- or a NanoDrop- spectrophotometer.

3.2.2. Plasmid Construction

Polymerase Chain Reaction (PCR): Optimized PCR conditions are shown in Table 3.4 The thermal cycler conditions were as follows: initial denaturation at 95°C for 5 min followed by 30 (or 35) cycles of denaturation step (at 95°C, for 30 seconds), annealing step (at a temperature specific for every primer pair, for 30 seconds) and an extension step (at 72°C, for 1 min for every 1 kilo base of DNA). These cycles were then followed by a final extension step at 72°C for 10 min.

PCR Reaction	Volume	Final Concentration
Water- Nuclease free	Up to 25 μ l	-
10X PCR buffer - $MgCl_2$	2.5 μ l	1 X
50 μ M $MgCl_2$	0.75 μ l	1.5 mM
10 mM dNTP mix	0.5 μ l	0.2 mM each
10 μ M Forward primer	0.5 μ l	0.2 μ M
10 μ M Reverse primer	0.5 μ l	0.2 μ M
Template DNA	Variable	<500 ng
Platinum™ <i>Taq</i> DNA Polymerase	0.1 μ l	2 U/rxn

Table 3.4: Optimized PCR conditions

Restriction Enzyme Digestion: Restriction enzyme digestion reactions were performed by mixing the required amount of DNA with the desired enzymes and their compatible buffers in 1.5 mL centrifuge tube, followed by incubation in a water-bath set to a temperature optimum for the enzymes for a duration of 2 hours. For diagnostic digestions 1 μ g of DNA was used. 10 μ g or more DNA was digested for gel extraction and cloning purposes. If the plasmid DNA was digested with a single restriction enzyme and was planned to be used in a ligation reaction, then the linear plasmid was dephosphorylated by calf intestinal alkaline phosphatase (CIAP) enzyme for an additional 45 min at 37°C.

Agarose Gel Electrophoresis: PCR products, digestion reaction products and other DNA samples were separated and visualized by agarose gels. Gels were prepared by dissolving the required amount of agarose (ranging from 0.5 g to 3 g depending on the sizes of the DNA fragments in the samples) in 100mL 0.5X TBE. In order to fully dissolve the agarose, the mixture was heated in a microwave oven. The solution was then cooled down and 2 μ l of ethidium bromide was added. After mixing properly, the gel was cast in a gel apparatus and cooled down and solidified. DNA samples were mixed with DNA loading dye were loaded into the gel, which was run at 100V for 75 min in 0.5X TBE and the bands were visualized using UV light on a Biorad Imager.

Desired DNA bands were excised from the gel and extracted using a Qiagen Gel Extraction Kit according to the manufacturer protocol.

Ligation: Ligation reactions were performed by using T4 DNA Ligase, in 1:3, 1:5 or 1:10 vector versus insert ratio, using 50 ng of the plasmid DNA. Ligation reactions were incubated at 16°C for overnight. The next day, the ligation mixture was transformed into chemically competent DH5 α bacteria and plated onto antibiotic selective-LB/agar petri dishes and incubated at 37°C.

3.2.3. Mammalian Cell Culture

Maintenance of Cell Lines: HEK293T, HCT116, and HCT116p53^{-/-} cell lines were maintained in DMEM medium in tissue culture plates in an incubator set to 37°C with 5%CO₂. When the confluency of the cells reached over 80%, the cells were split into pre-warmed, fresh medium with a ratio of 1:10. In order to freeze cells for later use, cells at the exponential growth phase were resuspended in ice- cold freezing medium and transferred to cryovials. Tubes were stored at -80°C for at least 24 h and then transferred to liquid nitrogen tank for long- term storage. After thawing the cells, they were immediately washed with growth medium to remove any residual DMSO.

Transient Transfection of Cell Lines Using Polyethylenimine (PEI): One day before the transfection, 1-3 x 10⁶ cells were split onto 10 cm tissue culture plates. On the day of the transfection, 10 μ g of plasmid DNA was mixed in 1 mL serum-free DMEM in a sterile micro centrifuge tube. PEI (1 μ g/ μ l) was added to the DNA-DMEM mix at a 3:1 ratio of PEI (μ g) to total plasmid DNA (μ g) and mixed immediately by vortexing. After 15 minutes of incubation at room temperature, the mixture was added drop wise on the cells.

Cell Lysis, SDS Gel, Transfer and Western-Blot: Cells were harvested from their cell culture plates either using trypsin or a cell scraper. Cells were centrifuged at 1000 rpm for 5 min and the supernatant was discarded. The cells were washed once with 1X PBS and the pelleted again. The pellet was dissolved in an appropriate amount of protein loading buffer and the mixture was boiled at 95°C for 10 min. The lysates

were either kept at -80°C for later use or used immediately. The SDS gels used in this project had a 10% separating part and a 4% stacking part. After the samples were loaded into the SDS gels, the gels were run with 1X running buffer at 80 V (constant voltage) for 1.5 - 2 h using a BIORAD Mini Protean Tetra Cell. After running, the gels were transferred to 0.45 µm PVDF membranes (Thermo Scientific) in 1X transfer buffer at 250 mA (constant current) for 1.5 h at 4°C using BIORAD Mini Trans-blot. Membranes were then blocked in 10 mL PBST - milk at room temperature for 1 hour with constant shaking. Primary antibody incubations were done overnight at 4°C and secondary antibody incubations were done for 1 hour at room temperature. After incubation, membranes were washed with PBST 3 times for 10 min each. After the final washing step, the membranes were incubated with an enhanced chemiluminescent substrate for 5 min at room temperature in the dark room and exposed to X-Ray films (Fuji); ImageQuant™ LAS4000 Biomolecular imager could also analyze membrane directly.

3.2.4. TALEN Protein Assembly

TALEN Target Site: The software used for design of transcription activator like effectors (TALE) and transcription activator like effector nucleases (TALEN) is available online (TAL Effector Targeter; <https://tale-nt.cac.cornell.edu/>). DNA sequence entered is scanned for potential TALEN recognition sites based on either preset design guidelines defined by four different articles or user-provided spacer and RVD lengths. The software gives coordinates and sequences of recognition sites for right and left TALEN monomers and the spacer sequence. In addition, RVD sequences necessary for construction of custom TALENs were also provided as software output.

Golden Gate Assembly: TAL effector DNA binding domain is composed of tandem repeat modules. 12th and 13th amino acids within each repeat module, called repeat-variable di-residues (RVDs), are responsible for nucleotide recognition. NI, NN, NG and HD are the four most common RVDs, each preferentially bind to nucleotides A, G, T, and C, respectively (Figure. 4.1). Design of custom TALENs were performed using TALEN Golden Gate Kit, which was obtained from Addgene. The Golden Gate

TALEN kit, reported by Cermak *et al* (2011), contains a set of module plasmids with each individual RVDs, array plasmids for intermediate cloning, and backbone expression plasmids to make final TALEN expression constructs.

The custom TALEN is assembled using successive rounds of Golden Gate cloning, in which digestion by restriction endonucleases such as BsaI and Esp3I is performed to create unique 4 bp overhangs on DNA fragments. These unique overhangs flanking each RVD were designed such that up to 10 RVD-encoding repeat module plasmids can be ligated in a single reaction. The desired array is cloned into a final expression vectors. Construction of TALEN construct was achieved in 5 days. All cloning and assembly procedure was performed exactly according to Cermal *et al*. Golden Gate Cloning protocol.

3.2.5. CRISPR/Cas9 and CRISPR/Cas9n Gene Editing

CRISPR guide RNA selection: CRISPR/Cas9 system could be designed against almost any desired target site; the only limitation is the presence of protospacer adjacent motive (PAM) sequence (5' NGG 3') down stream of the target region. We used an online tool to find CRISPR targets with the highest score, meaning those that have the lowest number of off-targets in the coding-sequence and other regions of the whole genome. (<http://crispr.mit.edu/>).

Preparing CRISPR/Cas9 and CRISPR/Cas9n plasmid: After selecting the best possible CRISPR target on the region of interest, guide RNA oligonucleotides were obtained commercially as top and bottom strand, from Midland Certified Reagent Co. (midland, TX). These oligonucleotides consist guide RNA and BbsI overhangs at the 5' end of each of oligonucleotides. These oligonucleotides are then annealed and double stranded guide RNA is then cloned into mammalian expression pSpCas9(BB)-Puro (or pSpCas9n(BB)-Puro) plasmid (Figure4.3). All the plasmid preparation procedure is according to Ann Ran et al. protocol (Nature protocols, 2013).

CRISPR gene editing procedure: Final CRISPR/Cas9 or Cas9n constructs are transfected into the HEK293 and HCT116 using PEI transfection method. If a specific

mutation is considered, a single stranded oligo nucleotide (ss-oligo) with our desired mutation in its sequence is also co-transfected. 24h post-transfection Puromycin selection was applied to enrich transfection efficiency by creating a selective medium for transfected cells. Cells stay in Puromycin selection medium for at least 72h. After transfection enrichment, cells are grown in normal DMEM until the number of cells is sufficient for DNA extraction and single cell clone screening, a 1-day recovery is normally sufficient. The remaining procedure is the same for TALEN proteins and CRISPR transfected cells. Each single cell clone is screened by RFLP assay.

3.2.6. RNA-Sequencing

RNA Sequencing: HCT116WT, mut#4, mut#5, and mut#9 p53 CTM cell lines were either untreated or treated with 1 μ M doxorubicin for 24 hours. Total RNA was extracted, polyA selected and triplicate samples were sequenced at Beijing Genomics Institute on an Illumina HiSeq 2000 sequencing machine and analyzed using the R library DEseq. To identify biological processes influenced by CTM p53, further analysis on RNA sequencing results is ongoing.

4. RESULTS

4.1. Screening Homozygous CTM Cell Lines Created by Genome Editing Tools

In this study, we tried to characterize the p53 C-terminal regulatory domain by creating several p53 C-terminal mutant (CTM) human colon cancer cell lines. We identified the phenotypic differences between wild type p53 expressing and CTM p53 expressing HCT116 cells.

Here we describe three different homozygous mutant HCT116 human colon cancer cell lines that have mutations in the exon encoding the C-terminus of their *Tp53* gene in detail. Genome editing tools were used to create these mutants. We studied the properties of the endogenously expressed mutant p53 protein, by examining its expression, nuclear accumulation, DNA binding, protein interaction, ability to activate downstream genes and its influence on cell growth. The first step was to design genome-editing tools to create p53 CTM HCT116 cell lines. We first generated transcription activator like effector nuclease (TALEN) proteins targeting the last exon of the *Tp53* gene (Figure 4.1). Next we switched our genome editing methodology to CRISPR/Cas9 technique.

4.1.1. TALEN-Mediated CTM Cell Lines

We first attempted to mutate the p53 gene using TALENs by expressing pairs of TALEN proteins targeting the last exon of this gene. We constructed a pair of TALEN protein expressing plasmids containing the correct sequence of repeats that would bind the desired sequence in the p53 gene using the protocol developed by Cermak et al.¹⁴³. These two TALEN proteins were designed to bind to the top and bottom strands of the p53 gene exon 11 with a spacer of 15 base pairs. To generate expression constructs, we cloned TALEN repeats in the required order, into the final mammalian expression plasmid (pC-GoldyTALEN). After confirming the sequence of the TALEN expression constructs, we transfected HCT116 human colon cancer cell lines. To determine the transfection efficiency, we assessed the percentage of cells that express a GFP protein using fluorescent microscopy and by flow cytometry after transfecting cells with the pcDNA GFP plasmid (Figure 4.2). After transfecting cells with TALEN expression constructs, we generated single cell clones; PCR amplified the region of interest from genomic DNA and assessed mutation efficiency by RFLP and by sequencing. We made several attempts to obtain homozygous mutants with the TALEN method, but were not successful (Figure 4.2 and 4.3).

As an alternative option for a genome-engineering tool, we decided to use the CRISPR/Cas9 genome engineering system to target the p53 gene. Because the steps of generating single cell clones and assessment of mutation efficiency by RFLP are very similar between the TALEN and CRISPR/Cas9 methods and are described in detail below and because our attempts to generate homozygous mutant generation failed, our work on TALENs are not further described in detail here.

CTM cell lines were detected using the RFLP assay. As it is shown in figures 4.1 and 4.4, exactly at the site of TALENs and CRISPR binding regions, there is a *FauI* restriction site, which would be destroyed, in case genome-editing tools work. The results of the RFLP assay can be seen in figure 4.7. The intensity of any remaining uncut PCR bands in amplicons derived from TALEN proteins and CRISPR/Cas9 transfected cells after the digestion indicate the approximate percentage of the mutated cells in the transfected pool. For TALEN transfected cells, the efficiency of the TALEN-induced DSB was low in comparison with the CRISPR system (Figure 4.3)

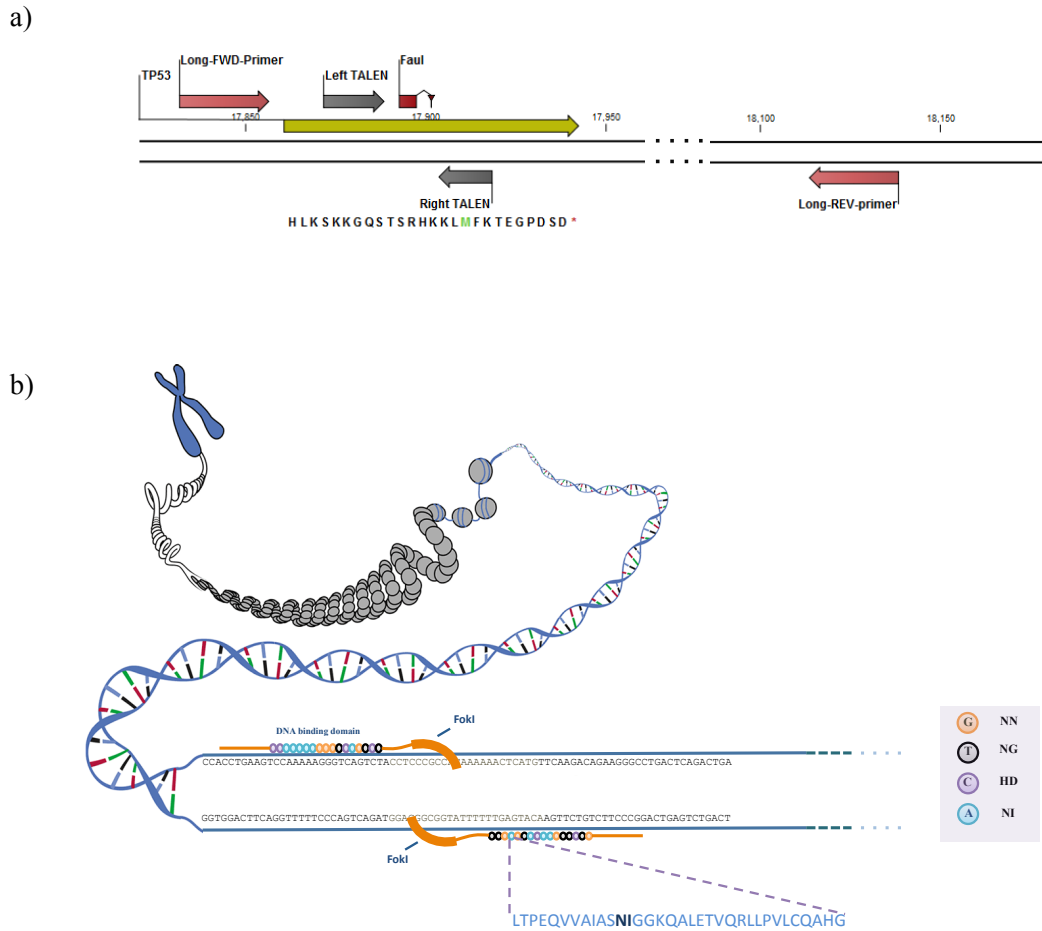


Figure 4.1: TALEN proteins designed to create P53 CTD mutant cells. a) Left and right TALEN proteins are shown in dark red. The last exon's coding sequence is represented in yellow and its translation product is shown. The FauI cut site used for the RFLP assay is shown in red. b) Illustration of TALEN proteins on the Tp53 gene's last exon. TALEN protein consists of an N-terminal tail, a DNA-binding domain, and a C-terminal domain to which FokI endonuclease enzyme is attached (all shown in orange); each of the FokI endonucleases introduce a nick in the DNA strand they bind. Each repeat of DNA-binding domain of the TALEN proteins are shown in a color-coded circle. Protein sequence of each repeat is magnified and the 12th and 13th RVD that differs in each repeat to bind to specific nucleotide is shown in dark blue. NN repeat binds to Guanine nucleotide, shown in orange; NG binds to Thymine, shown in gray; HD binds to Cytosine in purple; NI binds to Adenine, shown in blue.

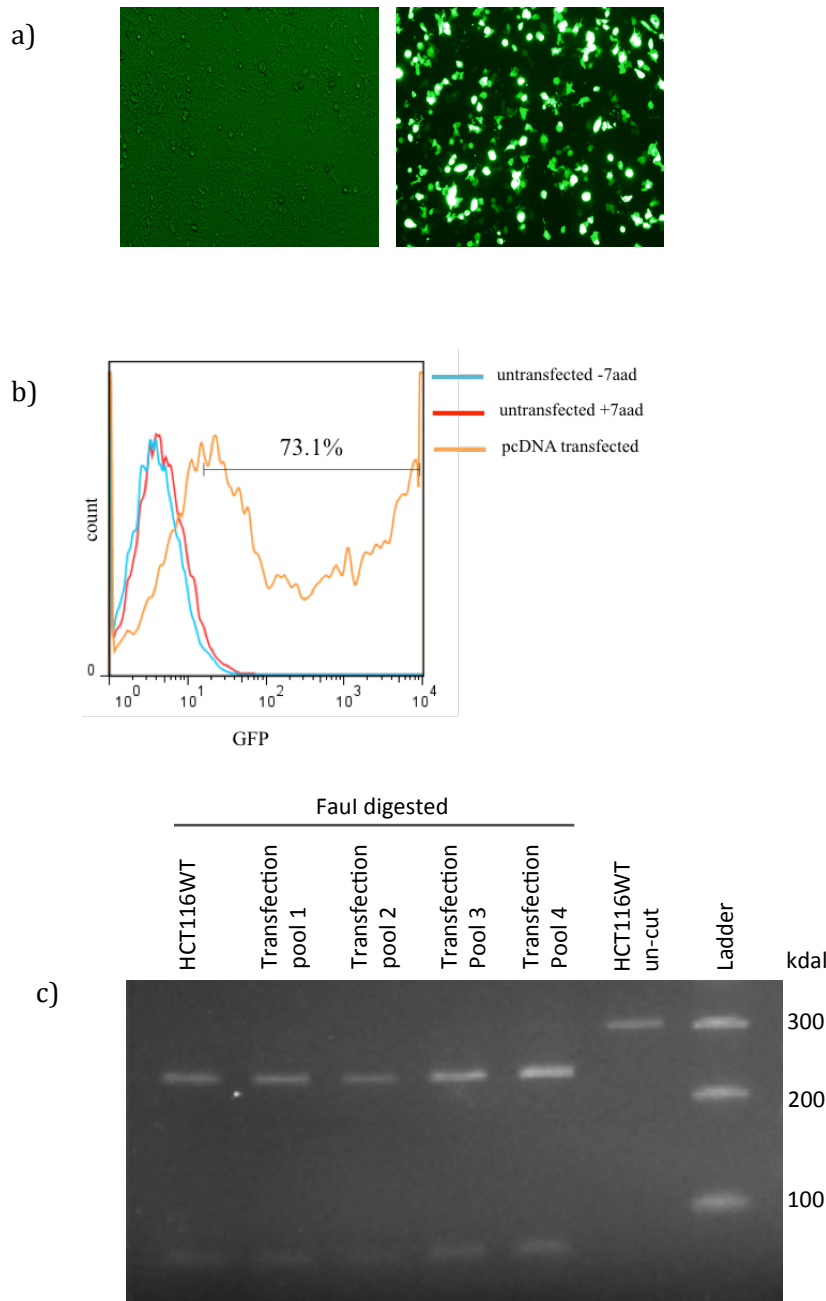


Figure 4.2: Determination of transfection and RFLP efficiency. Cells were transfected with pcDNA GFP plasmids and RFLP analysis was performed on TALEN transfected cell pools. a) On the left, HCT116 human colon cancer cells were imaged using the phase contrast technique on a fluorescent microscope. On the right, the same cells were imaged using a green fluorescent filter; green fluorescent cells correspond to those transfected successfully with the pcDNA GFP plasmid. b) Analysis of transfected cells using flow cytometry indicates transfection efficiency 73.1% for HCT116WT cells. Cell viability was determined by staining with 7AAD. c) RFLP analysis. A 300 bp PCR band was digested with the *FauI* restriction enzyme and generates two bands of size ~270 and ~30 bp. We conclude that TALEN transfected pools have a low mutation rate because the amount of uncut DNA after RFLP is not detectable.

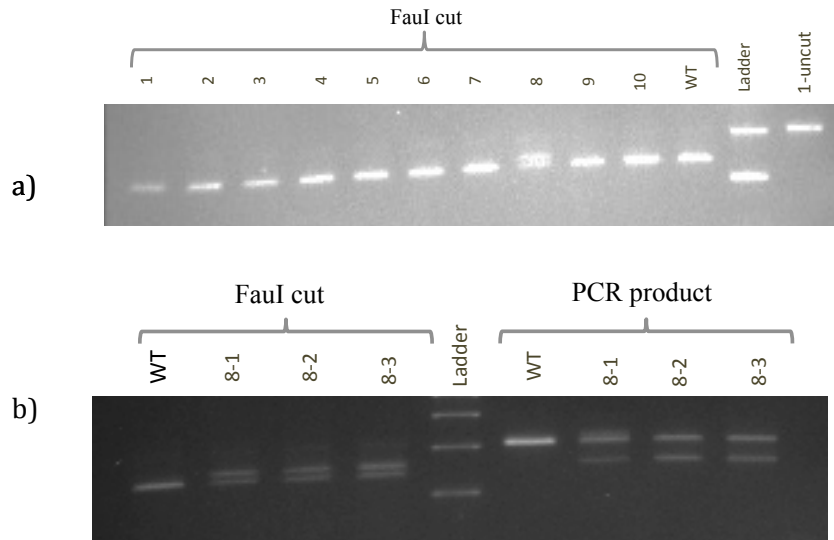


Figure 4.3: Identification of heterozygous mutants from single cell cloned TALEN transfected pools. a) Several single cell clones were screened by RFLP to find mutant clones; here several WT and one (clone #8) heterozygous mutant are shown. b) Clone #8 is diluted for the 2nd time to figure out if the clone is heterozygous or is actually coming from two clones, one WT, the other mutant. Three heterozygous mutants are shown after an RFLP screening of clone #8, diluted for the second time. PCR product from the WT allele of clone #8 gets cut, but other mutant allele stays intact after the digestion, indicating the heterozygosity of this clone.

4.1.2. CRISPR-Mediated CTM Cell Lines

As an alternative to the TALEN mediated genome engineering, we designed CRISPR/Cas9 and CRISPR/Cas9n plasmids against the last exon of the *Tp53* gene (Figure 4.3). To do this, we followed the protocol of Ran et al¹⁴⁶. This method expresses both the guide RNA component and the Cas9 cDNA from a single plasmid that can be transfected into eukaryotic cells. To generate CRISPR/Cas9 plasmids targeting the *Tp53* gene, we annealed oligonucleotides encoding the top and bottom strands of the guide RNA (Figure 4.5) and cloned these into the pSpCas9(BB)-puro plasmid (Figure 4.5). This plasmid includes: U6 promoter, CBh promoter (an altered version of CAG promoter), 3X FLAG epitope gene, nuclear localization signal (NLS), Cas9 restriction enzyme gene from *S. pyogenes* (SpCas9), 2A peptide self-cleaving

sequence, and bovine growth hormone Polyadenylation (bGH PA) as a specialized termination sequence for protein expression signal.

This assembled CRISPR/Cas9 expression vector was verified by sequencing and was introduced into HCT116 cells by the PEI (Polyethylenimine) transfection protocol. Pools of transfected cells theoretically contain a mixture of wild type cells, cells with one mutated allele (heterozygous mutants) and cells that are mutated in both alleles (carrying either the same mutation on both alleles or two independent mutations on each allele).

We designed the CRISPR/Cas9 system to target the last exon of the *Tp53* gene (Figure 4.4). The CRISPR/Cas9 enzyme is formed by the recruitment of the Cas9 endonuclease to the target site by the fused scaffold-guide RNAs. Recognition of the target site results in a DNA double strand break (DSB) (Figure 4.6). DNA DSBs are fixed efficiently in mammalian cells by either non-homologous end joining (NHEJ) or by homologous recombination. We assessed the formation of NHEJ mediated insertions and deletions (INDELs) by the restriction fragment length polymorphism assay conducted on PCR amplicons from genomic DNA isolated from cells that express CRISPR/Cas9. To enrich the population of cells that express the CRISPR/Cas9 endonuclease, we transiently selected the transfected cell pool with the antibiotic, puromycin, making use of the puromycin resistance gene in the pSpCas9(BB)-puro plasmid (Figure 4.6). To ensure that off target DSB and INDEL generation is kept to a minimum, we performed puromycin selection only for 72 hours, relieving the selection to ensure that the CRISPR/Cas9 expressing plasmid is lost from the majority of dividing cells after several rounds of cell division.

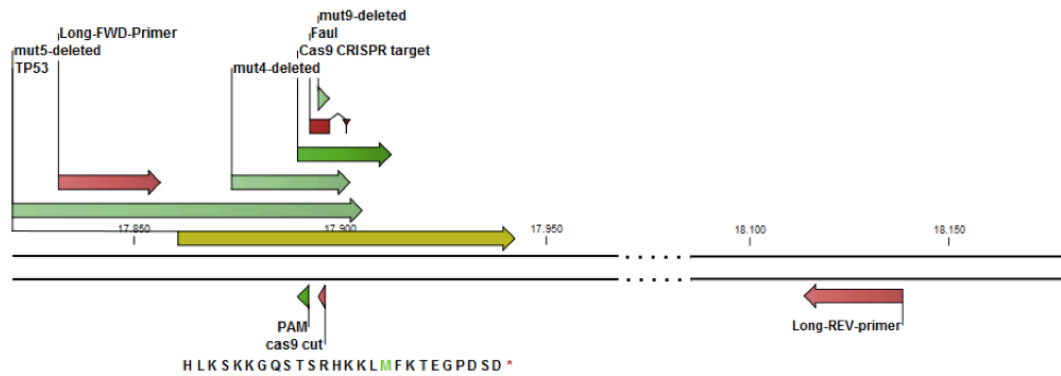


Figure 4.4: Annotation of primers used for RFLP and CRISPR target sites. The coding sequence of the last exon of the *Tp53* gene is shown in yellow; the translation product of this exon is shown in single letter amino acid code on the bottom. Forward and reverse primers used for RFLP analysis are annotated in light red (Long-FWD-primer and Long-REV-primer); mut#4, mut#5, and mut#9 deleted sequences (explained in detail later) are shown in light green and CRISPR/Cas9 target region is shown in dark green. The FauI restriction site used for RFLP is annotated in red.

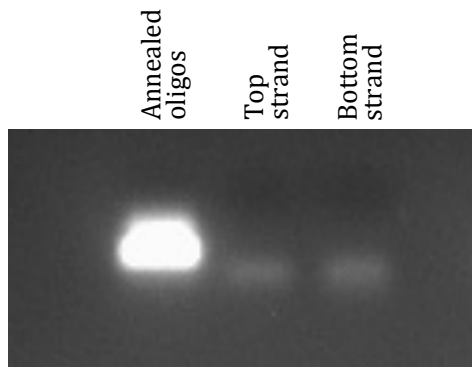


Figure 4.5: Annealing of DNA oligonucleotides for cloning into guide RNA expression plasmids.

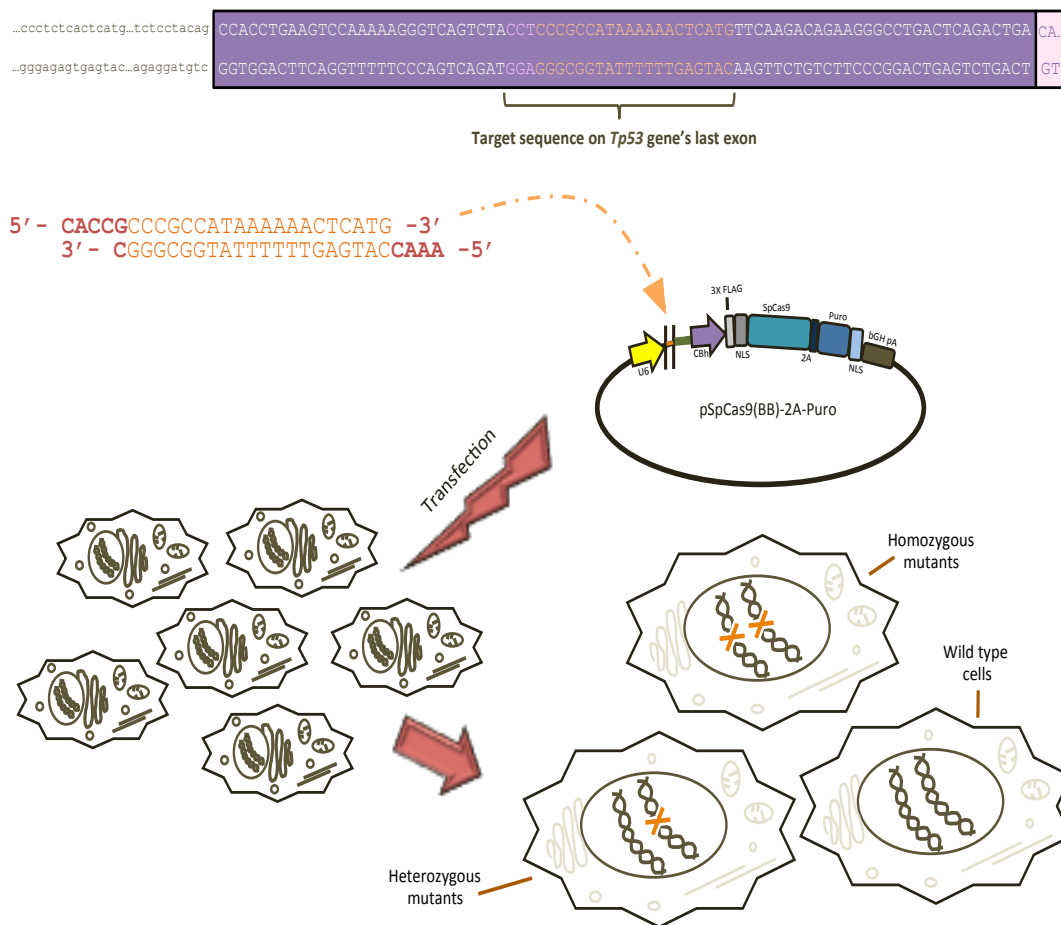


Figure 4.6: Experimental design of genome editing using the CRISPR/Cas9 system. At the top, a segment of the *Tp53* gene is shown that contains a partial exon 10, exon 11 and the intervening intron 10. The protein-coding region is shown in a purple box. A chosen CRISPR/Cas9 target sequence in this exon is indicated with 20 nt of yellow lettering, followed by the NGG PAM sequence,. Oligonucleotides corresponding to this guide sequence were cloned into the pSpCas9(BB)-2A-Puro plasmid. HCT116 cells were transfected with the pSpCas9(BB)-2A-Puro plasmid to generate mutations in the p53 CTD. The potential outcomes of *Tp53* gene targeting are shown in the bottom where cells could have mutations in one or both alleles, or remain wild type.

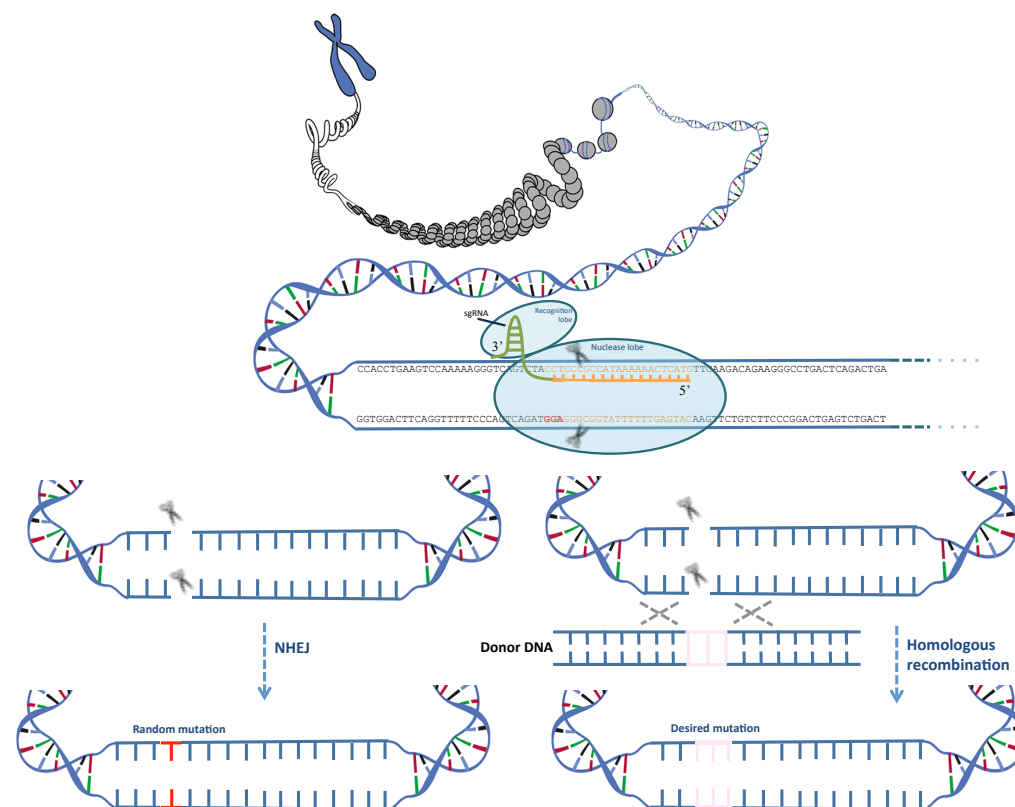


Figure 4.7: The mechanism of CRISPR/Cas9 interaction with DNA. Cas9, an RNA-directed DNA endonuclease, is recruited to the target of interest at the upstream of the PAM sequence with the help of single guide RNA (sgRNA). Cas9 introduces DNA double strand breaks in the *Tp53* gene, exactly 3 nt upstream of the PAM sequence. This break is repaired either by non-homologous end joining (NHEJ) in which a random mutation appears (shown on the left), or by homologous recombination, if a donor DNA is co-transfected into the cells to act as a template for DNA repair (shown on the right).

As done for TALEN transfected cells, RFLP analysis was conducted for CRISPR/Cas9 and CRISPR/Cas9n systems; CRISPR/Cas9n has a mutated Cas9 enzyme that could only introduce a nick to the strand it binds to, therefore two Cas9n proteins bind to top and bottom strands separately to create a DSB, similar to TALEN proteins. Following transfecting cells with CRISPR/Cas9 and Cas9n plasmids, we could confirm that a mutated population exists in our transfected pool, which was represented by a faint uncut band in the RFLP analysis. We cloned the undigested bands into a plasmid (PTZ57R/T in this case), transformed these plasmids into *E.coli* and sequenced the inserted DNA from several colonies derived from the transformed bacteria. At the same time, we performed single cell cloning by limiting dilution assays in 96-well plates.

4.2. Homology Directed CTMs

Our first trial in creating CTM cell lines, was to make a homology directed mutation in HEK293 cell lines. We co-transfected a donor-DNA that contained two homology arms, a restriction site for RFLP screening (that does not present in the wild type sequence), and Lysine to Alanine codon change (Figure 4.8).

HEK293 cells were transfected and RFLP experiment was conducted to check the efficiency of homology directed repair (HDR). HDR efficiency is not high as expected. Nevertheless, transfected pool was diluted to screen for K381A single cell clones. RFLP results showed that one clone seems to have the desired mutation (HR3 clone). Sequencing results confirmed the K381A mutation in HR3 clone. HR3 CTM cell line could accumulate p53 as efficient as WT cells (Figure 4.9). Our studies on this mutant are ongoing in a separate project. We moved on with p53 CTD characterization with other CTM cell lines that we obtained through NHEJ-induced random mutants.

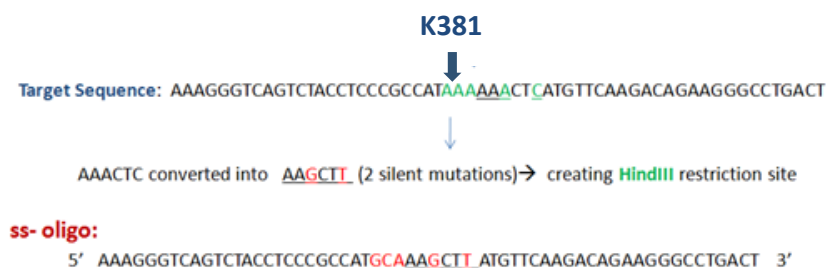


Figure 4.8: Design of the donor DNA for homology-directed mutation of HEK293 cells. Single-stranded oligonucleotides (ss-oligo) were designed to mutate the K381 amino acid of p53 protein to Alanine. This ss-oligo introduces a HindIII restriction site which generates a silent mutation that was designed to detect HDR(+) clones by RFLP. Silent mutations were designed by considering the abundance of the chosen codon in human cells.

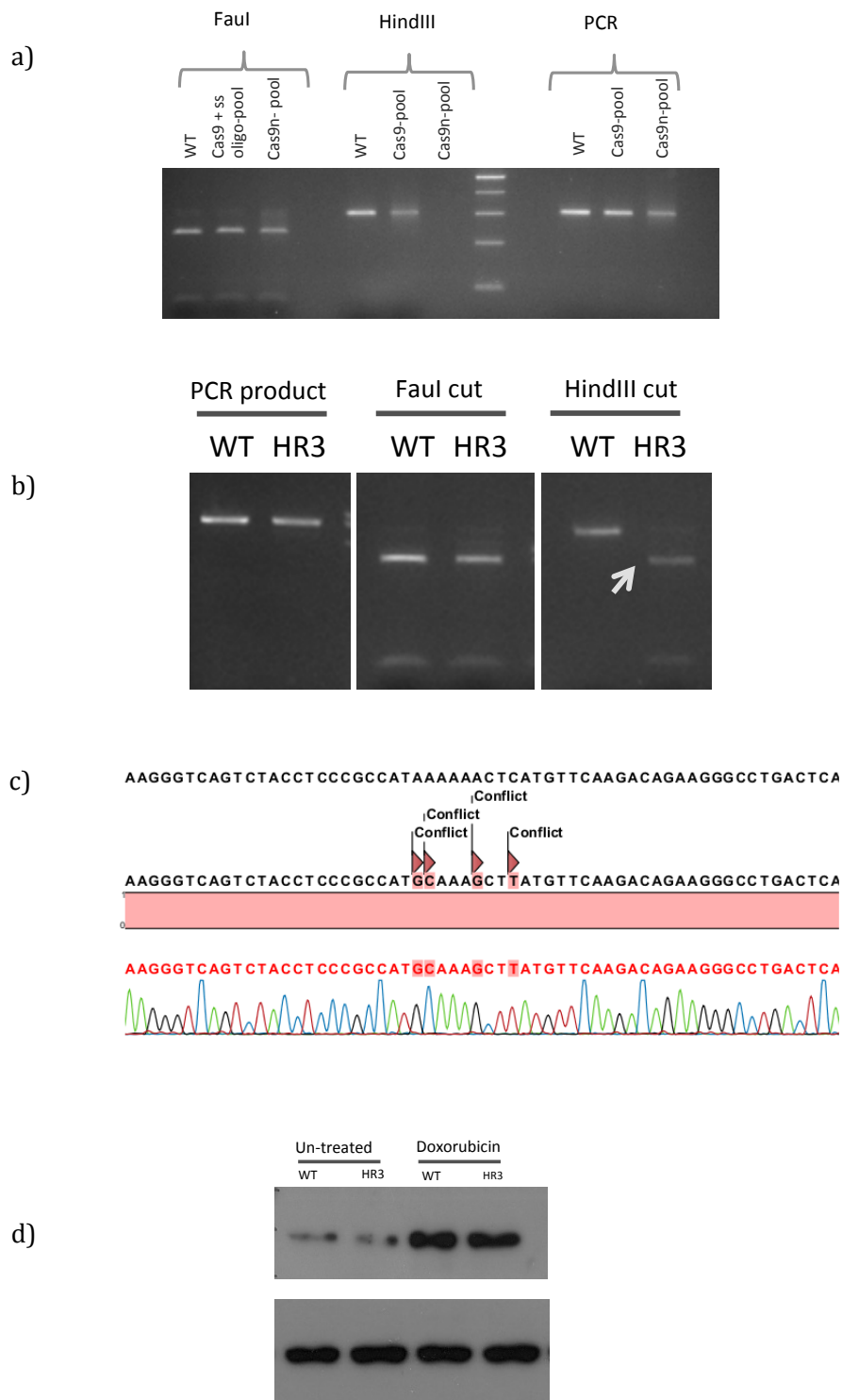


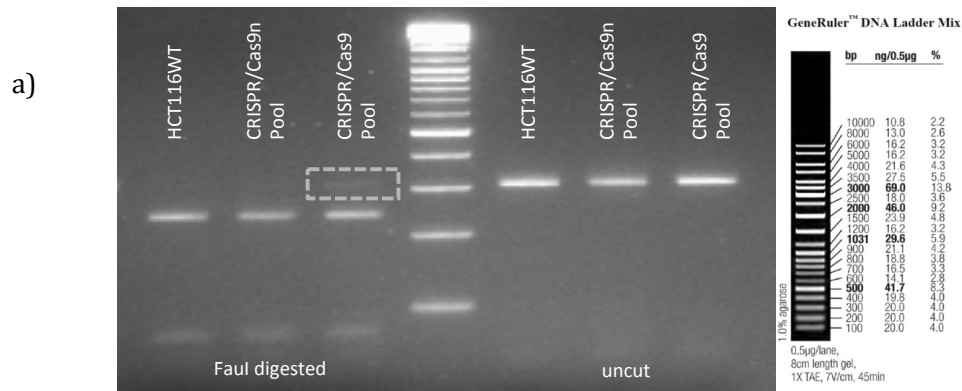
Figure 4.9: Homology directed mutagenesis using the CRISPR/Cas9 system with ss-oligonucleotides. a) CRSIPR efficiency was assessed by RFLP; an uncut band is detectable in the pool indicating the presence of a population of mutated cells. HindIII digestion is not detectable in the pool of CRISPR/Cas9, indicating a very low HDR efficiency. We could not detect any bands from CRISPR/Cas9n transfected cells because with donor DNA co-transfection was only performed with CRISPR/Cas9.

Single cell clones from CRISPR/Cas9 transfected pools were screened to find homozygous K382A mutant cells. b) HEK293 single cell clone screening after transfection. PCR products (left panel) were digested with FaeI (middle panel) indicating that the restriction site is intact. HindIII (right panel) cannot cut PCR products from WT cells, because there is no HindIII site in that region originally, but PCR products from HR3 are cut, indicating that HDR was successful. c) The presence of a mutation was confirmed by sequencing. WT sequence (top panel) and HR3 mutant (bottom panel) differ in the indicated positions identified by the Blast program d) No change in p53 accumulation after Doxorubicin treatment is detected for HR3 cells before and after Doxorubicin treatment. p53 western blot at the top and Actin loading control at the bottom is shown.

4.3. NHEJ Mediated CTM: mut#4, mut#5, and mut#9

The main focus of this study is three cell lines that we obtained from NHEJ repair mechanism after transfecting HCT116WT cells with CRISPR/Cas9 system. These homozygous mutants were detected after several single cell clone screening: mut#4, mut#5 and mut#9. mut#4 had 29 nucleotides deletion, 89 nucleotides were deleted in mut#5, and mut#9 lacked 3 nucleotides. These three mutants were first detected with RFLP, and then sequenced to confirm their homozygosity and deleted region (Figure 4.11 and 4.12).

Sequencing results were confirmed in more than 25 different clones to make sure of the same mutation in both alleles. The mRNA sequence of the mutated region after the transcription, and also estimated protein sequence is shown in schematic figures for wild type and CTM cells (Figure 4.13).



b)

HCT116WT:

ACAGCCACCTGAAGTCCAAAAAGGGTCAGTCTA**CCTCCCGGCCATAAAAACTCATG**TTCAAGACAGAAGGGCCTGACTCAGACT

CRISPR/Cas9 transfected cells (random mutations in CTD of the p53 gene):

ACAGCCACCTGAAGTCCAAAAAGGGTCAGTCTA**CCTCCCGGCCATAAAAACTCATG**TTCAAGACAGAAGGGCCTGACTCAGACT

ACAGCCACCTGAAGTCCAAAAAGGGTCAGTCTA**CCTCCC**-----**CTCATG**TTCAAGACAGAAGGGCCTGACTCAGACT

ACAGCCACCTGAAGTCCAAAAAGGGTCAGTCTA-----**AAAAAACTCATG**TTCAAGACAGAAGGGCCTGACTCAGACT

ACAGCCACCTGAAGTCCAAAAAGGGTCAGTCTA**CCTCCCGGCCATAAAAACTCATG**TTCAAGACAGAAGGGCCTGACTCAGACT

ACAGCCACCTGAAGTCCAAAAAGGGTCAGTCTA**CCTCCC**-----**CTCATG**TTCAAGACAGAAGGGCCTGACTCAGACT

ACAGCCACCTGAAGTCCAAAAAGGGTCAGTCTA**CCTCCCGGCCATAAAAACTCATG**TTCAAGACAGAAGGGCCTGACTCAGACT

ACAGCCACCTGAAGTCCAAAAAGGGTCA-----**TG**TTCAAGACAGAAGGGCCTGACTCAGACT

ACAGCCACCTGAAGTCCAAAAAGGGTCAGTCTA**CCTCCCGGCCATAAAAACTCATG**TTCAAGACAGAAGGGCCTGACTCAGACT

HCT116WT:

ACAGCCACCTGAAGT**CCAAAAAGGGTCAGTCTACCTCC**CGCCATAAA**AAACTCATGTTCAAGACAGAAGG**GCCTGACTCAGACT

CRISPR/Cas9n transfected cells (random mutations in CTD of the p53 gene):

ACAGCCACCTGAAGT**CAAAAAAGGGTC**-----**ATGTTCAAGACAGAAGG**GCCTGACTCAGACT

ACAGCCACCTGAAGT**CAAAAAAGGGTCAGTCTACCTCC**CG-----**ACAGAAGG**GCCTGACTCAGACT

ACAGCCACCTGAAGT**CAAAAAAGGGTC**-----**ATGTTCAAGACAGAAGG**GCCTGACTCAGACT

ACAGCCACCTGAAGT**CAAAAAAGGG**-----CCATAAA**AAACTCATGTTCAAGACAGAAGG**GCCTGACTCAGACT

Figure 4.10: Non-Homologous End Joining (NHEJ) mediated random mutations using the CRISPR/Cas9 system. a) HCT116 human colon cancer cells were transfected with CRISPR/Cas9 and CRISPR/Cas9n plasmids. RFLP analysis was performed on transfected pools. The third lane on the left shows a faint band (in the white rectangle), which represents the PCR product from the mutated cells that do not have a FauI site. b) The uncut bands were sequenced to identify various mutations in the pool of transfected cells. CRISPR/Cas9 mutation is shown at the top, and CRISPR/Cas9n at the bottom. Insertions are shown in green and the CRISPR binding site is highlighted.

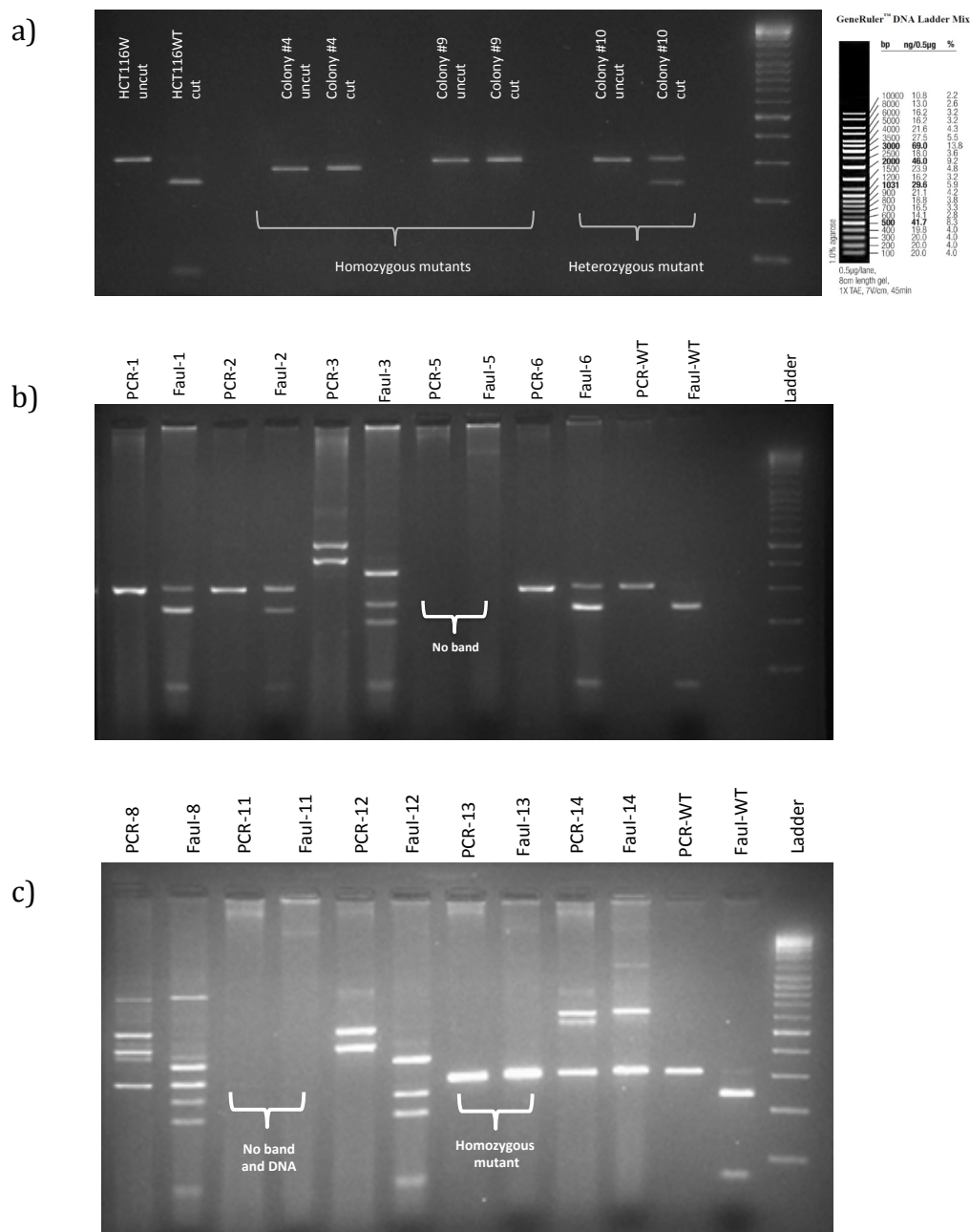
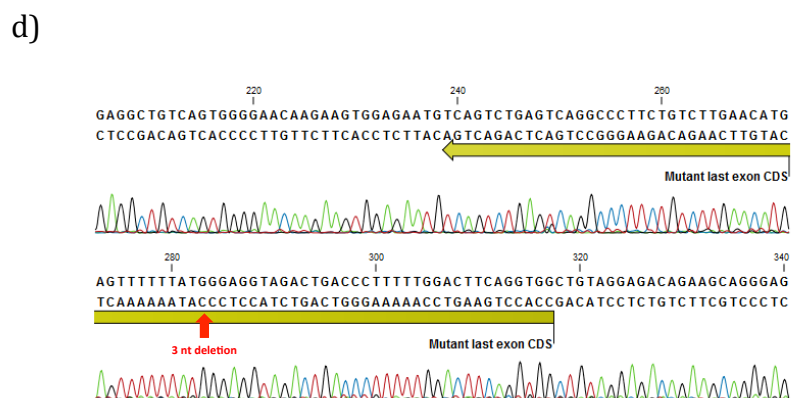
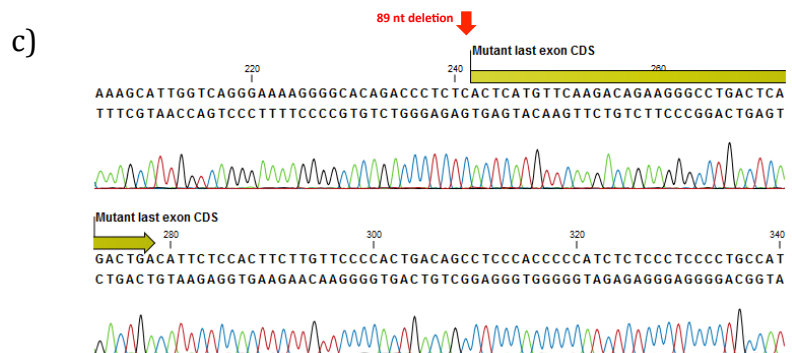
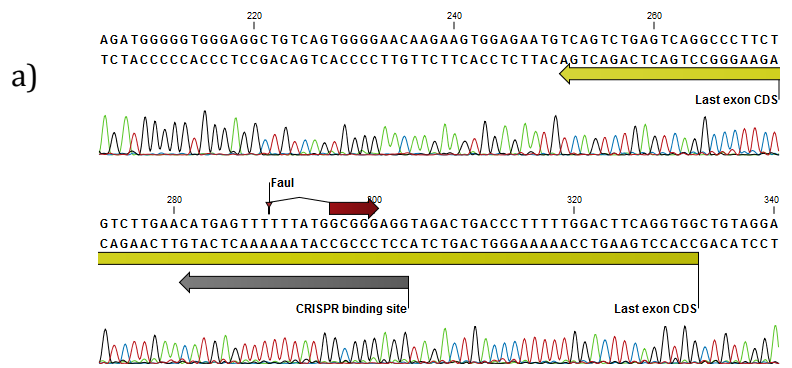


Figure 4.11: Single cell clone screening of CTM cell lines a) Single cell clone homozygous (#4 and #9) and heterozygous (#10) mutants' RFLP experiment after CRISPR/Cas9 transfection; from the left to the right, HCT116WT cells PCR amplicon (~300 nt) is cut into two fragments (~270 nt and 30 nt); mut#4 PCR amplicon is shorter than the WT and it cannot get cut (there are not *FauI* sites in any of the two alleles); mut#9 is not digested by *FauI* either; colony #10 is obviously mutated in one allele (there is an uncut band) and WT in the other allele (half of the PCR product is cut) b) RFLP analysis for several single cell clones show various mutations. Here, clone #5 is not amplified with our primes, which is due to a big mutation (89 nt) that includes our forward primer's binding site. We confirmed the exact deletion by selecting other primers with longer amplicons. c) Again, various mutations in which colony#13 looks homozygous (which was later confirmed to have R379 deletion, just like mut#9) and colony#11 has the exact mutation as mut#5 (89 nt deletion).



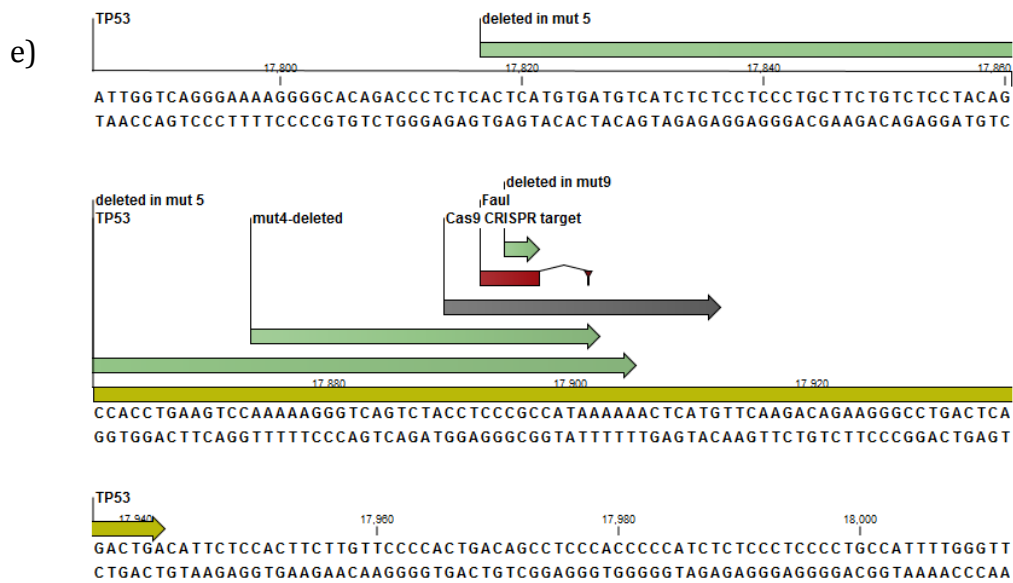


Figure 4.12: Sequencing analysis of mut#4, mut#5, and mut#9. a) Un-transfected cells sequencing results.. The coding sequence of the last exon of the *TP53* gene is shown in yellow. The CRISPR binding site is also shown in gray and the PstI enzyme restriction site is illustrated in red. b) 29 nt mutation both alleles of mut#4 is confirmed by sequencing several clones. c) 89 nt deletion in mut#5 starts from 10-11 intron and continues to the last exon. d) 3 nt deletion in mut#9 which follows R379 deleted p53 protein for these cell lines. e) All three mutations are illustrated on the *TP53* gene's last exon as green arrows.

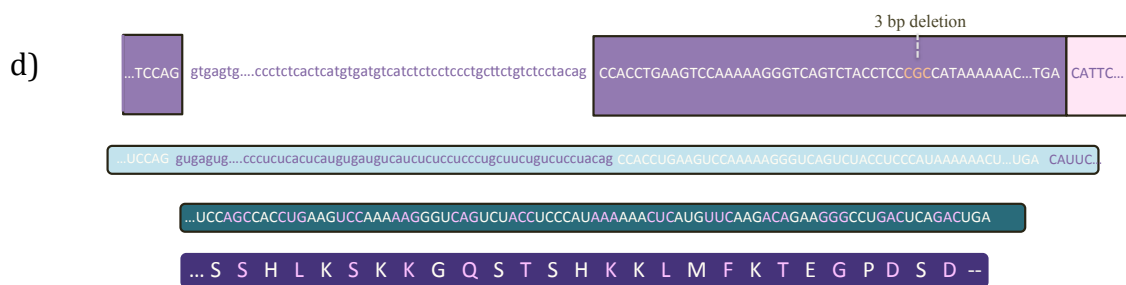
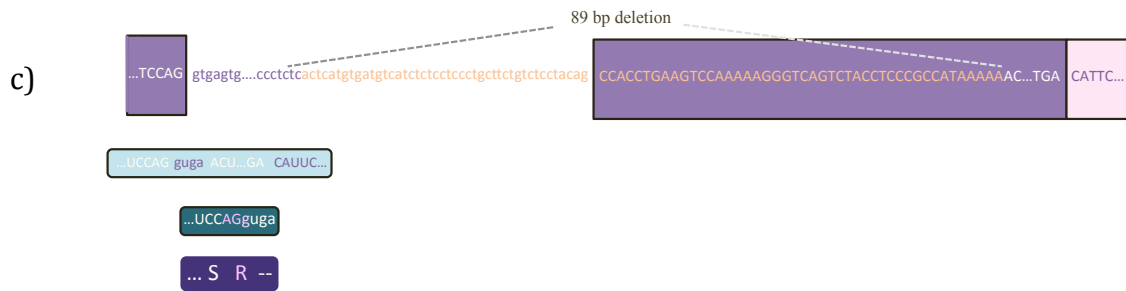
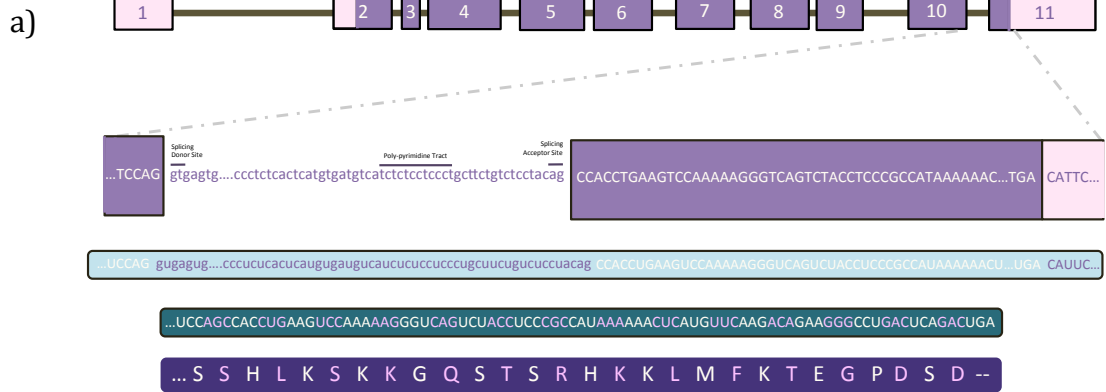


Figure 4.13: Predicted p53 gene DNA, RNA, and Protein structure of mut#4, mut#5, and mut#9. a) At the top, the *Tp53* gene is shown with its 11 exons. 3' un-translated region (UTR) and 5' UTR are shown in pink boxes. Coding region is shown in the purple box, and introns are the brown lines in between the exons. The end of the 10th exon, intron 10-11, and the last exon (11th exon) of the *Tp53* gene is magnified for wild type p53 and mut#4. Right under the illustration of the *Tp53* gene, a precursor RNA is shown in the light green box. Sequences transcribed from exons, are shown in pink letters and sequences transcribed from introns are shown in purple letters. Mature mRNA is displayed in dark green box; here splicing occurs and introns are removed from the pre-mRNA. The next step is translation; protein sequence is written in the dark purple box below the mature mRNA. The amino acids coming from the three-letter mRNA codes are shown. b) mut#4 has truncated p53 due to 29 nt deletion. It also has a non-WT tail coming from the frame-shift as well. The deleted part of the genome is removed from the precursor RNA as well as the mature mRNA. 29 nt deletion leads to frame-shift in the translation and a shorter non-WT tail is the consequence of this mutation. c) mut#5 completely lacks the last exon because of 89 nt deletion, starting from intron 10-11, that makes splicing between exon 10 and 11 impossible (polypyrimidine tract and also acceptor site of the intron is deleted which theoretically makes splicing impossible); therefore it most probably loses the last exon completely in the protein. d) mut#9 lacks one amino acid (R379) as the consequence of 3 nucleotide deletion. This deletion is shown in orange letters in the DNA sequence of the last exon. These three nucleotides are removed from the mRNA sequences, and the protein sequence of the mut#9 lacks R379 accordingly.

4.3.1. Phenotypic Specificities of the CTM Cell Lines

Different aspects Our CTM cell lines were investigated, trying to identify phenotypes specific to a mutant. We checked protein expression for several genes including p53, p21, PUMA, and MDM2. We also checked if p53 in CTM cell lines could bind to its DNA target as efficient as the wild type p53. Since p53 is a transcription factor, we looked at mRNA amount of a number of the p53 protein target genes in HCT116 human colon cancer cell lines with/without wild type p53, and compare them with the mRNA amount of the same group of genes in our CTM cell lines. During our studies, we found that some of the CTM cell lines grow slower than the HCT116 cells with wild type p53; we confirmed this cell doubling-time difference experimentally.

4.3.2. The p53 Protein Expression in CTM Cell Lines

Western blot experiment was conducted to compare the expression pattern of the p53 protein and some of its target genes (p21, PUMA, and MDM2). To induce p53 expression in our cells, we exposed them to various genotoxic stresses such as Doxorubicin (1 μ M), Cisplatin (100 μ M), or Nutlin (10 μ M) treatments. In figure 4.14, western blot experiment of HCT116WT and all CTMs is shown. WT cells mut#4, and mut#9 could accumulate p53 after Doxorubicin treatment, but mut#5 seems to have serious accumulation problems. p53 in mut#5 could be detected as a faint band in cytoplasm lysate though. p53 accumulation after Doxorubicin treatment is approximately the same for HCT115WT cells and mut#4 and mut#9 CTM cell lines. Shorter p53 protein is clearly presented in p53 western blot. After Doxorubicin treatment and also serum starvation (serum starvation stress is induced by keeping cells in EBSS medium (Biological Industries®) for 16 h), mut#9 p21 expression is significantly less than mut#4 and WT cells. PUMA expression in un-treated cells and cells under stress is very similar (Figure 4.15). Unlike other p53 CTM cell lines, mut#5 cannot accumulate p53 properly under stress. We compared p53 accumulation in mut#5 and mut#9 in different conditions such as un-treated, Nutlin treated (10 μ M 16h), Doxorubicin treated (1 μ M 24h), and Cisplatin treated (100 μ M 16h). In each case, p53 could not accumulate as much as mut#9 or wild type cells (Figure 4.16). p53 expression comparison between HCT116WT, HCT116KO, and mut#5 in western blot experiment was done as well which confirmed our previous findings (Figure 4.17).

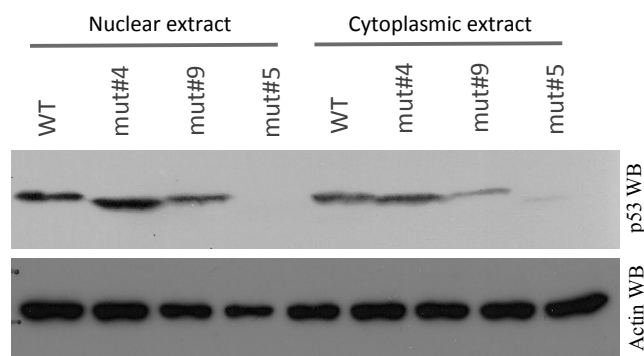


Figure 4.14: Analysis of p53 protein expression in HCT116WT and CTM cells by western blotting. WT cells and mut#4 accumulate p53 after Doxorubicin treatment, but mut#9 accumulates less and mut#5 almost cannot accumulate p53. p53 in mut#5 seems

to have translocation problem to the nucleus following DDR (DNA damage response) as it is present as a faint band in cytoplasm lysate but not nuclear lysate. Actin control is shown under the p53 western blot as well.

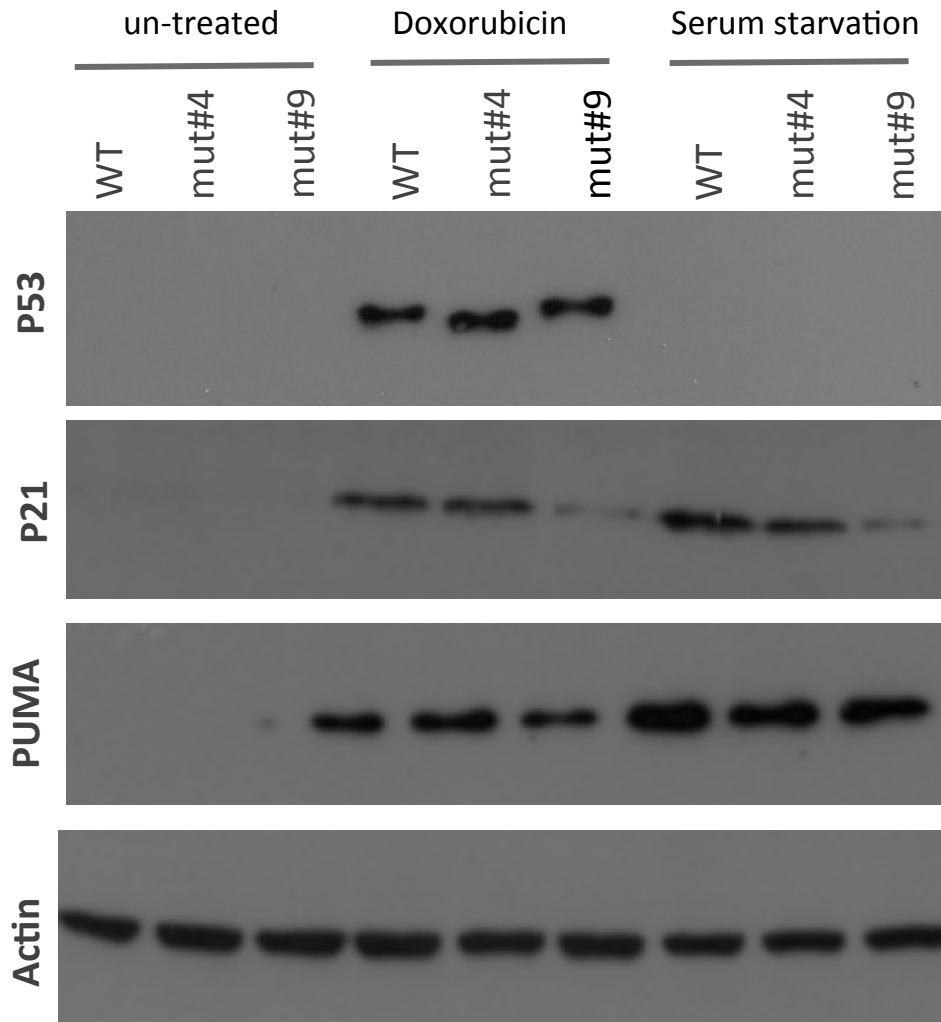


Figure 4.15: Analysis of p53, p21, PUMA protein expression in mut#4 and mut#9, under normal condition (un-treated), after Doxorubicin treatment (1 μ M for 24 h), and under serum starvation stress. p53 accumulation after Doxorubicin treatment is approximately the same for HCT116WT cells and CTMs. Shorter p53 protein is clearly presented in p53 blot. For p21 protein expression, after Doxorubicin treatment and also serum starvation, mut#9 p21 expression is significantly less than mut#4 and WT cells. PUMA expression in un-treated cells and cells under stress is very similar. The amount of loaded protein for each sample is equal as it is shown in Actin western blot.

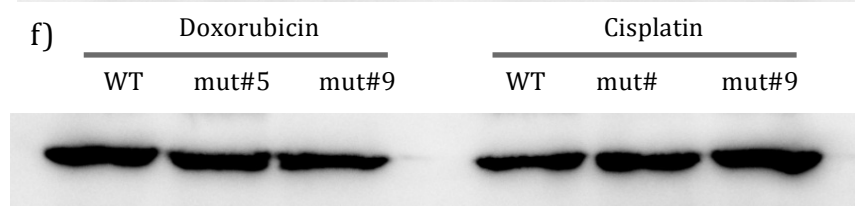
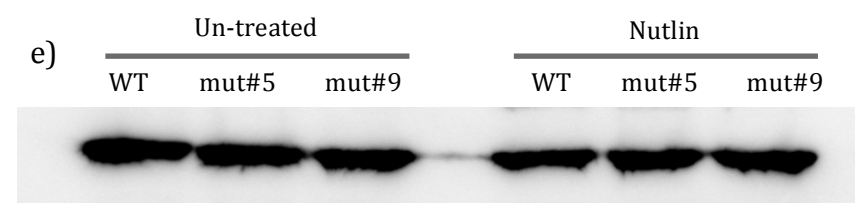
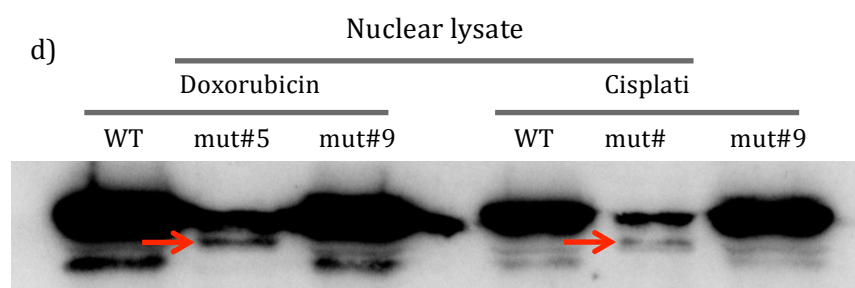
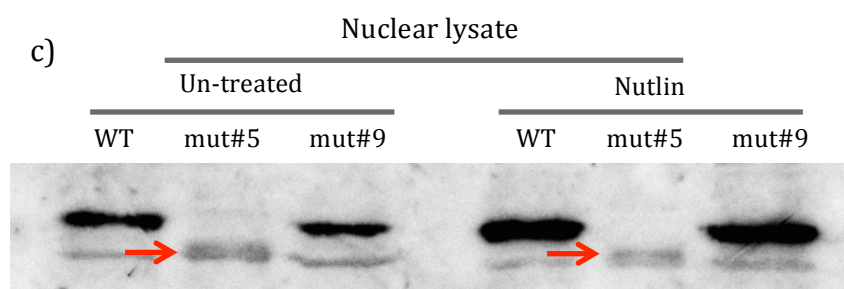
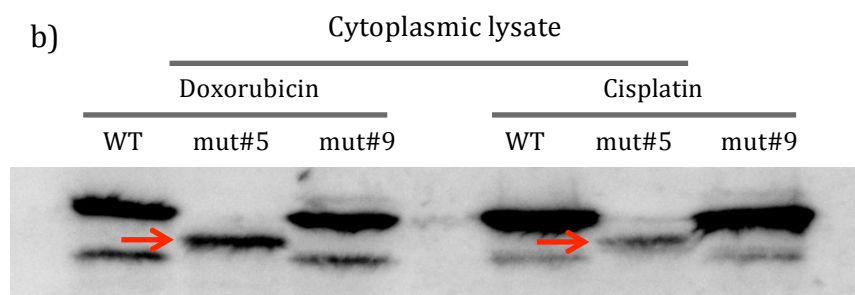
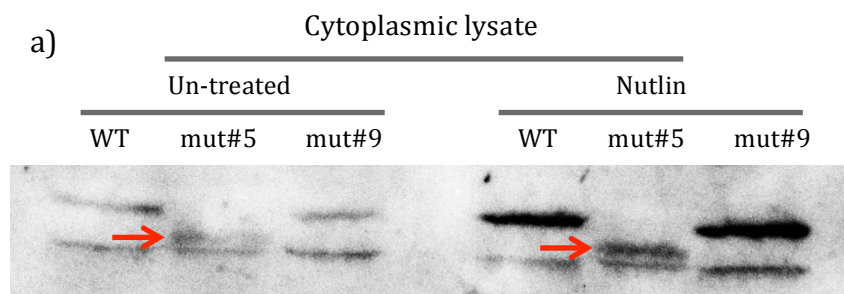


Figure 4.16: Analysis of p53 protein expression in WT, mut#9, and mut#5 under different types of genotoxic stress. a) The p53 protein amount is compared in WT, mut#5, and mut#9 cells under normal condition and also Nutlin treated; in cytoplasm, p53 is accumulated in three cell lines, but less in mut#5 (shown with red arrow); b) Doxorubicin and Cisplatin induces DNA double strand break and p53 is accumulated following both treatments. Again mut#5 accumulates less p53 in comparison. c) Untreated and Nutlin treated WT, mut#5 and mut#9 p53 expression in the nuclei. d) Doxorubicin and Cisplatin treated WT, mut#5, and mut#9; mut#5 seems not to be able to translocate into the nucleus, specially after Doxorubicin treatment. Although there is no nuclear export region in the last exon of the p53, still the absence of this part seems to create translocation problems. e) Actin control, showing that equal amounts of protein is loaded to each of the wells for un-treated and Nutlin treated samples. f) Actin control, showing that equal amount of protein is loaded to each of the wells for Doxorubicin and Cisplatin treated samples.

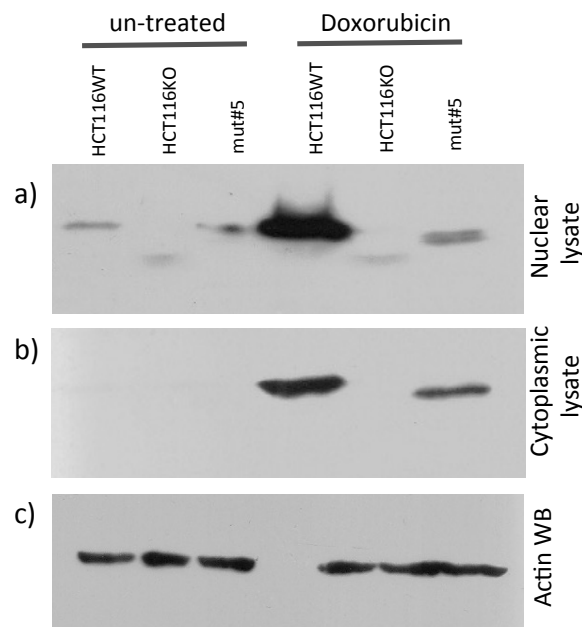


Figure 4.17: Analysis of p53 expression in WT, KO, and mut#5. a) Basal p53 expression for WT cells is more than mut#5. No p53 expression for HCT116KO. p53 accumulation is also less in mut#5 after Doxorubicin treatment. b) p53 accumulation is more obvious in the cytoplasm for mut#5 cells. c) Loading control; actin western blot shows the equal amounts of the loaded protein for each of the samples.

4.3.3. DNA-Binding Activity of p53 in CTM Cell Lines

To check whether p53 protein DNA binding activity is affected in the mutant cells or not, a pull-down experiment was conducted with DNA probes obtained from one of the p53 protein's transcription targets (GADD45 promoter). p53 of mut#9 binds less efficiently to its DNA target whereas mut#4 DNA binding efficiency is similar to the wild type cells (Figure 4.18).

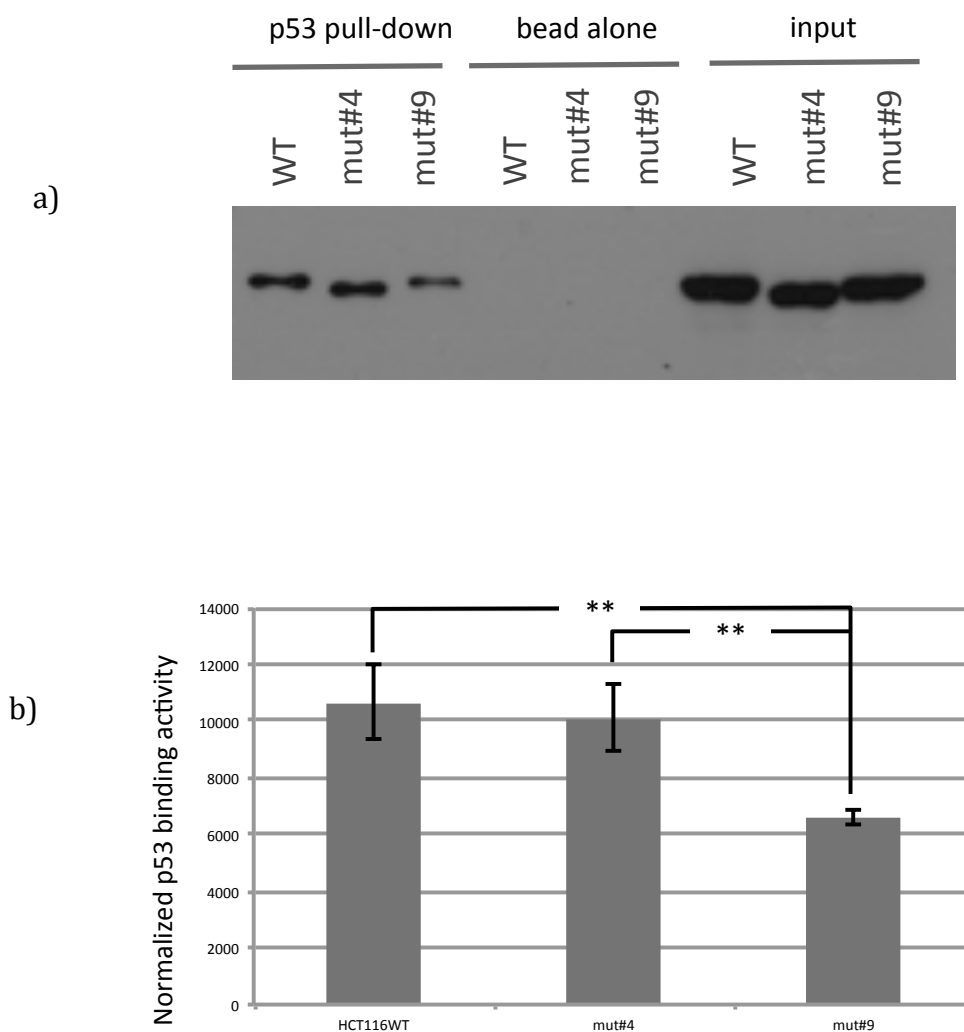


Figure 4.18: p53 protein expressed by mut#9 cells binds less efficiently to target DNA ($p=0.0069$). a) Here pull down experiment results show that the transcriptional activity of mut#9 drops compared to HCT116WT and also mut#4. b) Normalized p53 binding

activity is shown for three independent pull down experiments and compared in a graph; mut#9 binds less efficiently to its target DNA ($p=0.0069$).

4.3.4. p53 Translocation into the Nucleus in CTM Cell Lines

Another interesting observation was that p53 could not translocate into the nucleus under stress, unlike what happens in wild type cells (Figure 4.16). After several western blot experiments, we could almost conclude that mut#5 p53 cannot translocate efficiently into the nucleus after accumulation in the cytoplasm (Figure 4.19).

The p53 protein accumulation and translocation after Doxorubicin treatment was checked for HCT116WT and mut#5 under confocal microscopy as well. The results confirmed what we showed in western blot experiments. p53 cannot accumulate in the nucleus of the mut#5 cells after genotoxic stress, which is Cisplatin treatment in this case. Basal p53 expression is lower in mut#5 than HCT116WT cells. Another thing, which was clearly noticed under confocal microscopy, was disability of mut#5 in losing their volume (cell shrinking) as much as WT cells during apoptosis (Figure 4.20). This finding is clearly confirmed in xCELLigence experiments as well (Figure 4.27-b).

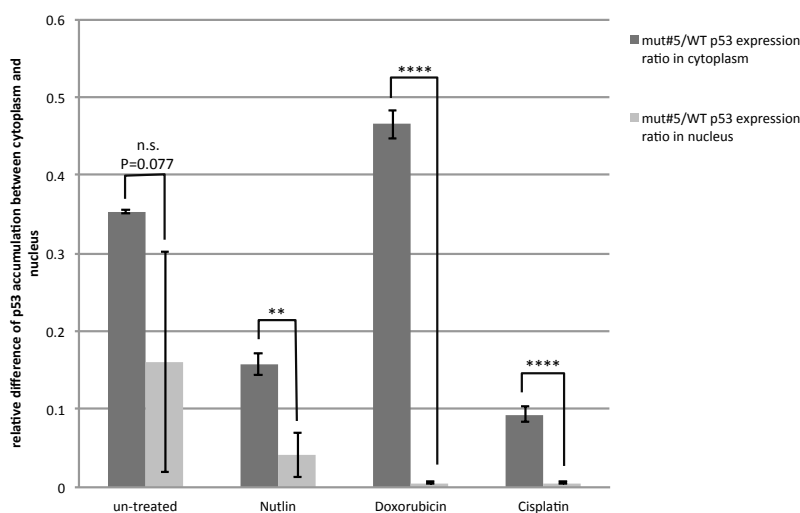


Figure 4.19: p53 nuclear translocation is inhibited in mut#5 cells under stress. p53 accumulation is calculated for three different stress conditions (Nutlin, Doxorubicin, and Cisplatin treated). p53 band intensity in mut#5 is divided by the p53 band intensity in the WT cells; here, the ratio for cytoplasmic p53 is compared with the ratio for

nuclear p53 and the difference between these amounts is significant, showing that the p53 protein cannot translocate into the nucleus.

$P > 0.05$: non-specific, $P \leq 0.05$: *, $P \leq 0.01$: **, $P \leq 0.001$: ***, *** $P \leq 0.0001$: ****.

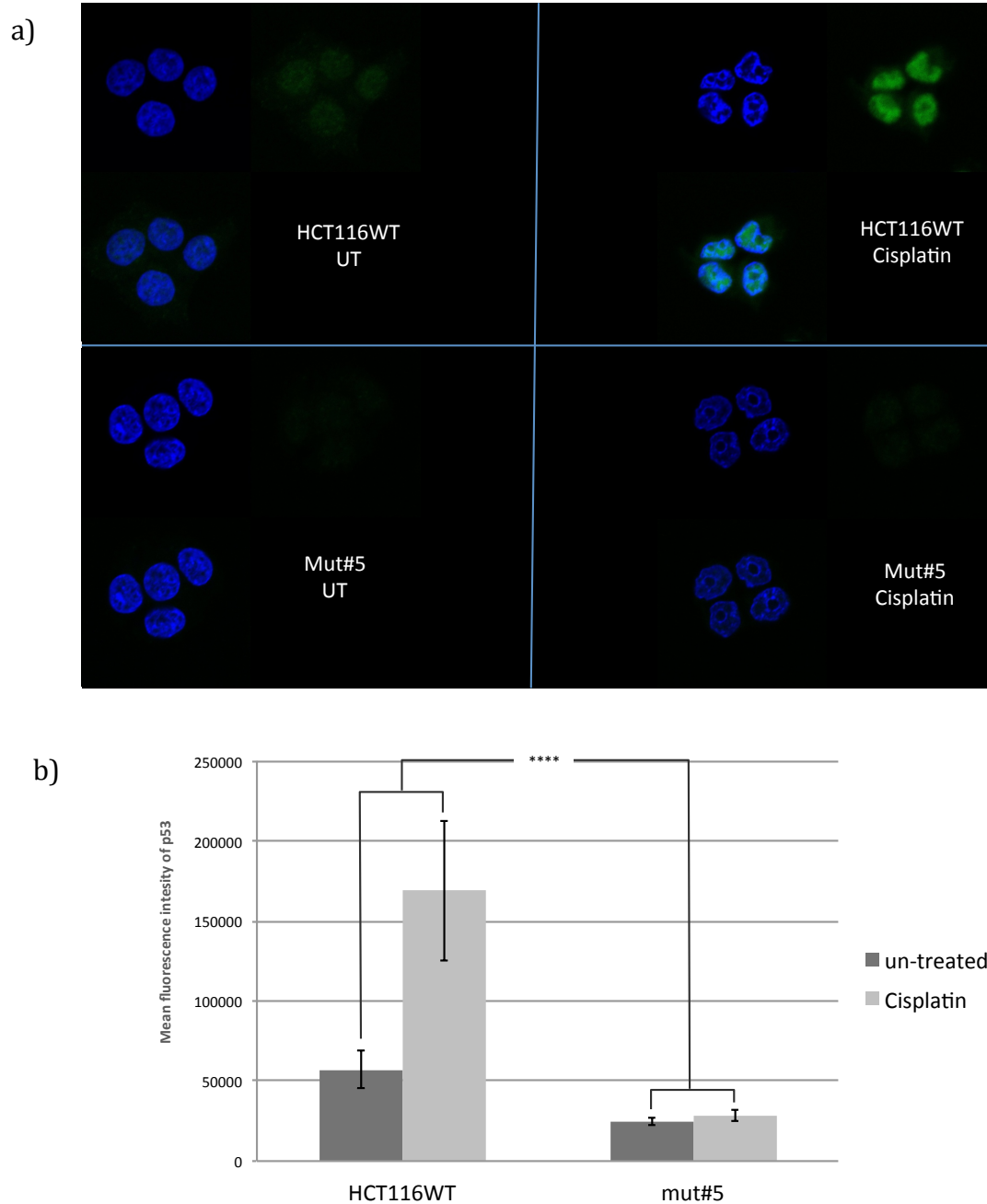


Figure 4.20: Confocal microscopic analysis of WT and mut#5 cells with and without stress. a) Confocal microscopy pictures of HCT116WT cells versus mut#5 showing p53 expression. The p53 protein is shown in green (488 2ndary antibody) and nuclei are shown in blue (DAPI staining). p53 is accumulated in the nuclei of HT116WT cells after treatment but no significant increase is detectable for mut#5 cells. b) p53 protein

amount in more than 200 cells are calculated for HCT116WT and mut#5 in normal condition and under genotoxic stress (Cisplatin treated in this case). Basal p53 amount is lower in mut#5 in comparison with WT cells, and it is not accumulated in the nuclei of mut#5 cells after Cisplatin treatment.

4.3.5. mRNA Amount for p53 and p53 Target Genes in CTM Cell Lines

To check if mRNA amount of the p53, p21, MDM2, and PUMA proteins in CTM cell lines and the WT cells are different, QRT PCR experiment was conducted, normalized to GAPDH gene transcription. The p53 target gene transcriptions are different in CTM cell lines; mRNA amount is significantly lower in p53 and all its target gene for mut#9 and mut#5 after Doxorubicin treatment. PUMA, p21, and p53 mRNA amounts are lower for mut#4 under stress. p53, p21, and MDM2 basal mRNA amount is significantly different in mut#5. Also, mut#9 has higher basal mRNA amount for MDM2 and PUMA genes (Figure 4.21).

The QRT PCR results are analyzed in a different way to check the change in mRNA amount of the p53, p21, PUMA, and MDM2 proteins before and after Doxorubicin treatment by normalizing each sample to its own un-treated mRNA amount (Figure 4.22).

To compare mRNA amount of p53 and its target genes, HCT116WT, HCT116KO, and mut#5 transcription patterns were compared separately. HCT116KO and mut#5 mRNA pattern is very similar in normal conditions and under stress (Figure 4.23).

According to some recent studies on CTD of the p53 protein and its relation with the telomere length, we compared mRNA amount for four telomere genes since cells with truncated p53 C-terminus tend to have shorter Telomeres¹⁴⁸. QRT PCR results showed different telomere gene transcription under normal conditions and after Doxorubicin treatment (Figure 4.23).

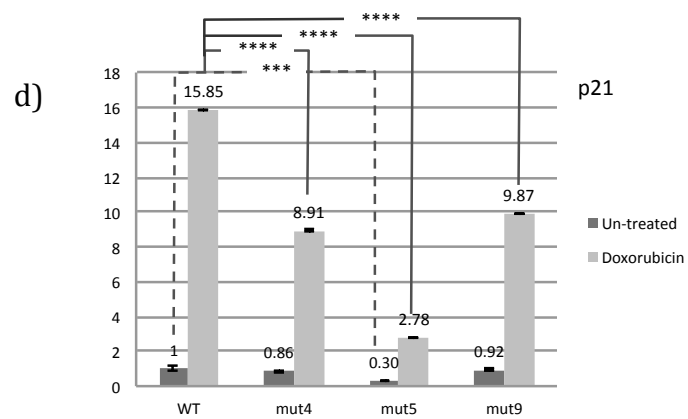
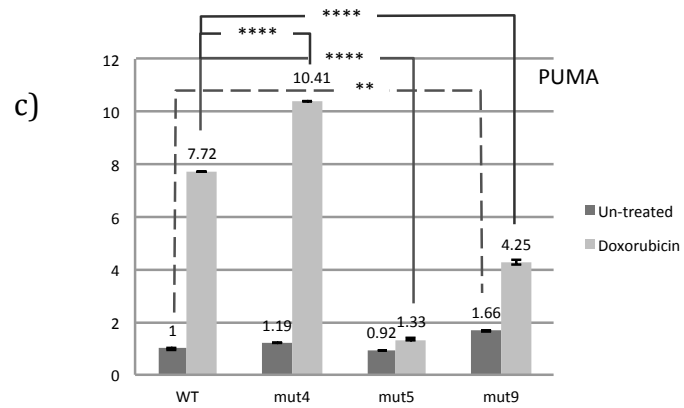
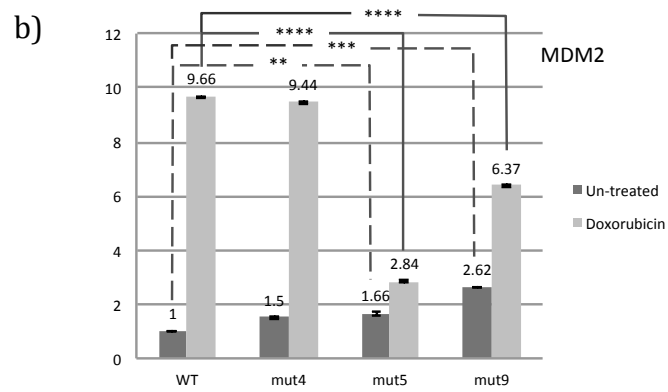
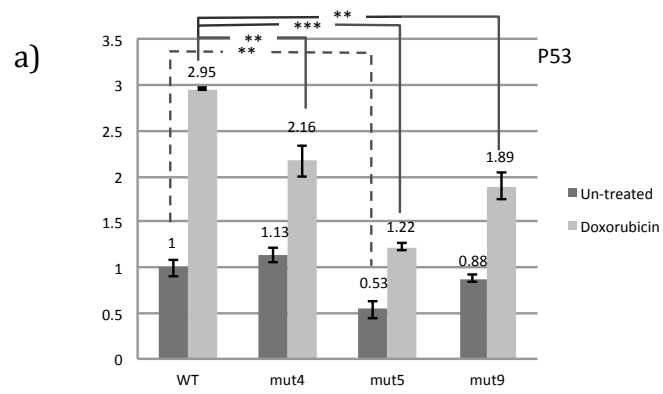


Figure 4.21: Quantitative realtime PCR analysis of p53, p21, MDM2, PUMA mRNA expression from WT, mut#4, mut#5, mut#9 cells (all normalized to HCT116WT untreated). a) p53 transcription drops in the CTM cell lines. Even under normal conditions, p53 mRNA amount of the WT cells is more than mut#5. b) MDM2 mRNA amount is higher in mut#5 and mut#9 under normal conditions, but they increase less than the WT cells after Doxorubicin treatment. c) PUMA mRNA amount in mut#5 is higher compared with WT cells, but the transcription of this gene is not increased as much in mut#5 and mut#9. d) p21 basal mRNA amount is lower in mut#5. After Doxorubicin treatment, p21 transcription is not increased as much as WT.

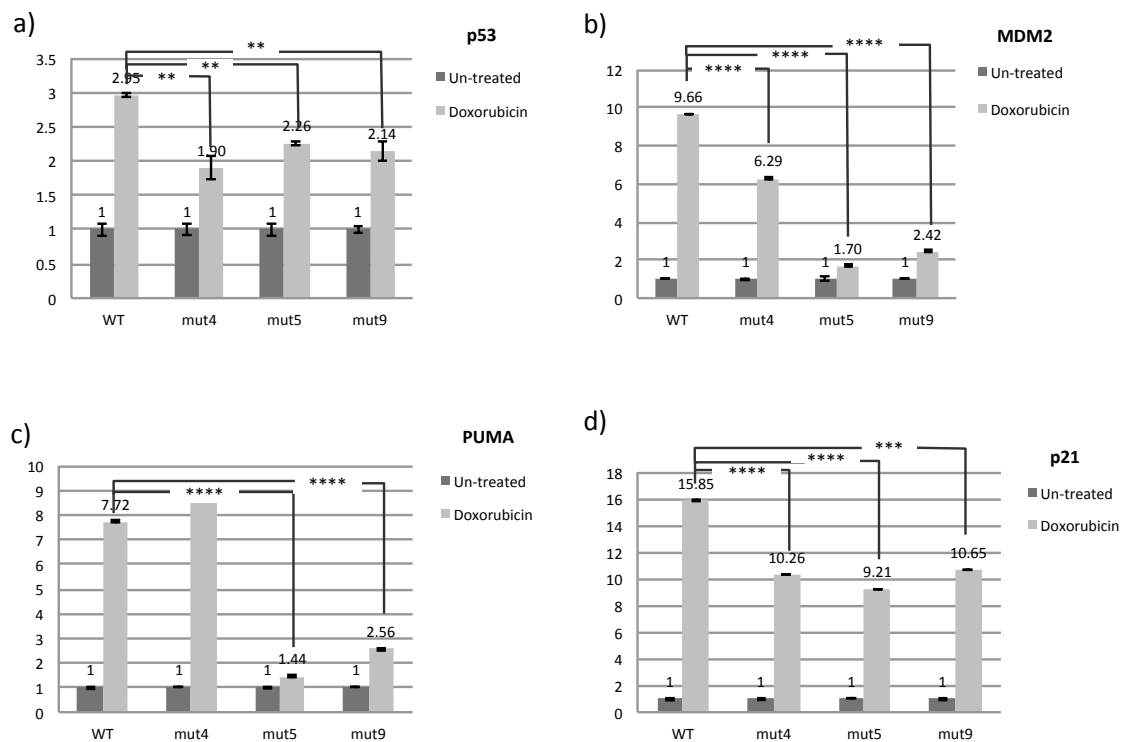


Figure 4.22: Quantitative realtime PCR analysis of p53, p21, MDM2, PUMA mRNA expression from WT, mut#4, mut#5, mut#9 cells (all normalized to their own untreated); transcription change in p53 and its target genes (p21, PUMA, MDM2) after Doxorubicin treatment (1 uM, 24h). a) p53 transcription does not increase as much as WT in CTM cell lines after Doxorubicin treatment. b) MDM2 mRNA amount shows the same pattern as p53 mRNA. c) PUMA transcription induces less than WT cells in mut#5 and mut#9. d) p21 mRNA amount increases not as much as WT in CTM cell lines.

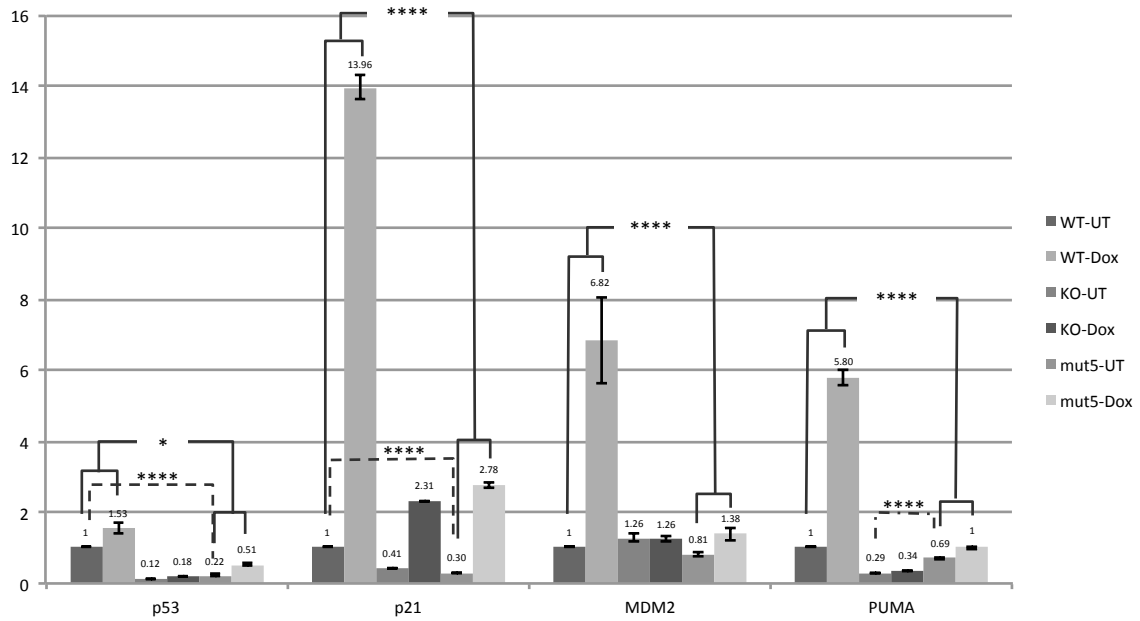
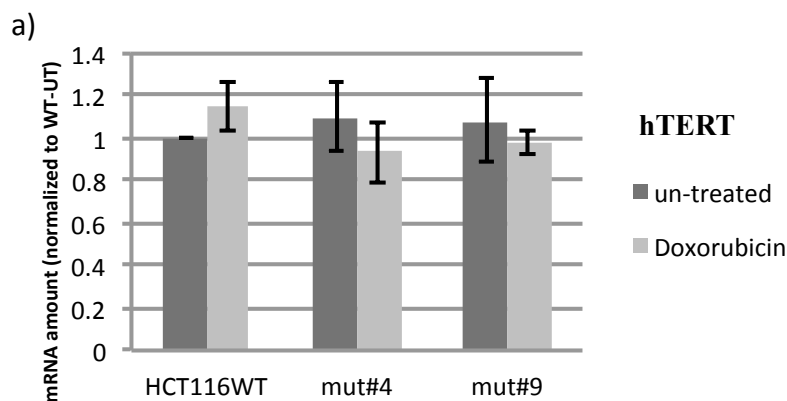


Figure 4.23: Quantitative real-time PCR analysis of p53, p21, MDM2, PUMA mRNA expression from HCT116WT, HCT116KO, and mut#5 under normal conditions (UT) vs. 24h 1 μ M Doxorubicin treatment (Dox). mut#5 transcription pattern for these genes is very similar to HCT116KO. The p53 protein in mut#5 lacks the last exon, but still its transcriptom resembles to HCT116KO that is p53 knock-out. p53 basic transcription is also lower (5 fold) in mut#5 compared to WT, and it doesn't increase as much under stress; the most robust difference is seen for p21. MDM2 transcription does not increase for HCT116KO and mut#5 under stress; PUMA mRNA amount for mut#5 is twice as much as HCT116KO, but still many folds less than HCT116WT.



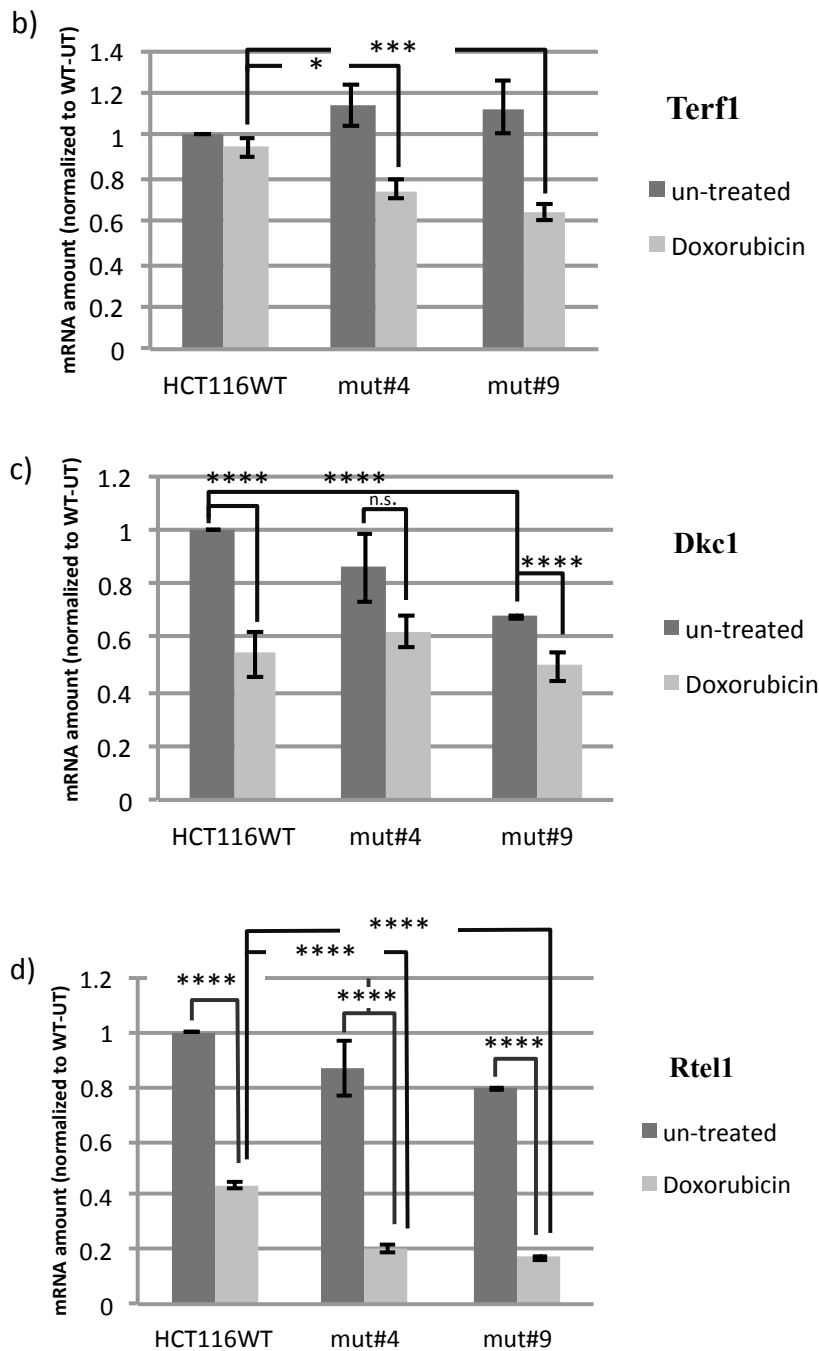


Figure 4.24: CTM cell lines have differentially expressed telomere genes. a) hTERT, the gene for catalytic subunit of the telomerase enzyme, is not differentially expressed in CTM cell lines. b) Terf1 encodes telomere specific protein, which is an inhibitor of telomerase. The mRNA amount drops more significantly for CTM cell lines after Doxorubicin treatment ($p=0.0044$ for mut#4 and $p=0.0009$ for mut#9). c) Dkc1 is a member of Shelterin protein complex that protect telomere tails. mut#9 and mut#4 decrease is less than HCT116WT after Doxorubicin treatment ($p=0.0001$). mRNA amount of Dkc1 gene in mut#9 is also less compared to WT cells. d) Rtel1 is the major determinant of the Telomere length; this gene's transcription drops significantly after Doxorubicin treatment in WT and mutant cells. mRNA amount of this gene in CTMs are significantly less than WT after Doxorubicin treatment ($p=0.0001$).

4.3.6. Cell Doubling Time Increase in CTM Cell Lines

During routine splitting of our CTM cell lines, we recognized a lower growth rate for mut#9 and mut#5 compared to HCT116WT cells. We experimentally confirmed this observation with xCELLigence experiment results, shown in Figure 4.25-28.

Although mut#5 and HCT116KO transcription pattern for p53, p21, PUMA, and MDM2 genes were very similar (Figure 4.23), but mut#5 cell doubling time is significantly longer than HCT116KO cells (Figure 4.26). To compare mut#5 and mut#9 doubling times, another xCELLigence experiment was conducted. We concluded that mut#5 grows slower than mut#9 and HCT116WT (Figure 4.27 and 7.28).

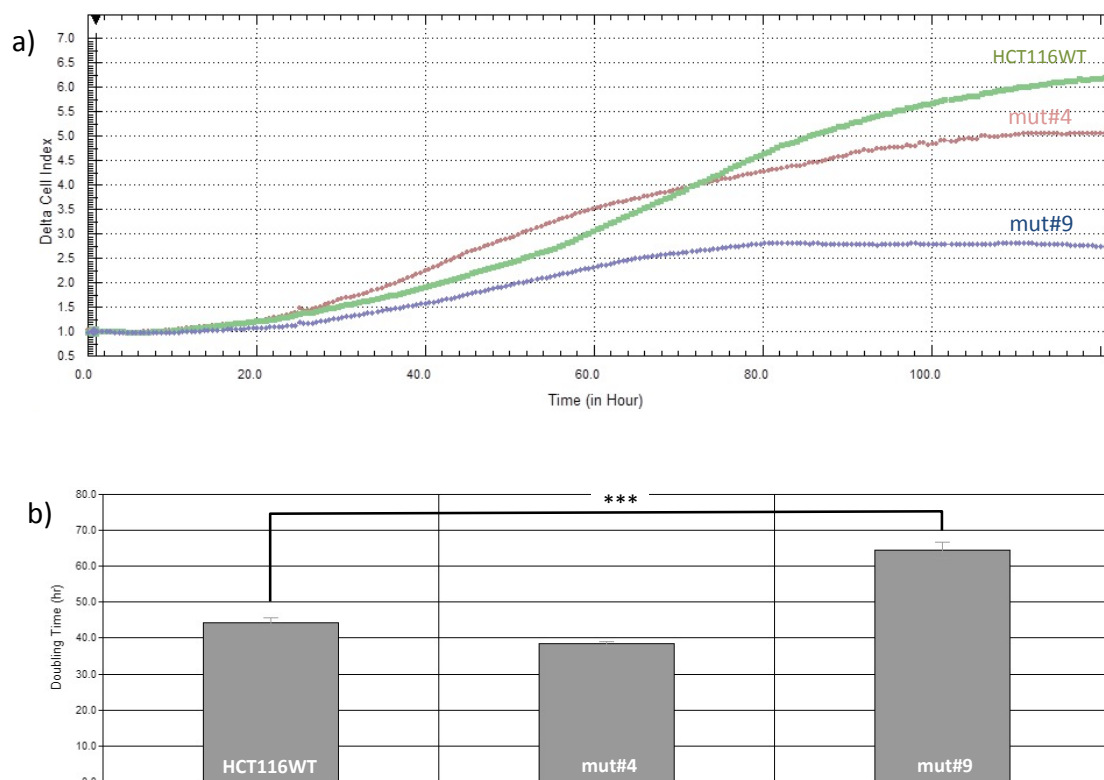


Figure 4.25: Doubling time analysis of HCT116WT cells in comparison with mut#4 and mut#9. a) HCT116WT cells divide faster than mut#9. b) The difference between doubling time of the three cell lines are shown; HCT116WT cells significantly (p=

0.0003) grow faster than mut#9. The difference between cell doubling time of mut#4 and HCT116WT is not significant ($p=0.02$).

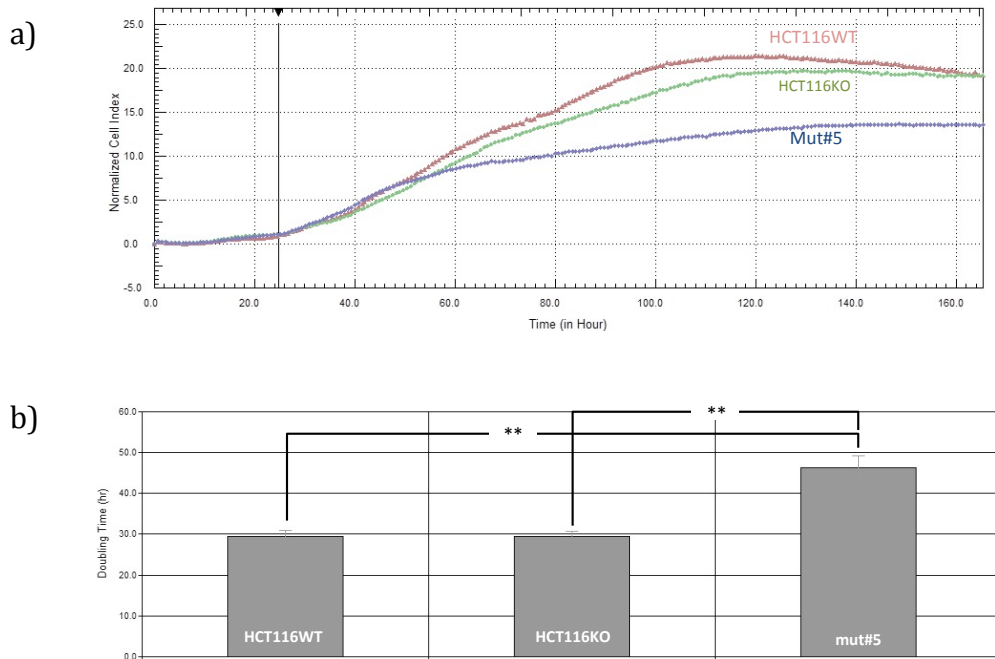


Figure 4.26: Growth rate comparison of HCT116WT and HCT116KO and mut#5 cells. a) mut#9 grows slower than HCT116WT and HCTKO, this can be an indicator of a mutant dominant effect of the p53 protein in mut#5. b) A significant difference ($p=0.0023$) between cell doubling time in HCT116WT/HCT116KO and mut#5.

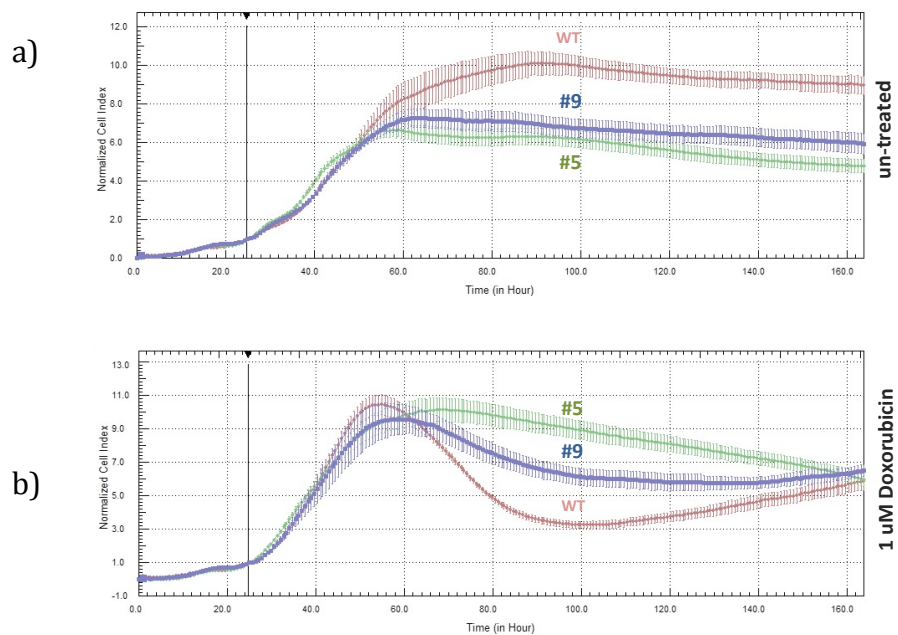


Figure 4.27: Analysis of doubling time in WT, mut#5, and mut#9 cells with or without stress. a) Real-time cell growth is shown for HCT116WT, mut#5, and mut#9 under normal condition (growth phase and plateau) or under stressed condition (1 uM Doxorubicin 24h treatment); mut#5 and mut#9 b) mut#5 cell doubling time is significantly higher than wild type cells and they do not lose volume as much as WT cells during apoptosis.

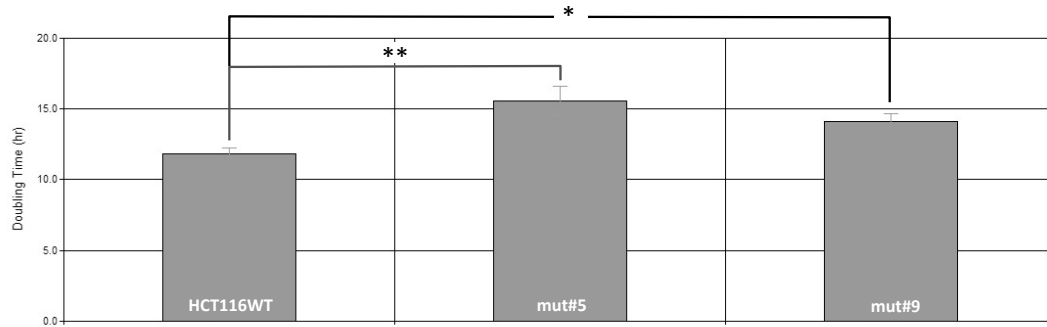


Figure 4.28: mut#5 and mut#9 cells grow slower than HCT116WT cells. Both CTM cell lines grow slower than HCT116WT. The difference between HCT116WT and mut#5 is more significant ($p = 0.01$) than the difference between HCT116WT and mut#9 ($p = 0.04$).

5. DISCUSSION

We demonstrated that p53 C-terminal is extremely crucial for the protein's function by studying the behavior of p53 CTM cell lines in basal condition and under different types of cellular stress, such as treatment by Doxorubicin, Cisplatin, or Nutlin and serum starvation. In this study, we investigated the different aspects of the p53 tumor suppressor protein, its transcriptional targets and also proteins that regulate p53 activation. We studied endogenous p53 by creating homozygous mutants using CRISPR/Cas9 technology. The focus of this study was three CTM cell lines that encode three different mutant types of p53 protein: 1) a truncated p53 protein (p53 $\Delta 21$ / $\Delta 21$) called mut#4; 2) a p53 protein missing the C-terminus encoded by the last p53 exon (p53 $\Delta 26$ / $\Delta 26$) called mut#5, and 3) a single amino acid deleted p53 protein (p53 $\Delta R379$ / $\Delta R379$) called mut#9.

p53 $\Delta 21$ / $\Delta 21$: p53 $\Delta 21$ / $\Delta 21$ or as mentioned in the thesis, mut#4, did not show any differences in the accumulation of the p53, p21, and PUMA proteins in the stressed cells. This CTM cell line could also bind to its DNA target as efficiently as the wild type cells. Therefore we concluded that p53 truncation of this mutant, is not affecting p53 accumulation, tetramerization, and DNA binding efficiency. The interesting point about this mutant was that unlike mut#5, which lacks the last 26 amino acids of its p53 protein, mut#4 had a non-wild type tail with the amino acid sequence (T

H V Q D R R A). This change in C-terminal amino acid sequence arises from a frame shift mutation. This tail could potentially behave similar to WT p53 protein by compensating for the important amino acid R379. Even though, in total, mut#4 is 13 amino acids shorter than the wild type p53 the presence of arginine amino acids in the last three positions may cause it to fold into a three dimensional shape and behave similar to WT p53. mut#4 does not demonstrate a very different transcription pattern from wild type cells in comparison with other two CTM cell lines (mut#5 and mut#9). It can increase the transcription of MDM2 and PUMA efficiently after Doxorubicin treatment. This shows the transcription factor activity of this mutant is not damaged as much as other CTM cell lines. Here we could refer to a target-dependent manner in which CTD influences DNA binding efficiency to its different targets^{128,131}. As for mut#4, p21 (high affinity distal binding site) mRNA amount is affected whereas PUMA (medium affinity distal binding site) and more specifically MDM2 (closely-spaced low affinity binding site) mRNA levels are not changed as much. This is consistent with the literature on the selective DNA anchoring ability of the CTD¹²⁸.

mut#4 also shows a different transcription pattern for some genes that play important roles in ribosome biogenesis stress. As mentioned in the introduction, ribosomal protein RPL11 is important in the recruitment of p300/CBP, which leads to p53 K382 acetylation and activation¹⁹. It is possible that the differentially transcribed ribosome biogenesis genes could partially be influenced by the absence of the K382 residues in this mutant.

p53 Δ 26 / Δ 26: p53 Δ 26 / Δ 26 totally lacks the last exon of the *Tp53* gene. This mutant, also called mut#5, displays a very different transcriptional pattern in comparison with wild type cells and also with our other CTM cell lines. The most robust phenotype detected in this mutant was the low accumulation of the p53 protein in the nucleus after genotoxic stress. The accumulation is almost undetectable in the nucleus, but not in the cytoplasm. Although there is no nuclear localization signal encoded by the last exon of the *Tp53* gene, the protein encoded by this mutant cannot translocate into the nucleus. It could be discussed that since p53 CTD post-translational modification plays an important role in p53 function⁵⁹, the deletion of the last exon that includes many PTM sites, influences p53 conformational change which in turn causes its translocation problem. It is expected that the p53 in mut#5 cannot induce its target genes because not only the p53 is not accumulated efficiently, but also it cannot enter

the nucleus to play its transcription factor role; this was validated by QRT PCR results. Furthermore, apoptotic mut#5 cells do not go through nuclear shrinkage properly; we observed this phenotype in the xCELLigence and confocal microscopy results.

In accordance to previous studies that proved the relationship between p53 CTD and telomere length, differentially transcribed genes Dkc1 and Rtel1 might be the main reason that mut#5 grows slower than HCT116WT¹⁴⁸. Another possibility is the effect of this deletion mutation on the Glycolysis pathway and consequently to the metabolism of the mutated cell. This mutant cell line transcribes p53 and several other genes that play crucial role in cell cycle arrest and apoptosis, in lower amounts, regardless of stress conditions. Furthermore, the transcription pattern of this mutant resembles HCT116KO that does not express p53 at all. On the contrary, HCT116KO cell doubling time is the same as HCT116WT. This contradiction could be explained by the presence of p47, which is a shorter isoform of p53 protein that is not detected in mut#5. It is reported that p47 accumulates under stress and can fulfill some of p53 responsibilities, such as cell death¹⁴⁹. This truncated protein is negatively regulated by p53, and is normally suppressed by the accumulation of the p53 protein, in the cell lines in which p53 is not expressed (e.g. HCT116KO). As a result p47 is expressed and accumulated possibly for the compensation of p53 protein. It is arguable that the difference in the cell growth rate of mut#5 and HCT116KO, while their transcription pattern for p53, p21, MDM2, and PUMA is very similar, is due to the presence of p47 in HCT116KO cells.

p53 ΔR379 / ΔR379: p53 ΔR379 / ΔR379 (mut#9) lacks one amino acid in its CTD. It is unexpected to observe significant phenotypic differences in this mutant since it lacks only one amino acid, which is barely mentioned in the literature. However, it is demonstrated that p53 in mut#9 cannot bind to its DNA target efficiently. It is very intriguing that one amino acid, that wasn't previously shown to play an important role in PTM in p53 studies, could make such an effect in the most important activity of the protein. As a result of this deficiency, it is presumable that transcription of p53 target genes in mut#9 is significantly lower, as we confirmed in our QRT PCR results. Moreover, telomere gene mRNA amount drops in this mutant. Additionally, we showed that mut#9 grows slower just like mut#5. This finding is interesting since this increase in cell doubling time is apparent in mut#9 and mut#5 (both lack R379), but not in mut#4 (which theoretically has R379). According to all these findings, it is possible to claim that R379 is extremely important in p53-dependant cell metabolism. In order

to further explore this argument, we are currently conducting mass spectrophotometry experiments with our CTM cell lines to compare their PTM pattern with wild type cells. Then we would be able to reach a more certain conclusion.

In conclusion, we showed how different mutations in the CTD of the p53 protein affect cells in various ways. Our contribution to the literature was to identify R379 as a very critical amino acid in the C-terminus, that influences cellular metabolism. We also demonstrated that the p53 CTD influences ribosome biogenesis by controlling the transcription of ribosomal protein genes (RNA-seq data). Finally we identify the region of the p53 protein encoded by the last exon of the *Tp53* gene as being critical for the activity, accumulation, and translocation of this protein.

REFERENCES

1. Leroy B, Anderson M, Soussi T. TP53 mutations in human cancer: database reassessment and prospects for the next decade. *Hum Mutat.* 2014;35(6):672-88. doi:10.1002/humu.22552.
2. Vogelstein B, Lane D, Levine AJ. Surfing the p53 network. *Nature.* 2000;408(6810):307-10. doi:10.1038/35042675.
3. Li FP, Fraumeni JF. Soft-tissue sarcomas, breast cancer, and other neoplasms. A familial syndrome? *Ann Intern Med.* 1969;71(4):747-52. Available at: <http://www.ncbi.nlm.nih.gov/pubmed/5360287>. Accessed June 20, 2016.
4. Malkin D, Li FP, Strong LC, et al. Germ line p53 mutations in a familial syndrome of breast cancer, sarcomas, and other neoplasms. *Science.* 1990;250(4985):1233-8. Available at: <http://www.ncbi.nlm.nih.gov/pubmed/1978757>. Accessed February 1, 2016.
5. el-Deiry WS. Regulation of p53 downstream genes. *Semin Cancer Biol.* 1998;8(5):345-57. Available at: <http://www.ncbi.nlm.nih.gov/pubmed/10101800>. Accessed June 11, 2016.
6. Bieging KT, Mello SS, Attardi LD. Unravelling mechanisms of p53-mediated tumour suppression. *Nat Rev Cancer.* 2014;14(5):359-70. doi:10.1038/nrc3711.
7. Wade M, Li Y-C, Wahl GM. MDM2, MDMX and p53 in oncogenesis and cancer therapy. *Nat Rev Cancer.* 2013;13(2):83-96. doi:10.1038/nrc3430.
8. Linke K, Mace PD, Smith CA, Vaux DL, Silke J, Day CL. Structure of the MDM2/MDMX RING domain heterodimer reveals dimerization is required for their ubiquitylation in trans. *Cell Death Differ.* 2008;15(5):841-8. doi:10.1038/sj.cdd.4402309.
9. Popowicz GM, Czarna A, Holak TA. Structure of the human Mdmx protein bound to the p53 tumor suppressor transactivation domain. *Cell Cycle.* 2008;7(15):2441-3. doi:10.4161/cc.6365.
10. Chao CC-K. Mechanisms of p53 degradation. *Clin Chim Acta.* 2015;438:139-147. doi:10.1016/j.cca.2014.08.015.
11. Golomb L, Volarevic S, Oren M. p53 and ribosome biogenesis stress: The essentials. *FEBS Lett.* 2014;588(16):2571-2579. doi:10.1016/j.febslet.2014.04.014.
12. Montanaro L, Treré D, Derenzini M. Changes in ribosome biogenesis may induce cancer by down-regulating the cell tumor suppressor potential. *Biochim Biophys Acta - Rev Cancer.* 2012;1825(1):101-110. doi:10.1016/j.bbcan.2011.10.006.
13. Leary D, Huang S. Regulation of ribosome biogenesis within the nucleolus.

- FEBS Lett.* 2001;509(2):145-50. doi:FEBS Lett. 2001 Dec 7;509(2):145-50.
14. Ben-Shem A, Garreau de Loubresse N, Melnikov S, Jenner L, Yusupova G, Yusupov M. The structure of the eukaryotic ribosome at 3.0 Å resolution. *Science*. 2011;334(6062):1524-9. doi:10.1126/science.1212642.
 15. Shav-Tal Y, Blechman J, Darzacq X, et al. Dynamic Sorting of Nuclear Components into Distinct Nucleolar Caps during Transcriptional Inhibition. *Mol Biol Cell*. 2005;16(5):2395-2413. doi:10.1091/mbc.E04-11-0992.
 16. Rubbi CP, Milner J, Abrahams P, et al. Disruption of the nucleolus mediates stabilization of p53 in response to DNA damage and other stresses. *EMBO J*. 2003;22(22):6068-6077. doi:10.1093/emboj/cdg579.
 17. Pestov DG, Strezoska Z, Lau LF. Evidence of p53-Dependent Cross-Talk between Ribosome Biogenesis and the Cell Cycle: Effects of Nucleolar Protein Bop1 on G1/S Transition. *Mol Cell Biol*. 2001;21(13):4246-4255. doi:10.1128/MCB.21.13.4246-4255.2001.
 18. Yuan X, Zhou Y, Casanova E, et al. Genetic inactivation of the transcription factor TIF-IA leads to nucleolar disruption, cell cycle arrest, and p53-mediated apoptosis. *Mol Cell*. 2005;19(1):77-87. doi:10.1016/j.molcel.2005.05.023.
 19. Zhang Y, Wolf GW, Bhat K, et al. Ribosomal protein L11 negatively regulates oncoprotein MDM2 and mediates a p53-dependent ribosomal-stress checkpoint pathway. *Mol Cell Biol*. 2003;23(23):8902-12. Available at: <http://www.ncbi.nlm.nih.gov/pubmed/14612427>. Accessed July 20, 2016.
 20. Mahata B, Sundqvist A, Xirodimas DP. Recruitment of RPL11 at promoter sites of p53-regulated genes upon nucleolar stress through NEDD8 and in an Mdm2-dependent manner. *Oncogene*. 2012;31(25):3060-71. doi:10.1038/onc.2011.482.
 21. Marechal V, Elenbaas B, Piette J, Nicolas JC, Levine AJ. The ribosomal L5 protein is associated with mdm-2 and mdm-2-p53 complexes. *Mol Cell Biol*. 1994;14(11):7414-20. Available at: <http://www.ncbi.nlm.nih.gov/pubmed/7935455>. Accessed July 20, 2016.
 22. Joerger AC, Fersht AR. Structural biology of the tumor suppressor p53. *Annu Rev Biochem*. 2008;77:557-82. doi:10.1146/annurev.biochem.77.060806.091238.
 23. Uversky VN, Davé V, Iakoucheva LM, et al. Pathological unfoldomics of uncontrolled chaos: intrinsically disordered proteins and human diseases. *Chem Rev*. 2014;114(13):6844-79. doi:10.1021/cr400713r.
 24. Zhang X, Wen H, Shi X. Lysine methylation: beyond histones. *Acta Biochim Biophys Sin (Shanghai)*. 2012;44(1):14-27. doi:10.1093/abbs/gmr100.
 25. Wells M, Tidow H, Rutherford TJ, et al. Structure of tumor suppressor p53 and its intrinsically disordered N-terminal transactivation domain. *Proc Natl Acad Sci U S A*. 2008;105(15):5762-7. doi:10.1073/pnas.0801353105.
 26. Schon O, Friedler A, Bycroft M, Freund SM V, Fersht AR. Molecular

- mechanism of the interaction between MDM2 and p53. *J Mol Biol.* 2002;323(3):491-501. Available at: <http://www.ncbi.nlm.nih.gov/pubmed/12381304>. Accessed June 14, 2016.
27. Honda R, Tanaka H, Yasuda H. Oncoprotein MDM2 is a ubiquitin ligase E3 for tumor suppressor p53. *FEBS Lett.* 1997;420(1):25-7. Available at: <http://www.ncbi.nlm.nih.gov/pubmed/9450543>. Accessed June 23, 2016.
 28. Avantaggiati ML, Ogryzko V, Gardner K, Giordano A, Levine AS, Kelly K. Recruitment of p300/CBP in p53-dependent signal pathways. *Cell.* 1997;89(7):1175-84. Available at: <http://www.ncbi.nlm.nih.gov/pubmed/9215639>. Accessed June 23, 2016.
 29. Lin J, Chen J, Elenbaas B, Levine AJ. Several hydrophobic amino acids in the p53 amino-terminal domain are required for transcriptional activation, binding to mdm-2 and the adenovirus 5 E1B 55-kD protein. *Genes Dev.* 1994;8(10):1235-1246. doi:10.1101/gad.8.10.1235.
 30. Poyurovsky M V, Katz C, Laptenko O, et al. The C terminus of p53 binds the N-terminal domain of MDM2. *Nat Struct Mol Biol.* 2010;17(8):982-9. doi:10.1038/nsmb.1872.
 31. Chehab NH, Malikzay A, Stavridi ES, Halazonetis TD. Phosphorylation of Ser-20 mediates stabilization of human p53 in response to DNA damage. *Proc Natl Acad Sci U S A.* 1999;96(24):13777-82. Available at: <http://www.ncbi.nlm.nih.gov/pubmed/10570149>. Accessed June 23, 2016.
 32. Sakaguchi K, Saito S, Higashimoto Y, Roy S, Anderson CW, Appella E. Damage-mediated phosphorylation of human p53 threonine 18 through a cascade mediated by a casein 1-like kinase. Effect on Mdm2 binding. *J Biol Chem.* 2000;275(13):9278-83. Available at: <http://www.ncbi.nlm.nih.gov/pubmed/10734067>. Accessed June 23, 2016.
 33. Lambert PF, Kashanchi F, Radonovich MF, Shiekhata R, Brady JN. Phosphorylation of p53 serine 15 increases interaction with CBP. *J Biol Chem.* 1998;273(49):33048-53. Available at: <http://www.ncbi.nlm.nih.gov/pubmed/9830059>. Accessed June 23, 2016.
 34. el-Deiry WS, Kern SE, Pietenpol JA, Kinzler KW, Vogelstein B. Definition of a consensus binding site for p53. *Nat Genet.* 1992;1(1):45-9. doi:10.1038/ng0492-45.
 35. Wei C-L, Wu Q, Vega VB, et al. A global map of p53 transcription-factor binding sites in the human genome. *Cell.* 2006;124(1):207-19. doi:10.1016/j.cell.2005.10.043.
 36. Weinberg RL, Veprintsev DB, Fersht AR. Cooperative binding of tetrameric p53 to DNA. *J Mol Biol.* 2004;341(5):1145-59. doi:10.1016/j.jmb.2004.06.071.
 37. Stavridi ES, Chehab NH, Caruso LC, Halazonetis TD. Change in oligomerization specificity of the p53 tetramerization domain by hydrophobic amino acid substitutions. *Protein Sci.* 1999;8(9):1773-9. doi:10.1110/ps.8.9.1773.

38. Butler JS, Loh SN. Zn(2+)-dependent misfolding of the p53 DNA binding domain. *Biochemistry*. 2007;46(10):2630-9. doi:10.1021/bi062106y.
39. Cho Y, Gorina S, Jeffrey PD, Pavletich NP. Crystal structure of a p53 tumor suppressor-DNA complex: understanding tumorigenic mutations. *Science*. 1994;265(5170):346-55. Available at: <http://www.ncbi.nlm.nih.gov/pubmed/8023157>. Accessed June 23, 2016.
40. Bargonetti J, Reynisdóttir I, Friedman PN, Prives C. Site-specific binding of wild-type p53 to cellular DNA is inhibited by SV40 T antigen and mutant p53. *Genes Dev*. 1992;6(10):1886-98. Available at: <http://www.ncbi.nlm.nih.gov/pubmed/1398068>. Accessed June 23, 2016.
41. Bullock AN, Henckel J, DeDecker BS, et al. Thermodynamic stability of wild-type and mutant p53 core domain. *Proc Natl Acad Sci U S A*. 1997;94(26):14338-42. Available at: <http://www.ncbi.nlm.nih.gov/pubmed/9405613>. Accessed June 23, 2016.
42. Pfeifer GP, Denissenko MF, Olivier M, Tretyakova N, Hecht SS, Hainaut P. Tobacco smoke carcinogens, DNA damage and p53 mutations in smoking-associated cancers. *Oncogene*. 2002;21(48):7435-51. doi:10.1038/sj.onc.1205803.
43. Mochan TA, Venere M, DiTullio RA, Halazonetis TD. 53BP1 and NFB1/MDC1-Nbs1 function in parallel interacting pathways activating ataxia-telangiectasia mutated (ATM) in response to DNA damage. *Cancer Res*. 2003;63(24):8586-91. Available at: <http://www.ncbi.nlm.nih.gov/pubmed/14695167>. Accessed June 26, 2016.
44. Gorina S, Pavletich NP. Structure of the p53 tumor suppressor bound to the ankyrin and SH3 domains of 53BP2. *Science*. 1996;274(5289):1001-5. Available at: <http://www.ncbi.nlm.nih.gov/pubmed/8875926>. Accessed June 26, 2016.
45. Lee W, Harvey TS, Yin Y, Yau P, Litchfield D, Arrowsmith CH. Solution structure of the tetrameric minimum transforming domain of p53. *Nat Struct Biol*. 1994;1(12):877-90. Available at: <http://www.ncbi.nlm.nih.gov/pubmed/7773777>. Accessed June 25, 2016.
46. Clore GM, Ernst J, Clubb R, et al. Refined solution structure of the oligomerization domain of the tumour suppressor p53. *Nat Struct Biol*. 1995;2(4):321-33. Available at: <http://www.ncbi.nlm.nih.gov/pubmed/7796267>. Accessed June 25, 2016.
47. Hollstein M, Sidransky D, Vogelstein B, Harris CC. p53 mutations in human cancers. *Science*. 1991;253(5015):49-53. Available at: <http://www.ncbi.nlm.nih.gov/pubmed/1905840>. Accessed June 25, 2016.
48. Johnson CR, Morin PE, Arrowsmith CH, Freire E. Thermodynamic analysis of the structural stability of the tetrameric oligomerization domain of p53 tumor suppressor. *Biochemistry*. 1995;34(16):5309-16. Available at: <http://www.ncbi.nlm.nih.gov/pubmed/7727392>. Accessed June 25, 2016.

49. Shaulian E, Zauberman A, Ginsberg D, Oren M. Identification of a minimal transforming domain of p53: negative dominance through abrogation of sequence-specific DNA binding. *Mol Cell Biol.* 1992;12(12):5581-92. Available at: <http://www.ncbi.nlm.nih.gov/pubmed/1448088>. Accessed June 25, 2016.
50. McCoy M, Stavridi ES, Waterman JL, Wieczorek AM, Opella SJ, Halazonetis TD. Hydrophobic side-chain size is a determinant of the three-dimensional structure of the p53 oligomerization domain. *EMBO J.* 1997;16(20):6230-6. doi:10.1093/emboj/16.20.6230.
51. Mateu MG, Fersht AR. Mutually compensatory mutations during evolution of the tetramerization domain of tumor suppressor p53 lead to impaired hetero-oligomerization. *Proc Natl Acad Sci U S A.* 1999;96(7):3595-9. Available at: <http://www.ncbi.nlm.nih.gov/pubmed/10097082>. Accessed June 25, 2016.
52. Gaglia G, Guan Y, Shah J V, Lahav G. Activation and control of p53 tetramerization in individual living cells. *Proc Natl Acad Sci U S A.* 2013;110(38):15497-501. doi:10.1073/pnas.1311126110.
53. Kusano K, Sakaguchi M, Kagawa N, Waterman MR, Omura T. Microsomal p450s use specific proline-rich sequences for efficient folding, but not for maintenance of the folded structure. *J Biochem.* 2001;129(2):259-69. Available at: <http://www.ncbi.nlm.nih.gov/pubmed/11173528>. Accessed June 25, 2016.
54. Yu H, Chen JK, Feng S, Dalgarno DC, Brauer AW, Schreiber SL. Structural basis for the binding of proline-rich peptides to SH3 domains. *Cell.* 1994;76(5):933-45. Available at: <http://www.ncbi.nlm.nih.gov/pubmed/7510218>. Accessed June 25, 2016.
55. Walker KK, Levine AJ. Identification of a novel p53 functional domain that is necessary for efficient growth suppression. *Proc Natl Acad Sci U S A.* 1996;93(26):15335-40. Available at: <http://www.ncbi.nlm.nih.gov/pubmed/8986812>. Accessed June 25, 2016.
56. Gu W, Shi XL, Roeder RG. Synergistic activation of transcription by CBP and p53. *Nature.* 1997;387(6635):819-23. doi:10.1038/42972.
57. Xu Y. Regulation of p53 responses by post-translational modifications. *Cell Death Differ.* 2003;10(4):400-3. doi:10.1038/sj.cdd.4401182.
58. Ayed A, Mulder FA, Yi GS, Lu Y, Kay LE, Arrowsmith CH. Latent and active p53 are identical in conformation. *Nat Struct Biol.* 2001;8(9):756-60. doi:10.1038/nsb0901-756.
59. Appella E, Anderson CW. Signaling to p53: breaking the posttranslational modification code. *Pathol Biol (Paris).* 2000;48(3):227-45. Available at: <http://www.ncbi.nlm.nih.gov/pubmed/10858956>. Accessed June 25, 2016.
60. Avalos JL, Celic I, Muhammad S, Cosgrove MS, Boeke JD, Wolberger C. Structure of a Sir2 enzyme bound to an acetylated p53 peptide. *Mol Cell.* 2002;10(3):523-35. Available at: <http://www.ncbi.nlm.nih.gov/pubmed/12408821>. Accessed June 25, 2016.

61. Rustandi RR, Baldisseri DM, Weber DJ. Structure of the negative regulatory domain of p53 bound to S100B(betabeta). *Nat Struct Biol.* 2000;7(7):570-4. doi:10.1038/76797.
62. Denu JM. Linking chromatin function with metabolic networks: Sir2 family of NAD(+)-dependent deacetylases. *Trends Biochem Sci.* 2003;28(1):41-8. Available at: <http://www.ncbi.nlm.nih.gov/pubmed/12517451>. Accessed June 25, 2016.
63. Ferreira DMS, Afonso MB, Rodrigues PM, et al. c-Jun N-Terminal Kinase 1/c-Jun Activation of the p53/MicroRNA 34a/Sirtuin 1 Pathway Contributes to Apoptosis Induced by Deoxycholic Acid in Rat Liver. *Mol Cell Biol.* 2014;34(6):1100-1120. doi:10.1128/MCB.00420-13.
64. Du L, Lyle CS, Obey TB, et al. Inhibition of cell proliferation and cell cycle progression by specific inhibition of basal JNK activity: evidence that mitotic Bcl-2 phosphorylation is JNK-independent. *J Biol Chem.* 2004;279(12):11957-66. doi:10.1074/jbc.M304935200.
65. Shi Y, Nikulenkov F, Zawacka-Pankau J, et al. ROS-dependent activation of JNK converts p53 into an efficient inhibitor of oncogenes leading to robust apoptosis. *Cell Death Differ.* 2014;21(4):612-623. doi:10.1038/cdd.2013.186.
66. Belyi VA, Ak P, Markert E, et al. The origins and evolution of the p53 family of genes. *Cold Spring Harb Perspect Biol.* 2010;2(6):a001198. doi:10.1101/cshperspect.a001198.
67. Srivastava M, Simakov O, Chapman J, et al. The Amphimedon queenslandica genome and the evolution of animal complexity. *Nature.* 2010;466(7307):720-726. doi:10.1038/nature09201.
68. King N, Westbrook MJ, Young SL, et al. The genome of the choanoflagellate Monosiga brevicollis and the origin of metazoans. *Nature.* 2008;451(7180):783-8. doi:10.1038/nature06617.
69. Lu W-J, Amatruda JF, Abrams JM. p53 ancestry: gazing through an evolutionary lens. *Nat Rev Cancer.* 2009;9(10):758-62. doi:10.1038/nrc2732.
70. Dötsch V, Bernassola F, Coutandin D, Candi E, Melino G. p63 and p73, the ancestors of p53. *Cold Spring Harb Perspect Biol.* 2010;2(9):a004887. doi:10.1101/cshperspect.a004887.
71. Lane DP, Madhumalar A, Lee AP, et al. Conservation of all three p53 family members and Mdm2 and Mdm4 in the cartilaginous fish. *Cell Cycle.* 2011;10(24):4272-9. doi:10.4161/cc.10.24.18567.
72. Brandt T, Kaar JL, Fersht AR, Veprintsev DB. Stability of p53 homologs. *PLoS One.* 2012;7(10):e47889. doi:10.1371/journal.pone.0047889.
73. Khoo KH, Andreeva A, Fersht AR. Adaptive evolution of p53 thermodynamic stability. *J Mol Biol.* 2009;393(1):161-75. doi:10.1016/j.jmb.2009.08.013.
74. Joerger AC, Wilcken R, Andreeva A. Tracing the evolution of the p53 tetramerization domain. *Structure.* 2014;22(9):1301-10.

doi:10.1016/j.str.2014.07.010.

75. Heering J, Jonker HRA, Löhr F, Schwalbe H, Dötsch V. Structural investigations of the p53/p73 homologs from the tunicate species *Ciona intestinalis* reveal the sequence requirements for the formation of a tetramerization domain. *Protein Sci.* 2016;25(2):410-22. doi:10.1002/pro.2830.
76. Rutkowski R, Hofmann K, Gartner A. Phylogeny and function of the invertebrate p53 superfamily. *Cold Spring Harb Perspect Biol.* 2010;2(7):a001131. doi:10.1101/cshperspect.a001131.
77. Lane DP, Cheok CF, Brown C, Madhumalar A, Ghadessy FJ, Verma C. Mdm2 and p53 are highly conserved from placozoans to man. *Cell Cycle.* 2010;9(3):540-7. doi:10.4161/cc.9.3.10516.
78. Lane DP, Verma C. Mdm2 in evolution. *Genes Cancer.* 2012;3(3-4):320-4. doi:10.1177/1947601912458285.
79. Coffill CR, Lee AP, Siau JW, et al. The p53-Mdm2 interaction and the E3 ligase activity of Mdm2/Mdm4 are conserved from lampreys to humans. *Genes Dev.* 2016;30(3):281-92. doi:10.1101/gad.274118.115.
80. Momand J, Villegas A, Belyi VA. The evolution of MDM2 family genes. *Gene.* 2011;486(1-2):23-30. doi:10.1016/j.gene.2011.06.030.
81. Mendoza M, Mandani G, Momand J. The MDM2 gene family. *Biomol Concepts.* 2014;5(1):9-19. doi:10.1515/bmc-2013-0027.
82. Tai E, Benchimol S. TRIMming p53 for ubiquitination. *Proc Natl Acad Sci U S A.* 2009;106(28):11431-2. doi:10.1073/pnas.0905997106.
83. Cordani M, Pacchiana R, Butera G, D'Orazi G, Scarpa A, Donadelli M. Mutant p53 proteins alter cancer cell secretome and tumour microenvironment: Involvement in cancer invasion and metastasis. *Cancer Lett.* 2016;376(2):303-9. doi:10.1016/j.canlet.2016.03.046.
84. Ubertini V, Norelli G, D'Arcangelo D, et al. Mutant p53 gains new function in promoting inflammatory signals by repression of the secreted interleukin-1 receptor antagonist. *Oncogene.* 2015;34(19):2493-504. doi:10.1038/onc.2014.191.
85. Downing S, Bumak C, Nixdorf S, Ow K, Russell P, Jackson P. Elevated levels of prostate-specific antigen (PSA) in prostate cancer cells expressing mutant p53 is associated with tumor metastasis. *Mol Carcinog.* 2003;38(3):130-40. doi:10.1002/mc.10154.
86. Fontemaggi G, Dell'Orso S, Trisciuglio D, et al. The execution of the transcriptional axis mutant p53, E2F1 and ID4 promotes tumor neo-angiogenesis. *Nat Struct Mol Biol.* 2009;16(10):1086-93. doi:10.1038/nsmb.1669.
87. Zhang C, Liu J, Liang Y, et al. Tumour-associated mutant p53 drives the Warburg effect. *Nat Commun.* 2013;4:2935. doi:10.1038/ncomms3935.
88. Bensaad K, Tsuruta A, Selak MA, et al. TIGAR, a p53-inducible regulator of

- glycolysis and apoptosis. *Cell*. 2006;126(1):107-20. doi:10.1016/j.cell.2006.05.036.
89. Zhang C, Lin M, Wu R, et al. Parkin, a p53 target gene, mediates the role of p53 in glucose metabolism and the Warburg effect. *Proc Natl Acad Sci U S A*. 2011;108(39):16259-64. doi:10.1073/pnas.1113884108.
 90. Petitjean A, Mathe E, Kato S, et al. Impact of mutant p53 functional properties on TP53 mutation patterns and tumor phenotype: lessons from recent developments in the IARC TP53 database. *Hum Mutat*. 2007;28(6):622-9. doi:10.1002/humu.20495.
 91. Li XL, Jones MF, Subramanian M, Lal A. Mutant p53 exerts oncogenic effects through microRNAs and their target gene networks. *FEBS Lett*. 2014;588(16):2610-5. doi:10.1016/j.febslet.2014.03.054.
 92. Santoro R, Strano S, Blandino G. Transcriptional regulation by mutant p53 and oncogenesis. *Subcell Biochem*. 2014;85:91-103. doi:10.1007/978-94-017-9211-0_5.
 93. Kung C-P, Leu JI-J, Basu S, et al. The P72R Polymorphism of p53 Predisposes to Obesity and Metabolic Dysfunction. *Cell Rep*. 2016;14(10):2413-25. doi:10.1016/j.celrep.2016.02.037.
 94. Lane D. p53: out of Africa. *Genes Dev*. 2016;30(8):876-7. doi:10.1101/gad.281733.116.
 95. Muller PAJ, Vousden KH. Mutant p53 in cancer: new functions and therapeutic opportunities. *Cancer Cell*. 2014;25(3):304-17. doi:10.1016/j.ccr.2014.01.021.
 96. Butler JS, Loh SN. Kinetic partitioning during folding of the p53 DNA binding domain. *J Mol Biol*. 2005;350(5):906-18. doi:10.1016/j.jmb.2005.05.060.
 97. Bullock AN, Henckel J, Fersht AR. Quantitative analysis of residual folding and DNA binding in mutant p53 core domain: definition of mutant states for rescue in cancer therapy. *Oncogene*. 2000;19(10):1245-56. doi:10.1038/sj.onc.1203434.
 98. Dearth LR, Qian H, Wang T, et al. Inactive full-length p53 mutants lacking dominant wild-type p53 inhibition highlight loss of heterozygosity as an important aspect of p53 status in human cancers. *Carcinogenesis*. 2007;28(2):289-98. doi:10.1093/carcin/bgl132.
 99. Ang HC, Joerger AC, Mayer S, Fersht AR. Effects of common cancer mutations on stability and DNA binding of full-length p53 compared with isolated core domains. *J Biol Chem*. 2006;281(31):21934-41. doi:10.1074/jbc.M604209200.
 100. Joerger AC, Ang HC, Fersht AR. Structural basis for understanding oncogenic p53 mutations and designing rescue drugs. *Proc Natl Acad Sci U S A*. 2006;103(41):15056-61. doi:10.1073/pnas.0607286103.
 101. Suad O, Rozenberg H, Brosh R, et al. Structural basis of restoring sequence-specific DNA binding and transactivation to mutant p53 by suppressor mutations. *J Mol Biol*. 2009;385(1):249-65. doi:10.1016/j.jmb.2008.10.063.

102. Butler JS, Loh SN. Structure, function, and aggregation of the zinc-free form of the p53 DNA binding domain. *Biochemistry*. 2003;42(8):2396-403. doi:10.1021/bi026635n.
103. Xu J, Reumers J, Couceiro JR, et al. Gain of function of mutant p53 by coaggregation with multiple tumor suppressors. *Nat Chem Biol*. 2011;7(5):285-95. doi:10.1038/nchembio.546.
104. DiGiammarino EL, Lee AS, Cadwell C, et al. A novel mechanism of tumorigenesis involving pH-dependent destabilization of a mutant p53 tetramer. *Nat Struct Biol*. 2002;9(1):12-6. doi:10.1038/nsb730.
105. Lang GA, Iwakuma T, Suh Y-A, et al. Gain of function of a p53 hot spot mutation in a mouse model of Li-Fraumeni syndrome. *Cell*. 2004;119(6):861-72. doi:10.1016/j.cell.2004.11.006.
106. Olive KP, Tuveson DA, Ruhe ZC, et al. Mutant p53 gain of function in two mouse models of Li-Fraumeni syndrome. *Cell*. 2004;119(6):847-60. doi:10.1016/j.cell.2004.11.004.
107. Keeling KM, Xue X, Gunn G, Bedwell DM. Therapeutics based on stop codon readthrough. *Annu Rev Genomics Hum Genet*. 2014;15:371-94. doi:10.1146/annurev-genom-091212-153527.
108. Lee H-LR, Dougherty JP. Pharmaceutical therapies to recode nonsense mutations in inherited diseases. *Pharmacol Ther*. 2012;136(2):227-66. doi:10.1016/j.pharmthera.2012.07.007.
109. Issaeva N, Bozko P, Enge M, et al. Small molecule RITA binds to p53, blocks p53-HDM-2 interaction and activates p53 function in tumors. *Nat Med*. 2004;10(12):1321-8. doi:10.1038/nm1146.
110. Vassilev LT, Vu BT, Graves B, et al. In vivo activation of the p53 pathway by small-molecule antagonists of MDM2. *Science*. 2004;303(5659):844-8. doi:10.1126/science.1092472.
111. Bista M, Petrovich M, Fersht AR. MDMX contains an autoinhibitory sequence element. *Proc Natl Acad Sci U S A*. 2013;110(44):17814-9. doi:10.1073/pnas.1317398110.
112. Chen L, Borchers W, Wu S, et al. Autoinhibition of MDMX by intramolecular p53 mimicry. *Proc Natl Acad Sci U S A*. 2015;112(15):4624-9. doi:10.1073/pnas.1420833112.
113. Gilmartin AG, Faltg TH, Richter M, et al. Allosteric Wip1 phosphatase inhibition through flap-subdomain interaction. *Nat Chem Biol*. 2014;10(3):181-7. doi:10.1038/nchembio.1427.
114. Lu X, Ma O, Nguyen T-A, Jones SN, Oren M, Donehower LA. The Wip1 Phosphatase acts as a gatekeeper in the p53-Mdm2 autoregulatory loop. *Cancer Cell*. 2007;12(4):342-54. doi:10.1016/j.ccr.2007.08.033.
115. Cheung EC, Athineos D, Lee P, et al. TIGAR is required for efficient intestinal regeneration and tumorigenesis. *Dev Cell*. 2013;25(5):463-77.

doi:10.1016/j.devcel.2013.05.001.

116. Webster NJ, Resnik JL, Reichart DB, Strauss B, Haas M, Seely BL. Repression of the insulin receptor promoter by the tumor suppressor gene product p53: a possible mechanism for receptor overexpression in breast cancer. *Cancer Res.* 1996;56(12):2781-8. Available at: <http://www.ncbi.nlm.nih.gov/pubmed/8665514>. Accessed June 21, 2016.
117. Blum R, Kloog Y. Metabolism addiction in pancreatic cancer. *Cell Death Dis.* 2014;5:e1065. doi:10.1038/cddis.2014.38.
118. Jiang L, Kon N, Li T, et al. Ferroptosis as a p53-mediated activity during tumour suppression. *Nature.* 2015;520(7545):57-62. doi:10.1038/nature14344.
119. Saleem A, Adhihetty PJ, Hood DA. Role of p53 in mitochondrial biogenesis and apoptosis in skeletal muscle. *Physiol Genomics.* 2009;37(1):58-66. doi:10.1152/physiolgenomics.90346.2008.
120. Wang P-Y, Ma W, Park J-Y, et al. Increased oxidative metabolism in the Li-Fraumeni syndrome. *N Engl J Med.* 2013;368(11):1027-32. doi:10.1056/NEJMoa1214091.
121. Lebedeva MA, Eaton JS, Shadel GS. Loss of p53 causes mitochondrial DNA depletion and altered mitochondrial reactive oxygen species homeostasis. *Biochim Biophys Acta.* 2009;1787(5):328-34. doi:10.1016/j.bbabo.2009.01.004.
122. Kulawiec M, Ayyasamy V, Singh KK. p53 regulates mtDNA copy number and mitochekpoint pathway. *J Carcinog.* 2009;8:8. doi:10.4103/1477-3163.50893.
123. Vazquez F, Lim J-H, Chim H, et al. PGC1 α expression defines a subset of human melanoma tumors with increased mitochondrial capacity and resistance to oxidative stress. *Cancer Cell.* 2013;23(3):287-301. doi:10.1016/j.ccr.2012.11.020.
124. Li L, Wang L, Li L, et al. Activation of p53 by SIRT1 inhibition enhances elimination of CML leukemia stem cells in combination with imatinib. *Cancer Cell.* 2012;21(2):266-81. doi:10.1016/j.ccr.2011.12.020.
125. Friedler A, Veprintsev DB, Freund SM V, von Glos KI, Fersht AR. Modulation of binding of DNA to the C-terminal domain of p53 by acetylation. *Structure.* 2005;13(4):629-36. doi:10.1016/j.str.2005.01.020.
126. Laptenko O, Prives C. Transcriptional regulation by p53: one protein, many possibilities. *Cell Death Differ.* 2006;13(6):951-61. doi:10.1038/sj.cdd.4401916.
127. Spolar RS, Record MT. Coupling of local folding to site-specific binding of proteins to DNA. *Science.* 1994;263(5148):777-84. Available at: <http://www.ncbi.nlm.nih.gov/pubmed/8303294>. Accessed June 21, 2016.
128. Laptenko O, Shiff I, Freed-Pastor W, et al. The p53 C terminus controls site-specific DNA binding and promotes structural changes within the central DNA binding domain. *Mol Cell.* 2015;57(6):1034-46.

doi:10.1016/j.molcel.2015.02.015.

129. Espinosa JM, Emerson BM. Transcriptional regulation by p53 through intrinsic DNA/chromatin binding and site-directed cofactor recruitment. *Mol Cell*. 2001;8(1):57-69. Available at: <http://www.ncbi.nlm.nih.gov/pubmed/11511360>. Accessed June 21, 2016.
130. Jayaraman J, Prives C. Activation of p53 sequence-specific DNA binding by short single strands of DNA requires the p53 C-terminus. *Cell*. 1995;81(7):1021-9. Available at: <http://www.ncbi.nlm.nih.gov/pubmed/7600571>. Accessed June 21, 2016.
131. Schlereth K, Beinoraviciute-Kellner R, Zeitlinger MK, et al. DNA binding cooperativity of p53 modulates the decision between cell-cycle arrest and apoptosis. *Mol Cell*. 2010;38(3):356-68. doi:10.1016/j.molcel.2010.02.037.
132. Chillemi G, Davidovich P, D'Abramo M, et al. Molecular dynamics of the full-length p53 monomer. *Cell Cycle*. 2013;12(18):3098-108. doi:10.4161/cc.26162.
133. D'Abramo M, Bešker N, Desideri A, Levine AJ, Melino G, Chillemi G. The p53 tetramer shows an induced-fit interaction of the C-terminal domain with the DNA-binding domain. *Oncogene*. 2015. doi:10.1038/onc.2015.388.
134. Stommel JM, Marchenko ND, Jimenez GS, Moll UM, Hope TJ, Wahl GM. A leucine-rich nuclear export signal in the p53 tetramerization domain: regulation of subcellular localization and p53 activity by NES masking. *EMBO J*. 1999;18(6):1660-72. doi:10.1093/emboj/18.6.1660.
135. Zhang Y, Xiong Y. A p53 amino-terminal nuclear export signal inhibited by DNA damage-induced phosphorylation. *Science*. 2001;292(5523):1910-5. doi:10.1126/science.1058637.
136. Gu J, Nie L, Wiederschain D, Yuan ZM. Identification of p53 sequence elements that are required for MDM2-mediated nuclear export. *Mol Cell Biol*. 2001;21(24):8533-46. doi:10.1128/MCB.21.24.8533-8546.2001.
137. Lohrum MA, Woods DB, Ludwig RL, Bálint E, Vousden KH. C-terminal ubiquitination of p53 contributes to nuclear export. *Mol Cell Biol*. 2001;21(24):8521-32. doi:10.1128/MCB.21.24.8521-8532.2001.
138. Morrow JF. Gene_for_Gene. *Ann N Y Acad Sci*. 1976;265:13-21. Available at: <http://onlinelibrary.wiley.com/doi/10.1111/j.1749-6632.1976.tb29316.x/epdf>.
139. Sambrook J, Westphal H, Srinivasan PR, Dulbecco R. The integrated state of viral DNA in SV40-transformed cells. *Proc Natl Acad Sci U S A*. 1968;60(4):1288-1295.
140. Jasln M. Genetic manipulation of genomes with rare-cutting endonucleases. *Cell Press*. 1996;12(6):224-228.
141. Nomura A, Sugiura Y. Sequence-selective and hydrolytic cleavage of DNA by zinc finger mutants. *J Am Chem Soc*. 2004;126(47):15374-15375. doi:10.1021/ja045663l.

142. Tong C, Huang G, Ashton C, Li P, Ying Q-L. Generating gene knockout rats by homologous recombination in embryonic stem cells. *Nat Protoc.* 2011;6(6):827-844. doi:10.1038/nprot.2011.338.
143. Cermak T, Doyle EL, Christian M, et al. Efficient design and assembly of custom TALEN and other TAL effector-based constructs for DNA targeting. *Nucleic Acids Res.* 2011;39(12):e82. doi:10.1093/nar/gkr218.
144. Bultmann S, Morbitzer R, Schmidt CS, et al. Targeted transcriptional activation of silent oct4 pluripotency gene by combining designer TALEs and inhibition of epigenetic modifiers. *Nucleic Acids Res.* 2012;40(12):5368-77. doi:10.1093/nar/gks199.
145. Mali P, Yang L, Esvelt KM, et al. RNA-guided human genome engineering via Cas9. *Science.* 2013;339(6121):823-6. doi:10.1126/science.1232033.
146. Ran FA, Hsu PD, Wright J, Agarwala V, Scott DA, Zhang F. Genome engineering using the CRISPR-Cas9 system. *Nat Protoc.* 2013;8(11):2281-308. doi:10.1038/nprot.2013.143.
147. Kim H-M, Colaiácovo MP. CRISPR-Cas9-Guided Genome Engineering in *C. elegans*. *Curr Protoc Mol Biol.* 2016;115:31.7.1-31.7.18. doi:10.1002/cpmb.7.
148. Simeonova I, Jaber S, Draskovic I, et al. Mutant mice lacking the p53 C-terminal domain model telomere syndromes. *Cell Rep.* 2013;3(6):2046-58. doi:10.1016/j.celrep.2013.05.028.
149. Phang BH, Othman R, Bougeard G, et al. Amino-terminal p53 mutations lead to expression of apoptosis proficient p47 and prognosticate better survival, but predispose to tumorigenesis. *Proc Natl Acad Sci U S A.* 2015;112(46):E6349-58. doi:10.1073/pnas.1510043112.

APPENDIX

APPENDIX A: Chemicals Used in the Study

Chemicals and Media Components	Supplier Company
2-Mercaptoethanol	Sigma, Germany
Acetic Acid	Merck, Germany
Acid Washed Glass Beads	Sigma, Germany
Acrylamide/Bis-acrylamide	Sigma, Germany
Agarose	peQLab, Germany
Ammonium Persulfate	Sigma, Germany
Ammonium Sulfate	Sigma, Germany
Ampicillin Sodium Salt	CellGro, USA
Bacto Agar	BD, USA
Bacto Tryptone	BD, USA
Boric Acid	Molekula, UK
Bradford Reagent	Sigma, Germany
Bromophenol Blue	Sigma, Germany
Chloramphenicol	Gibco, USA
D-Glucose	Sigma, Germany
Distilled water	Milipore, France
DMEM	PAN, Germany
DMSO	Sigma, Germany

DNA Gel Loading Solution, 5X	Quality Biological, Inc, USA
DPBS	CellGro, USA
EDTA	Applichem, Germany
Ethanol	Riedel-de Haen, Germany
Ethidium Bromide	Sigma, Germany
Fetal Bovine Serum (FBS)	Biological Industries, Israel
Glycerol Anhydrous	Applichem, Germany
Glycine	Applichem, Germany
HBSS	CellGro, USA
HEPES	Applichem, Germany
Hydrochloric Acid	Merck, Germany
Isopropanol	Riedel-de Haén, Germany
Kanamycin Sulfate	Gibco, USA
LB Agar	BD, USA
LB Broth	BD, USA
L-Glutamine	Hyclone, USA
Liquid nitrogen	Karbogaz, Turkey
Magnesium Chloride	Promega, USA
Methanol	Riedel-de Haen, Germany
Monoclonal Anti-HA Antibody	Sigma, Germany
p53 Mouse Antibody	Cell Signalling Technology, USA
p53 Polyclonal Antibody	Cell Signalling Technology, USA
PATZ1 (H-300) Antibody	Santa Cruz, USA
Penicillin-Streptomycin	Sigma, Germany
Phenol-Chloroform-Isoamylalcohol	Amersco, USA
PIPES	Sigma, Germany
Potassium Acetate	Merck, Germany
Potassium Chloride	Fluka, Germany
Potassium Hydroxide	Merck, Germany
Protease Tablets (EDTA-free)	Roche, Germany
ProtG Sepharose	Amersco, USA
RNase A	Roche, Germany
RPMI 1640	PAN, Germany
SDS Protein Gel Loading Pack	Fermentas, Germany
SDS Pure	Applichem, Germany
Skim Milk Powder	Fluka, Germany
Sodium Azide	Amresco, USA
Sodium Chloride	Applichem, Germany
SuperSignal Chemiluminescent Substrate	Thermo Scientific, USA
TEMED	Applichem, Germany
Tris Buffer Grade	Amresco, USA
Tris Hydrochloride	Amresco, USA
Triton X100	Promega, USA
Tween20	Sigma, Germany

APPENDIX B: Equipment Used in the Study

Equipment	Company
Autoclave	Hirayama, Hiclave HV-110, Japan
Balance	Sartorius, BP221S, Germany Schimadzu, Libror EB-3200 HU, Japan
Biomolecular Imager	ImageQuant LAS 4000 mini - GE Healthcare, USA
Cell Counter	Cole Parmer, USA
Centrifuge	Eppendorf, 5415D, Germany Hitachi, Sorvall RC5C Plus, USA
CO2 Incubator	Binder, Germany
Deepfreeze	-80°C, Forma, Thermo Electron Corp., USA -20°C, Bosch, Turkey
Distilled Water	Millipore, Elix-S, France
Electrophoresis Apparatus	Biogen Inc., USA Biorad Inc., USA
Electroporator	Neon Transfection System - Life Technologies, USA
Filter Membranes	Millipore, USA
Flow Cytometer	BDFACSCanto, USA
Gel Documentation	Biorad, UV-Transilluminator 2000, USA
Heater	Thermomixer Comfort, Eppendorf, Germany
Hematocytometer	Hausser Scientific, Blue Bell Pa., USA
Ice Machine	Scotsman Inc., AF20, USA
Incubator	Memmert, Modell 300, Germany Memmert, Modell 600, Germany
Laminar Flow	Kendro Lab. Prod., Heraeus, HeraSafe HS12, Germany
Liquid Nitrogen Tank	Taylor-Wharton, 3000RS, USA
Magnetic Stirrer	VELP Scientifica, ARE Heating Magnetic Stirrer, Italy
Microliter Pipettes	Gilson, Pipetman, France Eppendorf, Germany
Microscope	Olympus CK40, Japan Olympus CH20, Japan Olympus IX70, Japan Zeiss Confocal LSM710, German
Microwave Oven	Bosch, Turkey
pH meter	WTW, pH540 GLP MultiCal, Germany
Power Supply	Biorad, PowerPac 300, USA
Refrigerator	Bosch, Turkey

Shaker Incubator	New Brunswick Sci., Innova 4330, USA
Spectrophotometer	Schimadzu, UV-1208, Japan
	Schimadzu, UV-3150, Japan
Thermocycler	Eppendorf, Mastercycler Gradient, Germany
Vortex	Velp Scientifica, Italy

APPENDIX C: DNA and Protein Molecular Weight Markers

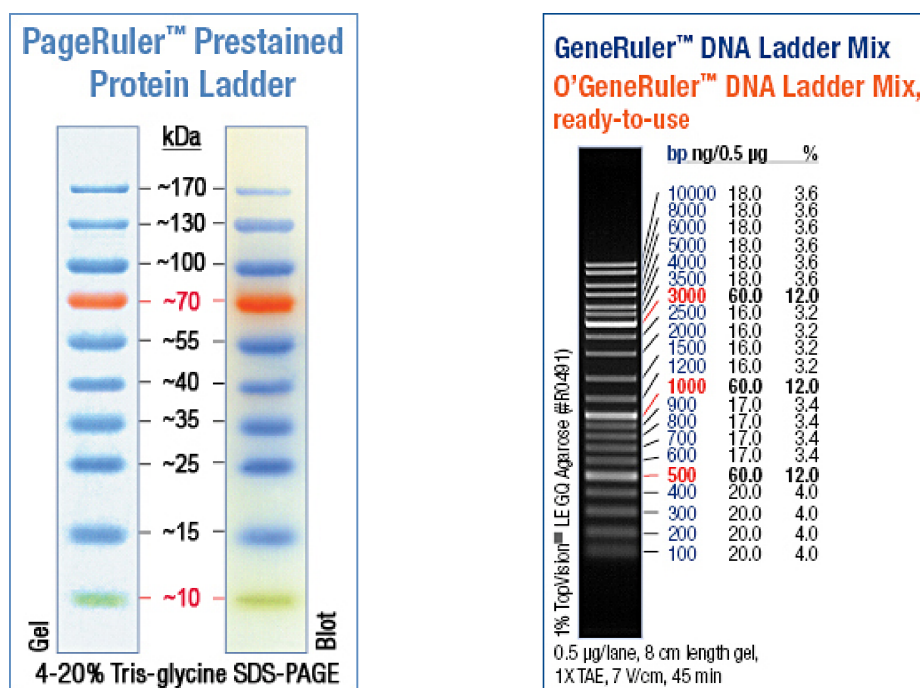


Figure C.1: DNA and Protein Molecular Weight Markers